To the Graduate Council:

I am submitting herewith a thesis written by Haisam Kassim Ido entitled "Six Degrees-of-Freedom Atmospheric Entry Characteristics of the NASA sponsored COMmercial Experiment Transporter (COMET) Recovery Vehicle using the Program to Optimize Simulated Trajectories (POST)". I have examined the final copy of this thesis for form and content and recommend that it be accepted in partial fulfillment of the requirements for the degree of Master of Science, with a major in Aerospace Engineering.

Firouz Shahrokhi

Dr. Firouz Shahrokhi, Major Professor

We have read this thesis and
recommend its acceptance:

George Garrison

Michael J. Chaney

Accepted for the Council:

C W Minkel

Associate Vice Chancellor
and Dean of The Graduate School

STATEMENT OF PERMISSION TO USE

In presenting this thesis in partial fulfillment of the requirements for a Master of Science degree at The University of Tennessee, Knoxville, I agree that the Library shall make it available to borrowers under rules of the Library. Brief quotations from this thesis are allowable without special permission, provided that accurate acknowledgment of the source is made.

Permission for extensive quotation from or reproduction of this thesis may be granted by my major professor, or in his absence, by the Head of Interlibrary Services when, in the opinion of either, the proposed use of the material is for scholarly purposes. Any copying or use of the material in this thesis for financial gain shall not be allowed without my written permission.

Signature ____________________

Date 5/26/92

SIX DEGREES-OF-FREEDOM ATMOSPHERIC ENTRY CHARACTERISTICS OF THE NASA SPONSORED COMMERCIAL EXPERIMENT TRANSPORTER (COMET) RECOVERY VEHICLE USING THE PROGRAM TO OPTIMIZE SIMULATED TRAJECTORIES (POST)

A Thesis

Presented for the

Master of Science

Degree

The University of Tennessee, Knoxville

Haisam Kassim Ido

هيثم قاسم عيدو

August 1992

DEDICATION

This Thesis is dedicated to my wife

Carol Jendre Ido

and

to my parents

Rita Büche Ido

and

Kassim Ali Ido

قاسم علي عيدو

ACKNOWLEDGEMENTS

I would like to thank Mr. Joe Pawlick, COMET Program Manager of the UT-Calspan Center of Space Transportation and Applied Research, for allowing me to pursue research on the COMET project. Dr. George Garrison, director of the UT-Calspan Center for Space Transportation and Applied Research, who was on my committee has shown great patience in my progress and research. Mr. Bert Allee's, chief engineer at the UT-Calspan Center of Space Transportation and Applied Research, continuous inquiries, expertise and help was invaluable. Mr. Brian Feather, of Arvin-Calspan was great in finding errors in my input file and assisting me in understanding some of the physics pertaining to entry. My thesis advisor, Dr. Firouz Shahrokhi, was very helpful in every step of the writing of this thesis. Dr. Mike Chaney, thesis committee member, has taught me what was necessary for understanding the flight mechanics of space vehicles. Mr. Richard W. Powell, of Langley Research Center, was extremely helpful in answering my POST questions.

ABSTRACT

The purpose of this thesis to to conduct an analysis on the flight dynnamic characteristics of COMmercial Experiment Transporter's (COMET) Recovery Vehicle (RV), with no controls. The COMET Service Module will not be considered in this work. The three and the six, translational and rotational, degrees-of-freedom atmospheric entry characteristics are numerically computed using the Program to Optimize Simulated Trajectories (POST). There are two versions of POST three and six degrees-of-freedom, 3D POST & 6D POST, respectively. POST has been implemented using the fourth order Runge-Kutta numerical integration algorithm for both degrees-of-freedom. An oblate spinning earth is considered. A 1976 U.S. Standard Atmosphere is used. All the aerodynamic coefficients used are input as functions of the local angle. It is found that the nominal conditions of entry, particularly the roll rate, greatly affects the behavior of the vehicle at lower altitudes. Oscillatory numerical solutions are discussed. Angular, axial and transverse accelerations are considered. Perturbing the roll rates changes the sensed acceleration on the body. There is a slight increase of the accelerations due to increased roll rates, which is due to increased centrifugal acceleration. Convergence/Divergence of oscillation envelopes is also examined. This vehicle, as all blunt nosed vehicles, such as the Mercury capsule, has been determined to have a divergence of the oscillation envelope after maximum dynamic pressure is reached. This occurs due to the fact that the drag coefficient of these vehicles is relatively larger than the lift coefficient. The roll rate greatly affects the touch down point of the vehicle. The

downrange error of the touchdown increases by about thirty percent as the roll rate is increased from two and a half to five revolutions per minute. The percentage of increase is virtually the same from five to seven and a half revolutions per minute. The heating rate calculations are determined by use of the three degrees-of-freedom version of POST.

TABLE OF CONTENTS

LIST OF FIGURES

NOMENCLATURE

Math Symbol	POST's Fortran Symbol	Definition
a	SEMJAX	Semimajor Axis, ft
A_s	ASM	Total sensed Acceleration in the Body Frame (fps^2)
A_{ZL}	AZL	Azimuth of the z_L Axis, (deg.)
A_{ZR}	AZVELR	Azimuth of the relative Velocity Vector, (deg.)
C	N/A	Used in the stagnation heating rate equation, 17000 Btu $ft^{-3/2}$ sec^{-1}
C_A, C_Y, C_N	CA, CY, CN	Axial, Side and Normal Aerodynamic Force Coefficients
C_D, C_L	CD, CL	Drag and Lift Coefficients
C_m, C_n	CM, CW	Pith and Yaw Moment Coefficients
C_s	CS	Speed of Sound, fps
D	DRAG	Aerodynamic Drag, lb
D_{ref}	---	Reference Length
D_R, D_P, D_Y	DREFR, DREFP, DREFY	Reference Lengths for Roll, Pitch, and Yaw Aerodynamic Moment Coefficients, ft (all equal in this analysis)
D_{ref}	N/A	Reference length in Chapter 2, (ft)
e	ECCEN	Orbital Eccentricity
$[e]^T=[e_0, e_1, e_2, e_3]^T$	EO(i)	Euler Parameters (Quaternion Elements)
F(r)	N/A	Central Force (lb)

$\bar{g}_x, g_y, g_z$	N/A	Local gravitational components on the body, (ft/s^2)
$\underline{G_I}=(G_{XI}, G_{YI}, G_{ZI})$	GXI, GYI, GZI	Total Gravitational Acceleration in the ECI-Frame (fps^2)
h	ALTITO	Oblate Altitude, (ft)
i	INC	Orbital Inclination, (deg)
[IB]	IB(i)	Matrix Transformation from the ECI-Frame to the Body-Frame
[IG]	IG(i)	Matrix Transformation from the ECI-Frame to the Geographic-Frame.
[IL]	IL(i)	Matrix Transformation from the ECI-Frame to the Launch-Frame.
[IP]	IP(i)	Matrix Transformation from the ECI-Frame to the Rotating Planet-Frame.
I_{xx}, I_{yy}, I_{zz}	IXX, IYY, IZZ	Moments of Inertia about the Vehicle Body Axis System (slug-ft^2)
I_{xy}, I_{xz}, I_{yz}	IXY, IXZ, IYZ	Products of Inertia about the Vehicle Body Axis System (slug-ft^2)
J_2, J_3, J_4	J2, J3, J4	Gravitational Constants
L	LIFT	Aerodynamic Lift, (lb)
[LB]	LB(i)	Matrix Transformation from the Launch-Frame to the Body-Frame.
l	LREF	Aerodynamic Reference Length (ft)
$\underline{M}$	---	Pitch and Yaw Moments in the Moment Equations

$\underline{\bar{M}}_{AB}$	AMXB(i), i=1,2,3	External Moments about the Roll, Pitch and Yaw axes owing to Aerodynamic forces, (ft-lb)
p, q, r	ROLBD, PITBD, YAWBD	Angular rates about roll, pitch and yaw, (deg/s)
$p^{'}$, $q^{'}$, $r^{'}$	PND, QND, RND	Nondimensional Roll, Pitch, and Yaw Vehicle Body Rates.
Q	TLHEAT	Total Heat, (Btu/ft^2)
q (q_∞ in Chapter 2)	DYNP	Dynamic Pressure, (lb/ft^2)
R_E, R_P	RE, RP	Equatorial and Polar Radii, (ft)
R_N	RN	Nose Radius, (ft)
S_{ref}	SREF	Aerodynamic Reference Area, (ft^2)
t	TIME	Time, s
$\bar{u}$	N/A	Chapman's nondimensional independent variable
v_r, v_θ	N/A	Radial and Tangential Velocities, (fps)
V_R	VELR	Relative Velocity, (fps)
v_x, v_y, v_z	N/A	Body velocity components, (fps)
W	N/A	Weight, (lb)
W_G	WEIGHT	Gross Vehicle Weight, (lb)
X, Y, Z	N/A	The Axial, Side and Vertical Aerodynamic body forces, (lb)

x_{cg}, y_{cg}, z_{cg}	XCG, YCG, ZCG	Coordinates of the Center-of-Gravity in the Body Reference System (ft)
$\overline{z}$	N/A	Chapman's nondimensional dependent variable.
α, β, σ	ALPHA, BETA, BNKANG	Aerodynamic Angle-of-Attack, Sideslip, and Bank, (deg)
α_T	ALPTOT	Total Angle-of-Attack, (deg)
β (In Chapter 2)	N/A	The reciprocal of Scale Height, 1/23500 ft^{-1}
γ_R	GAMMAR	Relative Flight Path Angles, (deg)
Δt	DT	Increment in Time or Integration step-size, s
θ_a	---	True Anomaly, (deg)
θ_I	LONGI	Inertial Longitude, (deg)
λ	AZREF	Azimuth Reference, (deg)
μ	MU	Gravitational Constant (ft^3/s_2)
μ^*	N/A	The Atmospheric Dynamic Viscosity.
$\rho(h)$	DENS	Atmospheric Density, ($slug/ft^3$)
ϕ_c	GCLAT	Geocentric Latitude, (deg)
ϕ_g	GDLAT	Geodetic Latitude, (deg)
$\underline{\omega}=(\omega_x, \omega_y, \omega_z)$	ROLBD, PITBD, YAWBD	Inertial Angular Velocity Components about the body Axes, (deg/s)

$\underline{\dot{\omega}}$	ROLBDD, PITBDD, YAWBDD	Inertial Angular Acceleration Components about the Body Axes, (deg/s^2)
ω_p	ARGP	Argument of Perigee, (deg)
Ω	LAN	Inertial Longitude of the Ascending Node, (deg)

CHAPTER 1: INTRODUCTION

1.1 COMET Program Background

"It has been recognized for some time that the United States space industry does not offer the commercial R&D community dependable and economical access to a space environment. This need was defined and focused by the NASA-sponsored Centers for the Commercial Development of Space (CCDSs) reflecting their requirements and those of their industrial partners. As a result, the Center for Space Transportation and Applied Research (CSTAR) located at the University of Tennessee Space Institute (UTSI) in Tullahoma, Tennessee was given the authority by NASA to establish and implement the COMmercial Experiment Transporter (COMET) Program with funding provided by a NASA grant."(CSTAR March 23 1992, pp. ii)

"COMET is a fully integrated space transportation and recovery service to meet the needs of the United States' research and development community. This service, with three launches planned for the 1993-1995 time frame -- the first launch scheduled for March 1993 -- will carry experiments to microgravity of space and return, providing basic utilities such as electric power, controlled temperature, orientation, data management, and communications while in orbit.

The modular design of COMET provides flexible payload accommodations for a wide variety of materials and equipment ... each mission will launch a two-part Free-Flyer - which will carry experiments into a nominal 300 nautical mile orbit - consisting of a

Service Module for 130 days and a **Recovery System** which returns to land by parachute after 30 days in orbit.

The Recovery System is separated from the Service Module 30 days into the mission. The capsule is recovered on land with a parachute landing ..." (CSTAR March 23, 1992, 1-2). COMET is well suited for life sciences, materials processing, remote sensing, space propulsion, and automation and robotics experiments.

"The Recovery System consists of a reentry vehicle with the necessary structural and support systems to accommodate a variety of experiments. It will be attached to the Service Module by bolting to an interface ring. The Recovery System has all the required components to start-up, operate, deorbit and make a controlled parachute landing at a selected recovery site. The Recovery System will accommodate a 300-lb payload in a pressurized environment ... Standard pressurized volume is 10 cubic feet ... The maximum payload volume available for unpressurized experiments is 12 cubic feet." (CSTAR March 23 1992, 14)

1.2 Purpose of present research

The Service Module (fig. 1-2-1) will not be considered here. The purpose of this thesis is to conduct an analysis on the flight dynamic characteristics of the atmospheric entry vehicle (fig. 1-2-2) with no controls, which is a component of COMET's Recovery System. The analysis will include axial, transverse and angular loads that a payload may encounter in its flight trajectory. Also, the time history of all pertinent angles of the body to the local velocity vector will be determined. The necessity of that will be apparent when

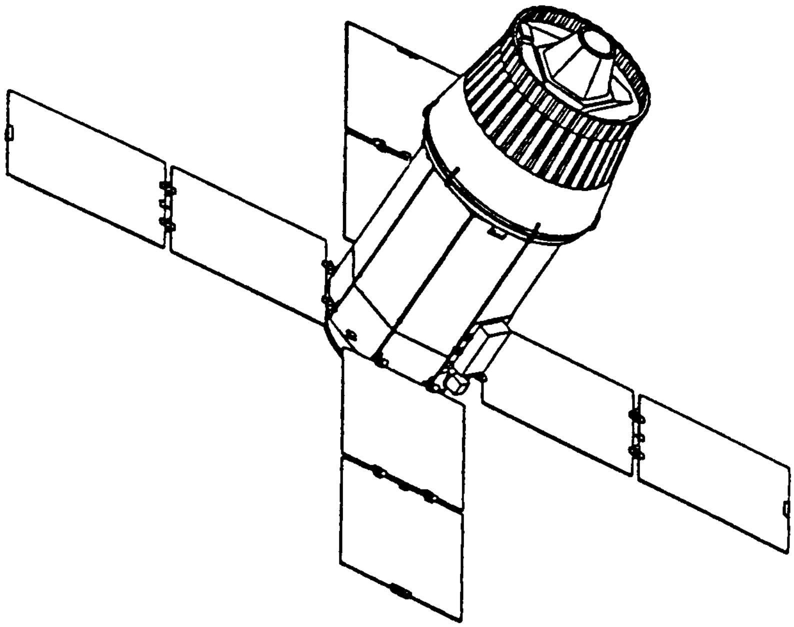

Figure 1-2-1, COMET FreeFlyer.
(CSTAR March 23 1992, ii)

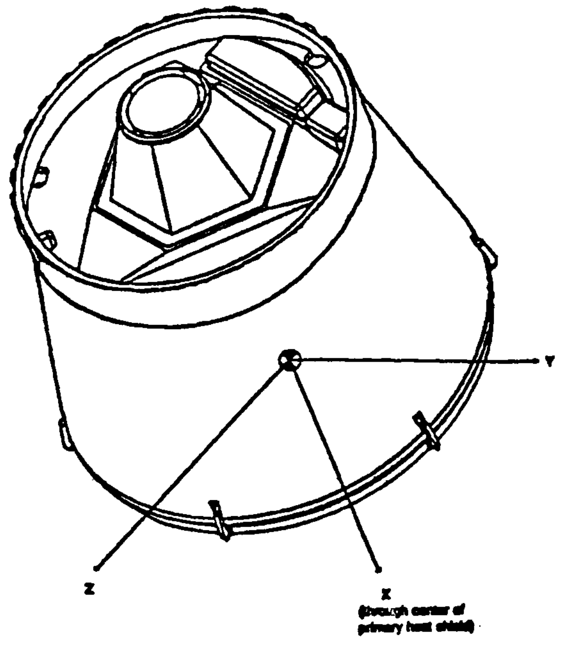

Figure 1-2-2, COMET's Recovery Vehicle.

the angle of attack or the sideslip angle is larger than the half cone angle of the vehicle. The time variance of the angles will also contribute to the loading on the vehicle. The analysis will also deal with targeting to the landing point, i.e. crossrange and downrange estimates. The heat accumulation on the heat shield will also be determined. However, this thesis will emphasize analysis of the dynamical behavior rather than the aerodynamics heating rate.

1.3 Methodology used

The approach taken here is to implement software that has been already developed for flight dynamic analysis. The Martin Marietta Corporation developed the Program to Optimize Simulated Trajectories (POST), for the NASA Langley Research Center, has been selected for this analysis. POST was selected since it can be implemented to numerous N-stage flight vehicles with or without controls and an option of optimization of chosen parameters. It has been used to simulate the Space Shuttle, and Titan missile dynamics, and also used to simulate Mars aerobraking. Both the three and six degree-of-freedom version of POST, 3D and 6D POST, have been implemented for this analysis. "6D POST is a general-purpose Fortran program for simulating and optimizing rigid-body trajectories of aerospace type vehicles. The program can be used to solve a wide variety of performance, guidance, and flight control problems for atmospheric and orbital vehicles. For example, typical applications of 6D POST include:

1) Guidance and flight control system simulation and analysis;

2) Loads and dispersion type analyses;

3) General-purpose 6D simulation of controlled and uncontrolled vehicles;

4) 6D performance validation." (Brauer September 1987, 6D POST V.1 1-1).

Every computational routine in the program can be categorized according to five basic functional elements. These elements are: the planet module, the vehicle module, the trajectory simulation module, the trajectory auxiliary calculations module, and the trageting/optimization module.

The Planet Module. -- This module is composed of an oblate spheroid model, a gravitational model, an atmospheric model, and a winds model. These models define the environment in which the vehicle operates.

The Vehicle Module. -- This module is composed of mass properties, propulsion, aerodynamics, aeroheating, an airframe model, a navigation and guidance model, and a flight control system model. These models define the basic vehicle simulation characteristics." (Brauer September 1987, 6D POST V.1 1-1). The documentation and development for POST was paid for by U.S. tax payers. Hence, the public may acquire copies from NASA.

The physical properties include the vehicle's moments of inertia and mass. It has been assumed that the vehicle is rigid and contains no propellant fuel after retro thrust burnout. The center of gravity is assumed to be fixed and is on the center line of the vehicle. Therefore, the analysis begins after the propellant has been exhausted and the vehicle has "entered" the atmosphere.

The aerodynamic properties of the vehicle are input in a table format, and POST interpolates for the appropriate values. The aerodynamic coefficients are input as functions of the local angle. POST can use trivariant tables.

POST contains both laminar and turbulent heat-rate options. Chapman's stagnation point equation, for either laminar and turbulent flow, can be used.

"The Trajectory Simulation Module. -- This module consists of the event sequencing module that controls the program cycling, the table interpolation routines, and several standard numerical integration techniques. These models are used in numerically solving the translational and rotational equations of motion [using a 4th order Runge-Kutta method]." (Brauer September 1987, 6D POST, V.1 1-2)

In the auxiliary calculation module only range calculations are implemented for this analysis. The targeting/optimization module was not implemented here.

1.4 Order of thesis

In Sections one and two of Chapter 2 the derivation of the point mass equations for atmospheric entry trajectories are covered. Section one derives the motion of a point mass under a central force with no aerodynamic forces. Section two includes the effects of the aerodynamic forces and derives Chapman's "Universal" equation. Section three covers the oscillatory motion of a vehicle as it descends through the atmosphere. The end of Chapter 2 applies the equations of section one to three to the nominal values of the recovery vehicle and has a brief analysis of the results.

Chapter 3 has three and six degrees-of-freedom results from using POST and has extensive figures. The complete nominal data on the COMET Recovery Vehicle are contained in this chapter.

Chapter 4 contains the conclusions and recommendations. It contains comparisons of some of the results in Chapter 2.

The bibliography is as inclusive as possible. By no means are all the items listed referred to in the text. The purpose of the bibliography is to assist readers in their future research and certainly for this author's future endeavors.

Appendix A contains some of the features in 6D POST and their applications. Appendix B contains the input file for the three degrees-of-freedom used in the POST programs. Appendix C contains the input file for the six degrees-of-freedom used in the POST programs. Appendix D contains the table of aerodynamic data used.

CHAPTER 2: ATMOSPHERIC ENTRY

2.1 Keplerian Equations

The Keplerian Equations can be used to model the motion of objects under central force systems and can, therefore, be used to describe the dynamics and mechanics of space vehicles entering a planet's atmosphere. This section summarizes the governing equations in vector form (Thompson 1986, 13-22), of a point mass vehicle moving around a planet.

$$\vec{F} = F(r)\,\vec{e}_r \tag{2.1.1}$$

where $F(r) = -\frac{GM_p m}{r^2}$ for a central force due to a point mass and where M_p is the mass of the planet and m is the mass of the vehicle (fig. 2-1-1). Neglecting other forces (fig. 2-2-1 includes aerodynamic forces), the moment equation due to gravity is

$$\vec{M} = \vec{r}\times\vec{F} = \frac{d\vec{H}}{dt} = \begin{vmatrix} \vec{e}_r & \vec{e}_\theta & \vec{e}_k \\ r & 0 & 0 \\ -\frac{GM_p m}{r^2} & 0 & 0 \end{vmatrix} = \vec{0} \tag{2.1.2}$$

and $\vec{r} \equiv r\vec{e}_r$. Defining the angular momentum by

$$\vec{H} = H\vec{e}_k$$

and since the moment equation turns out to be zero the angular momentum, $\vec{H}$, is a constant. Using the concept of angular momentum, H, the following equations are

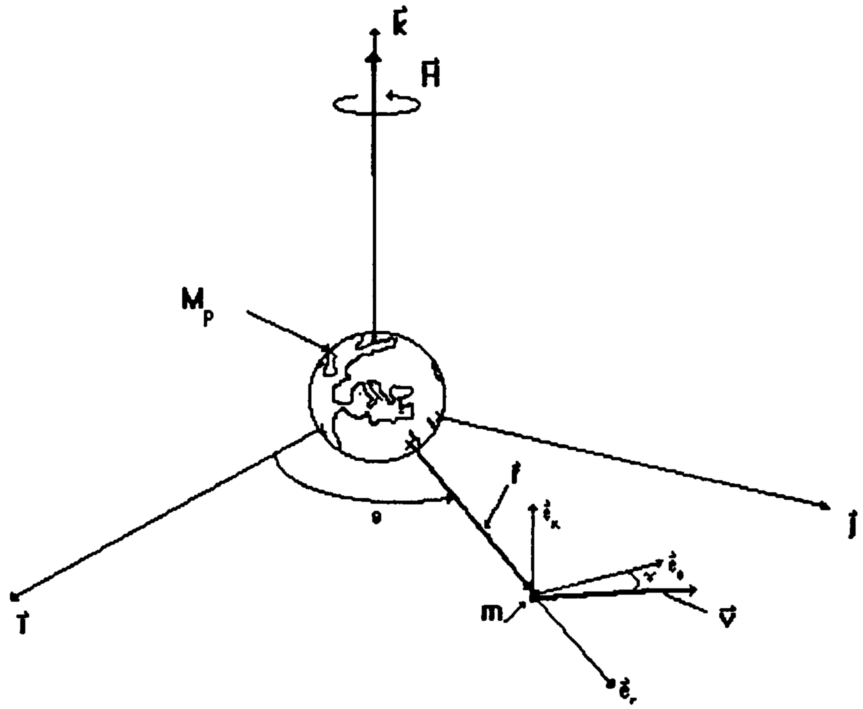

Figure 2-1-1, Point mass motion under a central force

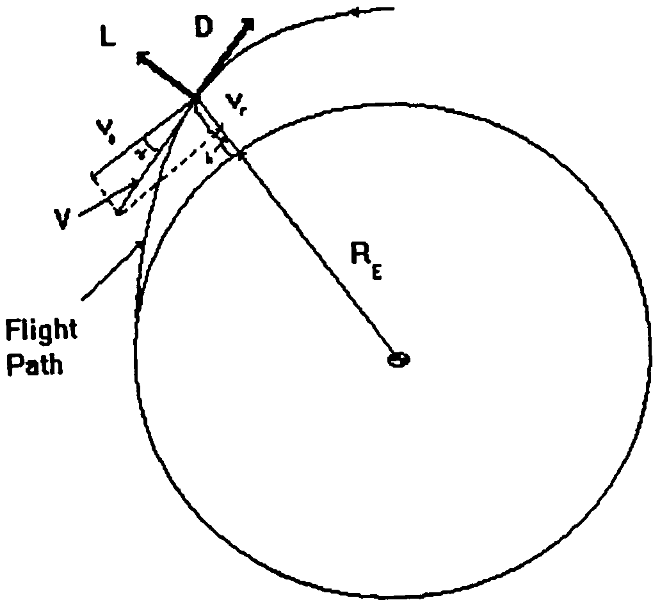

Figure 2-2-1, Flight Path of an Entry Vehicle derived,

$$\vec{H} = \vec{r}\times m\vec{v},$$
$$\vec{v} = \frac{d\vec{r}}{dt} = \left(\frac{d\vec{r}}{dt}\right)_{rel} + \vec{\omega}\times\vec{r}$$

where $\vec{\omega} = \dot{\theta}\vec{e}_k$, $()_{rel}$ is the change due to time only and not to rotating frame effects, and $\vec{v}$ is the local velocity vector. Hence,

$$\left(\frac{d\vec{r}}{dt}\right)_{rel} = \dot{r}\vec{e}_r\ , \ and\ \ \vec{\omega}\times\vec{r} = \begin{vmatrix} \vec{e}_r & \vec{e}_\theta & \vec{e}_k \\ 0 & 0 & \dot{\theta} \\ r & 0 & 0 \end{vmatrix} = r\dot{\theta}\vec{e}_\theta$$

therefore,

$$\vec{H} = \begin{vmatrix} \vec{e}_r & \vec{e}_\theta & \vec{e}_k \\ r & 0 & 0 \\ m\dot{r} & mr\dot{\theta} & 0 \end{vmatrix} = mr^2\dot{\theta}\vec{e}_k \qquad \textbf{2.1.3}$$

and

$$\frac{d\vec{r}}{dt} = \dot{r}\vec{e}_r + r\dot{\theta}\vec{e}_\theta \qquad \textbf{2.1.4}$$

The above equations are combined to arrive at the equation that describes the motion of a point mass under the central force described by eq. 2.1.1.

$$\vec{a} = \frac{d\vec{v}}{dt} = \frac{d^2\vec{r}}{dt^2} = \left(\frac{d^2\vec{r}}{dt^2}\right)_{rel} + \vec{\omega}\times\frac{d\vec{r}}{dt} \qquad \textbf{2.1.5}$$

where $\left(\frac{d^2\vec{r}}{dt^2}\right)_{rel} = \ddot{r}\vec{e}_r + (\dot{r}\dot{\theta} + r\ddot{\theta})\vec{e}_\theta$, which is arrived at by the differentiation of the velocity vector $\vec{v}$ (eq. 2.1.4). In addition,

$$\vec{\omega}\times\frac{d\vec{r}}{dt} = \begin{vmatrix} \vec{e}_r & \vec{e}_\theta & \vec{e}_k \\ 0 & 0 & \dot{\theta} \\ \dot{r} & r\dot{\theta} & 0 \end{vmatrix} = -r\dot{\theta}^2\vec{e}_r + \dot{r}\dot{\theta}\vec{e}_\theta$$

Therefore,

$$\frac{d^2\vec{r}}{dt^2} = (\ddot{r} - r\dot{\theta}^2)\vec{e}_r + (2\dot{r}\dot{\theta} + r\ddot{\theta})\vec{e}_\theta = -\frac{GM_p}{r^2}\vec{e}_r$$

$$\therefore \quad \ddot{r} - r\dot{\theta}^2 = -\frac{GM_p}{r^2} \quad (\textit{radial acceleration}) \qquad \textbf{2.1.6}$$

and

$$2\dot{r}\dot{\theta} + r\ddot{\theta} = \frac{1}{r}\frac{d}{dt}(r^2\dot{\theta}) = \frac{1}{mr}\left|\frac{d\vec{H}}{dt}\right| = 0 \quad (\textit{transverse acceleration})$$

Defining h=H/m and noting that $r\dot{\theta}^2 = \frac{H}{r^3}$, and combining it with the radial acceleration equation one arrives at the Keplerian equation for orbits (Thompson 1986, 56-57).

$$\ddot{r} - \frac{h}{r^3} = -\frac{GM_p}{r^2} \qquad \textbf{2.1.7}$$

2.2 Chapman's "Universal" Equation:

"Chapman's equation, ... , is universal in the sense that it is free of the physical characteristics of the vehicle. Hence, it is applicable to any type of entry vehicle regardless of its weight, dimensions and shape." (Vinh 1980, 183).

"Chapman derived a relatively simple non-linear differential equation of the second-order, free of the characteristics of the vehicle." (Vinh 1980, 178). He succeeded by introducing a set of completely nondimensionalized variables and arrived at the variables by trial and error (Chapman 1959, 7).

Including the drag and lift forces due to the atmosphere (fig. 2-2-1) in eq. 2.1.1 will change the force to the following, $\vec{F} = (\frac{-GM_p m}{r^2} + L\cos\gamma - D\sin\gamma)\,\vec{e}_r - (D\cos\gamma + L\sin\gamma)\,\vec{e}_\theta$, and the Moment equation becomes,

$$\vec{M} = \vec{r}\times\vec{F} = \begin{vmatrix} \vec{e}_r & \vec{e}_\theta & \vec{e}_k \\ r & 0 & 0 \\ -\frac{GM_p m}{r^2} + L\cos\gamma - D\sin\gamma & -D\cos\gamma - L\sin\gamma & 0 \end{vmatrix}$$

L, D and γ are the lift, drag and local flight path angle, respectively.

$$\vec{M} = -r\,(D\cos\gamma + L\sin\gamma)\,\vec{e}_k \qquad \textbf{2.2.1}$$

Using eqs. 2.1.6,

$$m\vec{a} = m\frac{d^2\vec{r}}{dt^2} = m\left((\ddot{r} - r\dot{\theta}^2)\,\vec{e}_r + (2\dot{r}\dot{\theta} + r\ddot{\theta})\,\vec{e}_\theta\right) =$$

$$\Rightarrow = (\frac{-GM_p m}{r^2} + L\cos\gamma - D\sin\gamma)\,\vec{e}_r - (D\cos\gamma + L\sin\gamma)\,\vec{e}_\theta$$

Grouping unit vector terms and dividing out m,

$$\ddot{r} - r\dot{\theta}^2 = -\frac{GM_p}{r^2} + \frac{L}{m}\cos\gamma - \frac{D}{m}\sin\gamma \quad \textit{(radial acceleration)} \qquad \textbf{2.2.2a}$$

$$2\dot{r}\dot{\theta} + r\ddot{\theta} = -\frac{D}{m}\cos\gamma - \frac{L}{m}\sin\gamma = \frac{\dot{h}}{r} \quad \textit{(transverse acceleration)} \qquad \mathbf{2.2.2b}$$

For brevity (Boltz 1963, 9) $v_\theta \equiv r\dot{\theta} \equiv V\cos\gamma$, $v_r \equiv \dot{r} \equiv V\sin\gamma$. v_r, and v_θ are the radial and tangential velocities, respectively. After algebraic manipulation and elementary calculus, eqs. 2.2.2 become

$$\begin{aligned} \dot{v}_r - \frac{v_\theta^2}{r} &= -g(r) + \frac{L}{m}\cos\gamma - \frac{D}{m}\sin\gamma \\ \dot{v}_\theta + \frac{v_r v_\theta}{r} &= -\frac{D}{m}\cos\gamma - \frac{L}{m}\sin\gamma \end{aligned} \qquad \mathbf{2.2.3}$$

Note that $r\dot{\theta}^2 = \frac{v_\theta^2}{r}$, $\dot{r}\dot{\theta} = \frac{v_r v_\theta}{r}$, $r\ddot{\theta} = \frac{d(r\dot{\theta})}{dt} - \dot{r}\dot{\theta}$, $g(r) \equiv \frac{GM_p}{r^2} \equiv \frac{\mu}{r^2}$. Also using the fact that

$$\begin{aligned} \dot{v}_r &= \dot{V}\sin\gamma + \dot{\gamma}V\cos\gamma \\ \dot{v}_\theta &= \dot{V}\cos\gamma - \dot{\gamma}V\sin\gamma \end{aligned} \qquad \mathbf{2.2.4}$$

and substituting eqs. 2.2.4 into 2.2.3, the following is obtained

$$\dot{V} + V\left(\frac{\cos\gamma}{\sin\gamma}\right)\dot{\gamma} - \frac{V^2}{r}\left(\frac{\cos^2\gamma}{\sin\gamma}\right) = -\frac{g(r)}{\sin\gamma} + \frac{L}{m}\left(\frac{\cos\gamma}{\sin\gamma} - \frac{D}{m}\right) \qquad \mathbf{2.2.5}$$

$$\dot{V} - V\dot{\gamma}\left(\frac{\sin\gamma}{\cos\gamma}\right) + \frac{V^2}{r}\sin\gamma = -\frac{D}{m} - \frac{L}{m}\left(\frac{\sin\gamma}{\cos\gamma}\right) \qquad \mathbf{2.2.6}$$

subtracting eq. 2.2.6 from eq. 2.2.5 and eliminating $V\dot{\gamma}$ from eq. 2.2.6 and eq. 2.2.5 the following equations are obtained

$$V\dot{\gamma} = \left(\frac{V^2}{r} - g(r)\right)\cos\gamma + \frac{L}{m} \qquad \mathbf{2.2.7a}$$

$$\dot{V} = -g(r)\sin\gamma - \frac{D}{m} \qquad \textbf{2.2.7b}$$

using the fact that $\dot{r} = V\sin\gamma$, the last two equations may be used to make r the independent variable.

$$\begin{aligned} \frac{dV}{dr} &= -\frac{g(r)}{V} - \frac{D}{mV\sin\gamma} \\ \frac{d\gamma}{dr} &= \left(\frac{V^2}{r} - g\right)\frac{\cos\gamma}{\sin\gamma V^2} + \frac{L}{mV^2\sin\gamma} \end{aligned} \qquad \textbf{2.2.8}$$

Define as an independent variable (Vinh 1980, 180) $\bar{u}$ and a dependent variable $\bar{Z}$

$$\bar{u} \equiv \frac{V\cos\gamma}{\sqrt{g(r)r}} \ , \quad \bar{Z} \equiv \frac{\rho S C_D}{2m}\sqrt{\frac{r}{\beta}}\,\bar{u} \qquad \textbf{2.2.9}$$

where $C_D \equiv D/((1/2)\rho V^2 S)$, ρ is the local atmospheric density of the planet, and S is the reference area. β is the reciprocal of the scale height (Vinh 1980, 4), and defined as

$$\beta = \frac{gM}{R^{*}T}$$

R^{*} is the universal gas constant and M is the mean molecular weight of the atmosphere, T is the local temperature and g is the local gravitational acceleration. Differentiating $\bar{u}$ *and* $\bar{Z}$ with respect to r gives

$$\begin{aligned} \frac{d\bar{u}}{dr} &= \frac{\cos\gamma}{\sqrt{g(r)r}}\frac{dV}{dr} - \frac{V\sin\gamma}{\sqrt{g(r)r}}\frac{d\gamma}{dr} + \frac{\bar{u}}{2r} \\ \frac{d\bar{Z}}{dr} &= -\frac{\bar{Z}^2}{\bar{u}\sin\gamma}\sqrt{\frac{\beta}{r}} - \beta\bar{Z}\left(1 - \frac{1}{2\beta r} + \frac{1}{2\beta^2}\frac{d\beta}{dr}\right) \end{aligned} \qquad \textbf{2.2.10}$$

Using the first of eqs. 2.2.3 in terms of the $\bar{u}$ *and* $\bar{Z}$ variables, the following transformation results

$$\frac{d\gamma}{dr} = \frac{\bar{Z}}{\bar{u}\sin\gamma}\sqrt{\frac{\beta}{r}}\left(\frac{L}{D} + \frac{\bar{u}\cos\gamma}{\sqrt{\beta r}\,\bar{Z}}\left(1 - \frac{\cos^2\gamma}{\bar{u}^2}\right)\right) \qquad \mathbf{2.2.11}$$

Chapman (Vinh 1980, 179) made two basic assumptions to reduce the equations of motion to a single ordinary, nonlinear differential equation of the second-order. They are,

i) The radial change in distance from the planet's center is small compared to the change in the horizontal component of the velocity. Mathematically (Vinh 1980, 179), this assumption is expressed as

$$\left|\frac{d(V\cos\gamma)}{V\cos\gamma}\right| >> \left|\frac{dr}{r}\right|$$

ii) For a lifting body, the flight path angle γ is considered small such that the lift component in the horizontal is small compared to the drag component in the same direction. Mathematically (Vinh 1980, 179) this assumption is expressed as

$$\left|\frac{L}{D}\tan\gamma\right| << 1$$

"It is erroneous to think that these assumptions will restrict Chapman's analysis to entry trajectories with small flight path angles and small lift-to-drag ratios ... On the contrary, these assumptions, applied simultaneously, constitute a well balanced set of hypotheses and make Chapman's theory applicable to a large family of entry trajectories." (Vinh 1980, 179).

Using assumptions (i), (ii), β = constant and $d\beta/dr=0$, β/g=constant in an isothermal atmosphere (Vinh 1980, 181) and βr is large eqs. 2.2.10 become

$$\frac{d\bar{u}}{dr} = -\frac{\bar{Z}}{\sin\gamma}\sqrt{\frac{\beta}{r}} \qquad \textbf{2.2.12a}$$

$$\frac{d\bar{Z}}{dr} = -\frac{\bar{Z}}{\sin\gamma}\sqrt{\frac{\beta}{r}}\left(\frac{\bar{Z}}{\bar{u}} + \sqrt{\beta r}\,\sin\gamma\right) \qquad \textbf{2.2.12b}$$

$$\frac{d\gamma}{dr} = \frac{\bar{Z}}{\bar{u}\,\sin\gamma}\sqrt{\frac{\beta}{r}}\left(\frac{L}{D} + \frac{\bar{u}\cos\gamma}{\sqrt{\beta r}\,\bar{Z}}\left(1 - \frac{\cos^2\gamma}{\bar{u}^2}\right)\right) \qquad \textbf{2.2.13}$$

Using the first equation in 2.2.12 to change the independent variable from r to $\bar{u}$ and the equations from $\bar{Z}$ and γ in eq. 2.2.13 the equations become

$$\frac{d\bar{Z}}{d\bar{u}} = \frac{d\bar{Z}}{dr}\Big/\frac{d\bar{u}}{dr} = \frac{\bar{Z}}{\bar{u}} + \sqrt{\beta r}\,\sin\gamma \qquad \textbf{2.2.14a}$$

$$\frac{d\bar{Z}}{d\bar{u}} - \frac{\bar{Z}}{\bar{u}} = \sqrt{\beta r}\;\sin\gamma \qquad \textbf{2.4.14b}$$

$$\frac{d\gamma}{d\bar{u}} = -\frac{1}{\bar{u}}\left(\frac{L}{D} + \frac{\bar{u}\cos\gamma}{\sqrt{\beta r}\,\bar{Z}}\left(1-\frac{\cos^2\gamma}{\bar{u}^2}\right)\right) \qquad \textbf{2.2.15}$$

The second equation of 2.2.14 is Chapman's first equation. It is used to evaluate the flight path angle. Taking the derivative of this equation with respect to $\bar{u}$ and using eq. 2.2.15 and considering βr (Vinh 1980, 181) as constant the following is derived

$$\bar{u}\frac{d}{d\bar{u}}\left(\frac{d\bar{Z}}{d\bar{u}} - \frac{\bar{Z}}{\bar{u}}\right) + \frac{\cos^2\gamma\,(\bar{u}^2 - \cos^2\gamma)}{\bar{Z}\bar{u}} + \sqrt{\beta r}\,\frac{L}{D}\cos\gamma = 0 \qquad \mathbf{2.2.16}$$

Transforming the above equation (Chapman 1959, 8) to Chapman's second-order nonlinear differential equation by using the second equation in 2.2.14 and using the fact that $\cos\gamma = \sqrt{1 - \sin^2\gamma}$ and noting that

$$\frac{\cos^2\gamma\,(\bar{u}^2 - \cos^2\gamma)}{\bar{Z}\,\bar{u}} = -\frac{(1-\bar{u}^2)\cos^4\gamma}{\bar{Z}\,\bar{u}} + \frac{\bar{u}\cos^2\gamma\sin^2\gamma}{\bar{Z}}$$

$$\sqrt{\beta r}\,\frac{L}{D}\cos\gamma = \sqrt{\beta r}\,\frac{L}{D}\left(\cos^3\gamma + \cos\gamma\sin^2\gamma\right)$$

and substituting them into eq. 2.2.16 yields

$$\bar{u}\frac{d^2\bar{Z}}{d\bar{u}^2} - \left(\frac{d\bar{Z}}{d\bar{u}} - \frac{\bar{Z}}{\bar{u}}\right) - \frac{(1-\bar{u}^2)\cos^4\gamma}{\bar{Z}\,\bar{u}} + \sqrt{\beta r}\,\frac{L}{D}\cos^3\gamma$$
$$+ \frac{\bar{u}\cos^2\gamma\sin^2\gamma}{\bar{Z}} + \sqrt{\beta r}\,\frac{L}{D}\cos\gamma\sin^2\gamma = 0 \qquad \mathbf{2.2.17}$$

Using assumptions (i) and (ii), which is equivalent to neglecting the terms containing $\sin^2\gamma$ (Vinh 1980, 182) yields

$$\bar{u}\frac{d^2\bar{Z}}{d\bar{u}^2} - \left(\frac{d\bar{Z}}{d\bar{u}} - \frac{\bar{Z}}{\bar{u}}\right) = \frac{(1-\bar{u}^2)\cos^4\gamma}{\bar{Z}\,\bar{u}} - \sqrt{\beta r}\,\frac{L}{D}\cos^3\gamma \qquad \mathbf{2.2.18}$$

This equation is the second Chapman equation. The first term on the left hand side represents vertical acceleration, the second represents the vertical component of drag force. The first term on the right hand side represents the gravity minus centrifugal force and the second represents the lift force. This is a nonlinear differential equation that must be integrated numerically. For a nonlifting body, L/D=0, the equation is applicable to large flight path angles (Vinh 1980, 182). This closely resembles the COMET Recovery Vehicle. For further details look at Chapter 3. The equation can also be used for lifting bodies if (L/D)tanγ is small.

Deceleration and aerodynamic heating rate per unit area are crucial for the survivability of a vehicle entering an atmosphere. The deceleration along the flight trajectory is simply dV/dt. The second equation of eqs. 2.2.7 and the definitions of the nondimensional variables yields (Vinh 1980, 184)

$$-\left(\frac{dV}{dt}/g\right) = \frac{\sqrt{\beta r}\,\bar{Z}\bar{u}}{\cos^2\gamma} + \sin\gamma \approx \sqrt{\beta r}\,\bar{Z}\bar{u} \qquad \textbf{2.2.19}$$

Chapman gives plots for $\sqrt{\beta r}\,\bar{Z}\bar{u}$ versus $\bar{u}$ for different types of entry (fig. 2-2-2). The deceleration due to the combined lift and drag forces, as sensed by an accelerometer during entry (Vinh 1980, 184), is

$$\frac{a}{g} = \sqrt{\left(\frac{L}{mg}\right)^2 + \left(\frac{D}{mg}\right)^2} = \frac{\sqrt{\beta r}\,\bar{Z}\bar{u}}{\cos^2\gamma}\sqrt{1 + \left(\frac{L}{D}\right)^2} \qquad \textbf{2.2.20}$$

For entry at small angles, the deceleration due to aerodynamic force is obtained simply by multiplying the vehicle deceleration, given by eq. 2.2.19, by the constant factor $\sqrt{1 + \left(\frac{L}{D}\right)^2}$. The Local density can also be expressed in terms of $\bar{Z}$ and $\bar{u}$

$$\frac{\rho}{\rho_o} = \left(\frac{2m}{SC_D r \rho_0}\right)\frac{\sqrt{\beta r}\,\bar{Z}}{\bar{u}} \qquad \textbf{2.2.21}$$

For a strictly exponential atmosphere, the altitude y is given by

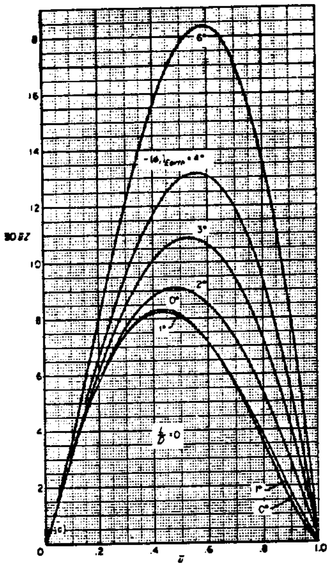

Figure 2-2-2, Values of Z functions for ballistic entry.
(Chapman 1959, 15)

$$\frac{\rho}{\rho_0} = e^{-\beta h} \, , \quad h = \frac{1}{\beta} \ln\left[\left(\frac{SC_D r\rho_0}{2m}\right)\frac{\bar{u}}{\sqrt{\beta r}\,\bar{Z}}\right]$$

Another parameter of interest in this analysis is the dynamic pressure exerted on a vehicle (Vinh 1980, 185),

$$\bar{q}_\infty = \frac{1}{2}\rho V^2 = \left(\frac{mg}{SC_D}\right)\frac{\sqrt{\beta r}\,\bar{Z}\bar{u}}{\cos^2\gamma} \approx \left(\frac{mg}{SC_D}\right)\sqrt{\beta r}\,\bar{Z}\bar{u} \qquad \textbf{2.2.22}$$

Therefore, after assuming a small flight path angle, the dynamic pressure is proportional to the deceleration of the vehicle, eq. 2.2.19. The Reynolds number per unit length is, where μ^* is the atmospheric dynamic viscosity. Eq. 2.2.23 indicates that the Reynolds number per unit length is proportional to $\bar{Z}$.

$$\frac{R_e}{l} = \frac{V\rho}{\mu^*} = \frac{2\sqrt{\beta g}}{\mu^* \cos\gamma}\left(\frac{m}{SC_D}\right)\bar{Z} \qquad \textbf{2.2.23}$$

The heating rate q at any point on a body (Lees 1960, 259) is equal to a fraction of the heating rate at the stagnation point q_s (Vinh 1980, 185) of radius of curvature R_N. The heating rate in hypersonic flow at the stagnation point, q_s can be expressed as

$$q_s = \frac{C}{\sqrt{R_N}}\left(\frac{\rho}{\rho_0}\right)^n\left(\frac{\bar{u}}{\cos\gamma}\right)^m \left(\frac{Btu}{ft^2 \sec}\right) \qquad \textbf{2.2.24}$$

C, n, and m depend on the type of boundary layer flow. For laminar flow, n=1/2 and m=3 corresponds to a gas with viscosity proportional to the square root of temperature (Chapman 1959, 10). C is equal to 17000 Btu $ft^{-3/2}$ sec^{-1} (Chapman 1959, 10).

<u>Application to COMET's Recovery Vehicle</u>

This section will use Chapman's equations to approximate the entry characteristics of the COMET Recovery Vehicle. To determine the characteristics eq. 2.2.18 should be numerically integrated. However, since eq. 2.2.18 is only an approximation it would suffice it to use the tables that have been generated for different nominal entry parameters. Before using the tables $\bar{u}$ *and* $\bar{Z}$ have to be calculated for the nominal values. The nominal values are listed below,

h	=	301,830.438 ft
V	=	24,816.715 ft/sec
γ	=	-3.008 °
S	=	14.74803219 ft^2

R_N = 2.166666667 ft

C_D = 1.51

L/D = 0.0

W = 926 lbs.

Values needed for other calculations are (Brauer 1987, 6D POST V.1 pp. 4-1)

g_0 = 32.174 ft/sec^2

μ = 1.407645794 x 10^{16} ft^3/sec^2 (Earth's gravitational constant, GM_p)

R = 2.08905824 x10^7 ft (Earth's average radius)

ϱ_0 = 0.0027 slug/ft^3 (Boltz February 1963, 7)

β = 1/23500 ft^{-1} (Boltz February 1963, 7)

Hence,

$$\bar{u}_i \approx .9616 \ , \quad \rho_i \approx 7.0 \times 10^{-9} \ \frac{slug}{ft^3}$$
$$\bar{Z}_i \approx 7.8 \times 10^{-8}$$

Reading from the table (Boltz February 1963, 82) for γ_i=-3.0° and for $\bar{u}_i = 1.0$ since that is reasonably close to 0.9616,

$\Delta y/r$ = .013985

$\bar{u}$ = .86

$\sqrt{\beta r}\ \frac{\bar{Z}}{\bar{u}}$ = 8.78

γ = -3.216°

To calculate the maximum heating rate per unit area eq. 2.2.24 would have to be used; however, to use it ρ would have to be calculated by use of eq. 2.2.21. Using $\Delta y/r$ to determine the local radius, r=R+Δy=2.118273719 x 10^7 ft., the local density would be about 1.071 x 10^{-7} slug/ft^3. Using eq. 2.2.22 the dynamic pressure is approximately 365.04 psf, which will be shown in Chapter 3 to be remarkably close to the results obtained from the POST codes.

Substituting the necessary values into eq. 2.2.24, the maximum stagnation heating rate per unit area is calculated to be $q_{s_{max}} \approx 147.0143$ Btu/(ft^2 sec). As will be shown in chapter 3 this is slightly higher than the three degrees-of-freedom calculation. According to the same table (Boltz February 1963, 58) the maximum sensed acceleration is about 10.05 g's. This is also a reasonable estimate as will be shown in Chapter 3. The nondimensional velocity $\bar{u}$ is equal to 0.56. In fact, a first order estimate of the velocity of maximum q_s is about 0.85 for laminar flow (Allen October 1957, 10-11) and the velocity at maximum sensed acceleration is about 0.61 (Allen October 1957, 9). These first order estimates turn out to be sensible estimates for even six degrees-of-freedom analysis. The value for sensed acceleration from the plot (fig. 2-2-2) for a flight path angle of -3.0° is about 10.8 g's.

This is a higher value since it assumes that the flight path angle is insignificant in the calculation (eq. 2.2.20).

2.3 Dynamic Motion Along the Trajectory

Newton's second law is $\vec{F} = m\frac{d^2\vec{r}}{dt^2}$, where $\vec{F}$ is the total external force acting on the rigid body and $\frac{d\vec{r}}{dt}$ is the absolute velocity of the center of mass. Expressing these vectors in terms of their instantaneous body-axis components (Greenwood 1988, 393), gives

$$\vec{F} = F_x \vec{i} + F_y \vec{j} + F_z \vec{k}$$
$$and$$
$$\frac{d\vec{r}}{dt} = u \vec{i} + v \vec{j} + w \vec{k}$$

where, $\vec{i}, \vec{j}, \vec{k}$ are the unit vectors which are fixed in the body. In order to find the absolute acceleration $\frac{d^2\vec{r}}{dt^2}$, eq. 2.1.5, would have to be used. The body angular rates are given by $\vec{\omega} \equiv p\ \vec{i} + q\ \vec{j} + r\ \vec{k}$. Hence, the resulting force equations of motion are

$$\begin{aligned} F_x &= m(\dot{u} + wq - vr) \\ F_y &= m(\dot{v} + ur - wp) \\ F_z &= m(\dot{w} + vp - uq) \end{aligned} \qquad \textbf{2.3.1}$$

The force elements can be any force acting on the body; however, here, concern is only with aerodynamic and gravitational forces. Therefore, one arrives at (Martin 1966, 51)

$$\begin{aligned} \frac{F_x}{m} &= \dot{u} + qw - rv = \frac{X}{m} - g_x = \frac{F_{x_{aero}}}{m} + \frac{F_{x_{grav}}}{m} \\ \frac{F_y}{m} &= \dot{v} + ru - pw = \frac{Y}{m} + g_y = \frac{F_{y_{aero}}}{m} + \frac{F_{y_{grav}}}{m} \\ \frac{F_z}{m} &= \dot{w} + pv - qu = \frac{Z}{m} + g_z = \frac{F_{z_{aero}}}{m} + \frac{F_{z_{grav}}}{m} \end{aligned} \qquad \textbf{2.3.2}$$

g is the local gravitational acceleration. X, Y and Z are the axial, side and vertical aerodynamical body force elements, respectively and are given by (Martin 1966, 52)

$$\begin{aligned} X &\approx -q_\infty S_{ref} C_A \\ Y &\approx q_\infty S_{ref} \left(-\beta C_{y_\beta}\right) \\ Z &\approx -q_\infty S_{ref} \left(\alpha C_{N_\alpha}\right) \end{aligned} \qquad \textbf{2.3.3}$$

where q_∞ is the dynamic pressure and where $-C_A$, C_Y, $-C_N$, are, the coefficients of forces in the longitudinal and transverse directions, respectively. α and β are the angles given by $\alpha=\tan^{-1}(w/u)$, and $\beta=\sin^{-1}(v/V_\infty)$ (fig. 2-3-1). They are defined as the angle of attack and the sideslip angle, respectively. V_∞ is the free stream flight speed given by $\sqrt{u^2 + v^2 + w^2}$. Applying the general moment equations in vector form (Greenwood 1988, 392)

$$[M] = [I]\cdot\frac{d(\vec{\omega})}{dt} + \vec{\omega}\times[I]\cdot\vec{\omega} \qquad 2.3.4$$

where [M] is the moment vector about the x, y and z body axes (Nelson 1989, 85), respectively and [I] is the mass moment of inertia dyadic tensor; each defined as

$$[M] = \begin{bmatrix} L \\ M \\ N \end{bmatrix}, \quad [I] = \begin{bmatrix} I_{xx} & -I_{xy} & -I_{xz} \\ -I_{xy} & I_{yy} & -I_{yz} \\ -I_{xz} & -I_{yz} & I_{zz} \end{bmatrix}$$

The aerodynamic moments are given by (Martin 1966, 52)

$$\begin{aligned} L &\approx q_\infty S_{ref} D_{ref} \left(\frac{pD_{ref}}{V_\infty} C_{l_p}\right) \\ M &\approx q_\infty S_{ref} D_{ref} \left(\alpha C_{m_\alpha} + \frac{qD_{ref}}{V_\infty}\left(C_{m_\alpha} + C_{m_q}\right)\right) \\ N &\approx q_\infty S_{ref} D_{ref} \left(-\beta C_{n_\beta} + \frac{rD_{ref}}{V_\infty}\left(C_{n_\beta} + C_{n_r}\right)\right) \end{aligned} \qquad 2.3.5$$

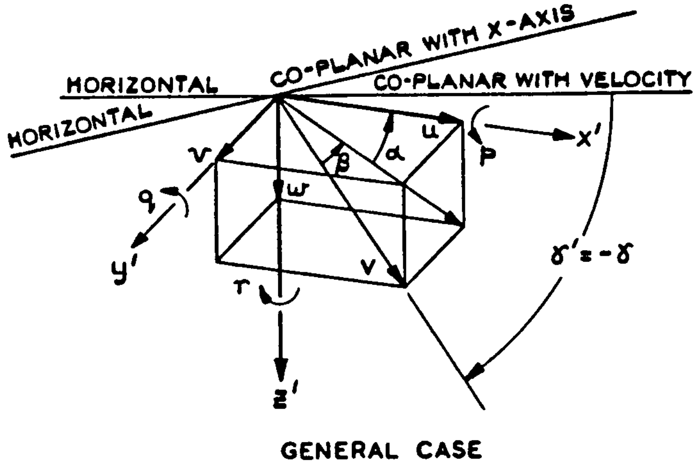

Figure 2-3-1, Reentry dynamic motion diagram
(Martin 1966, 51)

To gain a preliminary insight to oscillatory motion during atmospheric entry, some simplifications will be made. Considering only planar motion (yawing rate, $r \equiv 0$), nonrolling (rolling rate, $p \equiv 0$), damped, small angle of attack ($\alpha \approx w/u$), axially symmetric mass distribution of the vehicle's body ($I_{xy}=I_{yz}=I_{xz}=0$, and $I_{yy}=I_{zz}$) motion will display the dynamic aspects of entry body motion (Martin 1966, 59). Also the elements of gravity will be ignored, since their contribution is insignificant.

With the above assumptions the first equation from eqs. 2.3.2 has been uncoupled from the dynamic analysis, the second has been nulled and the third is retained. The assumption made for α produces $\dot{\alpha} \approx \dot{w}/u$, $u \approx V_\infty$ and $C_{N_\alpha} \approx C_{L_\alpha}$, then the equations of motion may be written as

$$V_\infty\left(\dot{\alpha} - q\right) = \frac{Z}{m} = -q_\infty S_{ref}\left(\alpha C_{L_\alpha}\right) \qquad \textbf{2.3.6}$$

The only element that remains from eq. 2.3.3 is M

$$I_{yy}\dot{q} = M = q_\infty S_{ref} D_{ref}\left(\alpha C_{m_\alpha} + \frac{qD_{ref}}{V_\infty}\left(C_{m_q} + C_{m_{\dot{\alpha}}}\right)\right) \qquad \textbf{2.3.7}$$

The first and third elements become trivial since p=r=0, and because moments of inertia due to asymmetries are zero. Solving for q in eq. 2.3.6 and then differentiating it and then substituting into eq. 2.3.7 yields (Tobak July 1958, 7),

$$\ddot{\alpha} + f_1(t)\dot{\alpha} + f_2(t)\alpha = 0 \qquad \textbf{2.3.8}$$

where,

$$\begin{aligned} f_1(t) &= \frac{q_\infty}{mV_\infty} S_{ref}\left(C_{L_\alpha} - \left(C_{m_q} + C_{m_{\dot{\alpha}}}\right)\frac{D_{ref}^2}{I_{yy}}\right) \\ f_2(t) &= \frac{C_{L_\alpha} S_{ref}}{2m}\,\frac{d(\rho_\infty V_\infty)}{dt} - \frac{C_{m_q} C_{L_\alpha} S_{ref}^2 D_{ref}^2}{I_{yy}m}\left(\frac{\rho_\infty V_\infty}{2}\right)^2 - \frac{C_{m_\alpha} S_{ref} D_{ref} q_\infty}{2I_{yy}} \end{aligned} \qquad \textbf{2.3.9}$$

and where derivatives of coefficients with respect to $\dot{\alpha}$ are considered to be negligible for hypersonic Mach numbers (Martin 1966, 60). Eq. 2.3.8 represents an ordinary differential equation with time variant coefficients. By transforming the independent variable from time to altitude, y, (Allen October 1957, 4-6) maximum frequency and maximum deceleration occur at (Allen October 1957, 9) the altitude

$$y = \frac{1}{\beta}\ln(k_o) \qquad \textbf{2.3.10}$$

and a velocity of

$$V_{(max\ drag)} = e^{-1/2}\ V_{entry} \approx 0.61\ V_{entry} \qquad \textbf{2.3.11}$$

The maximum frequency is

$$\omega_{max} = \sqrt{\frac{k_2}{k_0}}\left(\frac{\beta V_{entry} e^{-1/2}\ \sin(\gamma_{entry})}{2\pi}\right) \qquad \textbf{2.3.12}$$

$k_0 = (C_D\rho_0 S_{ref})/(\beta m \sin(\gamma_{entry}))$ and $k_2 = \ = \frac{\rho_0\ S_{ref}}{2\beta^2 m\ \sin^2\gamma_{entry}}\left(-\frac{C_{m_\alpha} D_{ref}\ m}{I_{yy}} + C_{L_\alpha}\beta\ \sin\gamma_{entry}\right)$,

and the corresponding amplitude is

$$\left(\frac{\alpha}{\alpha_{entry}}\right) = \frac{e^{\frac{k_1}{k_0}}}{\sqrt{\pi\sqrt{\frac{k_2}{k_0}}}} \qquad \textbf{2.3.13}$$

where $k_1 = \frac{\rho_0\ S_{ref}}{4\beta m\ \sin\gamma_{entry}}\left(C_D - C_{L_\alpha} + (C_{m_q} + C_{m_{\dot\alpha}})\frac{m}{I_{yy}}D_{ref}\right)$. The angle of attack is given by

$$\frac{\alpha}{\alpha_{entry}} = \frac{e^{k_1 e^{-\beta y}}\cos(\frac{\pi}{4} - 2\sqrt{k_2}\ e^{-\frac{\beta y}{2}})}{\sqrt{\pi\ \sqrt{k_2}\ e^{-\frac{\beta y}{2}}}} \qquad \textbf{2.3.14}$$

and the envelope value is

$$\left(\frac{\alpha}{\alpha_{entry}}\right)_{env} = e^{k_1 e^{-\beta y}} \Big/ \sqrt{\pi \sqrt{k_2}\, e^{-\frac{\beta y}{2}}} \qquad \textbf{2.3.15}$$

The frequency of oscillation is

$$\omega = \frac{\beta V_{entry} \sqrt{k_2}\, \sin\gamma_{entry}}{2\pi} e^{-\frac{k_0}{2} e^{-\beta y}} e^{-\frac{\beta y}{2}} \qquad \textbf{2.3.16}$$

<u>Application to COMET's Recovery Vehicle:</u>

In addition to the nominal values given in section 2.2 the following parameters for the RV will be used to evaluate the equations above

D_{ref} = 4.333 ft

C_{m_α} = -.12 rad^{-1}

C_{L_α} = -1.12 rad^{-1}

$C_{m_q} + C_{m_{\dot\alpha}}$ ≡ 0.0

I_{yy} = 48.14 slug-ft^2

Therefore,

k_0 = 938.2

k_1 = 408.85

k_2 = 4.337×10^7

$V_{(max\ drag)}$ = 15,138.2 ft/sec

ω_{max} = 1.15 rad/sec

$\left(\frac{\alpha}{\alpha_{entry}}\right)_{min\ amp}$ = .0595

$y_{max\ freq}$ = 160,833.134 ft

The variation of α/α_{entry} and its envelope with altitude is shown in fig. 2-3-2. The frequency oscillations is in fig. 2-3-3. As will be shown in Chapter 3 these results closely resemble the six degrees-of-freedom analysis. In fact, the COMET RV is a typical blunt nosed vehicle, such as Mercury or Gemini capsules, has a negative C_{L_α} and a very large C_D therefore, k_1, known as the dynamic stability coefficient, is usually positive which causes divergence at altitude y given above. Nevertheless, this is a very promising method for this preliminary analysis. However, more accurate investigations involving large atmospheric entry angles of attack will require a six degrees-of-freedom analysis with nonlinear aerodynamics.

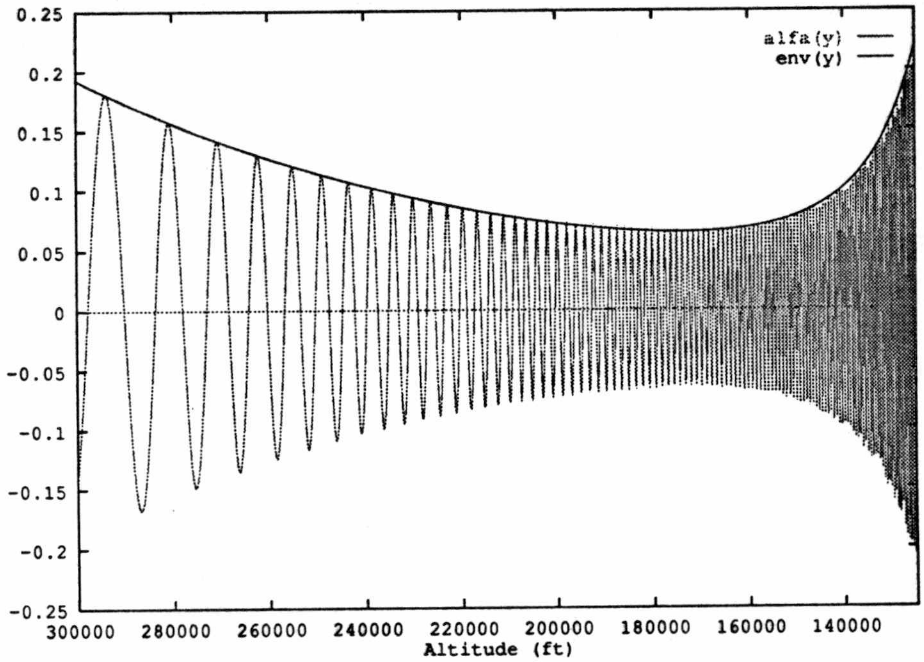

Figure 2-3-2, Angle of attack and its envelope vs. Altitude for the RV

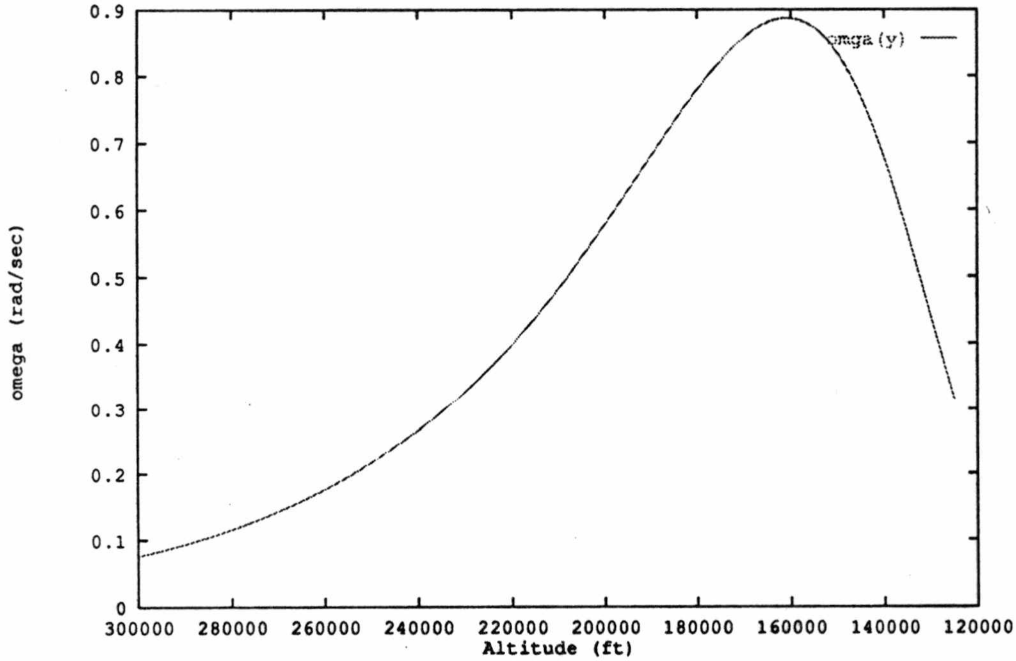

Figure 2-3-3, Frequency Oscillations vs. Altitude for the COMET RV

CHAPTER 3: DYNAMICAL ANALYSIS OF COMET'S RV

3.1 Objective

This chapter covers the entry characteristics of the recovery vehicle. The chapter is divided into several sections. Section 3.2 provides the nominal data used for the entire analysis. Section 3.3 provides the three degrees-of-freedom results and section 3.4 provides the six degrees-of-freedom results.

The simulation is initiated at the time that the recovery system has finished its retro motor burn and the vehicle is despun from 75 rpm to about 5 rpm. The nominal data has been provided by Space Industries Inc. (SII), Webster, TX., the manufacturer of the COMET Recovery System. The desired landing point is the Great Salt Lake Desert.

3.2 Nominal data used for analysis

Vehicle's Altitude, Velocity and Coordinates

Earth-Relative Local Horizontal Data			or	Orbital Elements Data
time	=	0.0 sec.		a = 21573603.7172 ft
h	=	301,830.438 ft		e = .05302982302
V_R	=	24,816.715 ft/sec		i = 40.3998437°
A_{ZR}	=	84.532°		Ω = 153.09365239°
ϕ_g	=	40.306°		ω_p = 157.58340925°
θ_I	=	-124.975°		θ = -72.745091096°

Reference Areas and Lengths

S_{ref}	=	14.748 32190 ft^2
D_{ref}	=	4.3333333333 ft
R_N	=	2.1666666667 ft

Mass Properties

I_{xx}	=	61.88 slug-ft^2

I_{yy} = 48.14 slug-ft^2

I_{zz} = 48.14 slug-ft^2

I_{xy} = 0.0 slug-ft^2

I_{xz} = 0.0 slug-ft^2

I_{yz} = 0.0 slug-ft^2

x_{cg}/D_{ref}= .1885

y_{cg}/D_{ref}= 0.0

z_{cg}/D_{ref}= 0.0

Vehicle's Orientation

γ_R = -3.008°

α = -62.651°

β = 0.0°

σ = 0.0°

ψ_R = 84.532°

θ_R = -65.659°

ϕ_R = 0.0°

Yaw, Pitch and Roll rates

ω_z (r) = 0.0 °/sec

ω_y (q) = 0.0 °/sec

ω_x (p) = 30 °/sec (5 rpm) (± 2.5 rpm for this analysis)

Yaw, Pitch and Roll Accelerations

$$[\dot{\omega}_x \ \ \dot{\omega}_y \ \ \dot{\omega}_z]^T = [\dot{p} \ \ \dot{q} \ \ \dot{r}]^T = [I]^{-1}\left[\vec{M} - [\dot{I}]\vec{\omega} - \vec{\omega}\times[I]\vec{\omega}\right]$$

and where $\vec{M} = [M_x \ \ M_y \ \ M_z]^T = [L \ \ M \ \ N]^T$

and [I] is

$$\begin{bmatrix} I_{xx} & -I_{xy} & -I_{xz} \\ -I_{xy} & I_{yy} & -I_{yz} \\ -I_{xz} & -I_{yz} & I_{zz} \end{bmatrix}$$

and $[\dot{I}]$ is the time variant of [I]. In our case we get

$$\begin{bmatrix} \dot{p} \\ \dot{q} \\ \dot{r} \end{bmatrix} = \begin{bmatrix} 0 \\ \dfrac{q_{\infty} S_{ref} d_{ref} C_m(\alpha)}{I_{yy}} \\ 0 \end{bmatrix} = \begin{bmatrix} 0 \\ 0.2328\ rad/\sec^2 \\ 0 \end{bmatrix} \triangleq \begin{bmatrix} 0 \\ 13.339\ ^\circ/\sec^2 \\ 0 \end{bmatrix}$$

Aerodynamic Data

The COMET Recovery Vehicle (RV) is a blunt-nosed capsule which has attributes similar to the Mercury capsule (fig. 3-2-1). This shape greatly influences the aerodynamic coefficients. The coefficient that is greatly affected is the drag coefficient (fig. 3-2-2), C_D. The maximum drag is experienced at zero angle of attack, α, which has a value of 1.5786 (SII). At zero angle of attack the normal force coefficient, C_N, is zero since the body is considered to be axisymmertic (fig. 3-2-3). This vehicle has a very stable static moment coefficient, C_m, i.e. an opposing moment at the equilibrium point. Since the vehicle is essentially an axisymmetric body the aerodynamic coefficients would be the same in magnitude for the transverse axes. Therefore, the yawing moment coefficient (fig. 3-2-4), C_n, has the same magnitude as C_m but the opposite sign. The side force, C_Y, also has the same magnitude as the normal force coefficient, C_N, but the opposite sign. This occurs since a positive side-slip angle, β, is defined positive with the nose of the vehicle to the left of the velocity vector.

The RV as all blunt-nosed vehicles has a negative lift curve slope between ± 20 degrees. In other words, at a positive angle of attack, nose up, the RV has negative lift.

Skirt height chosen by evaluating area moments about CG

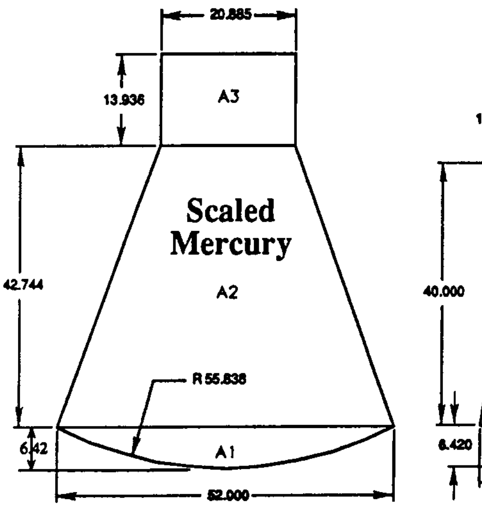

Figure 3-2-1, Comparison of Mercury to the COMET capsule (units are in inches) (SII)

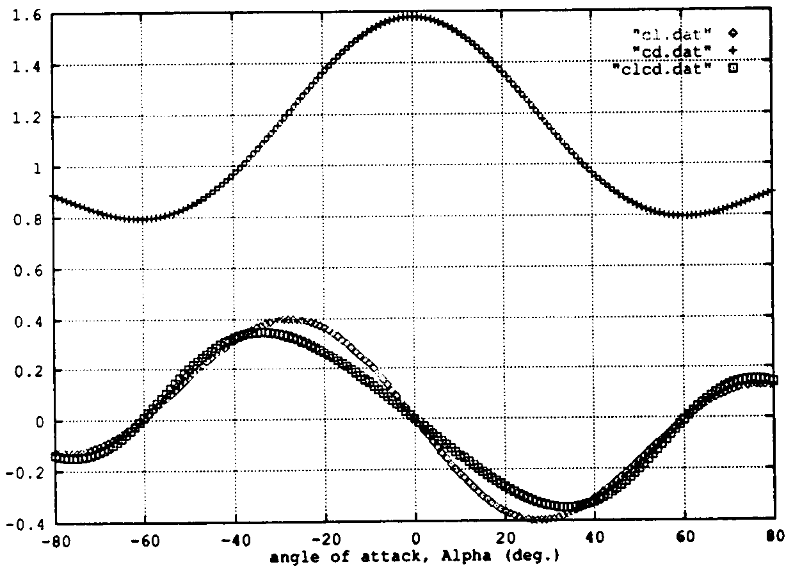

Figure 3-2-2, C_L, C_D and L/D vs. α of the RV

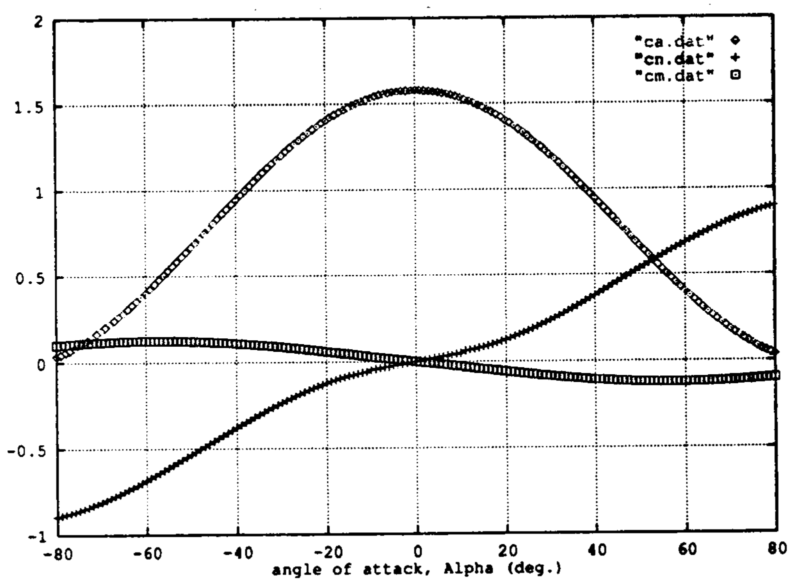

Figure 3-2-3, C_A, C_N and C_m vs. α of the RV

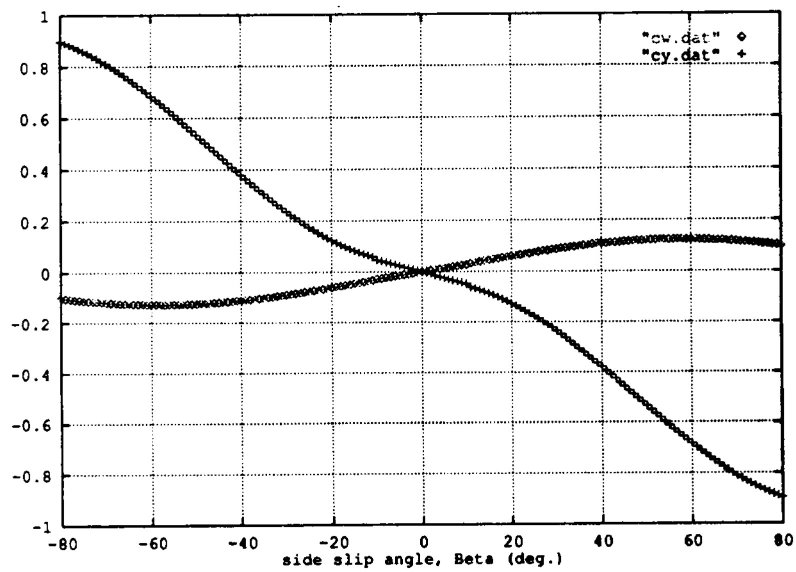

Figure 3-2-4, C_n, and C_Y vs. β of the RV

This occurs due to the fact that C_D is significantly larger than C_N.

The minimum C_D, encountered by the RV, is about .8 at α equal to 60°. The drag coefficient remains above 1.4 between ±20°. The maximum C_L is .4 which occurs at about 25° and the maximum L/D is about .3 which occurs at about 35°. The dynamic coefficients (fig. 3-2-5), C_{m_q} and C_{n_r} , are stabilizing until about ±60°, where they become positive. All the coefficients have been calculated by SII using hypersonic Newtonian estimates. They are more accurate from Mach 4 and higher. All the data points may be found in Appendix D.

3.3 Three degrees-of-freedom motion

The three degrees-of-freedom analysis will deal with the translational equations. Therefore, only a point mass is considered here. The mass moments of inertia and the angles of attack are irrelevant in the three degrees-of-freedom. The other nominal conditions used are in section 3.2. However, the drag coefficient, C_D, for this section has been assumed to be 1.51 (SII).

The vehicle maintains a virtually constant velocity to an altitude of 270,000 ft (fig. 3-3-1)and then rapidly decelerates as the dynamic pressure increases from 1.43 psf to a maximum of about 390 psf (fig. 3-3-2). This is the point in the trajectory that the maximum sensed deceleration is felt, which is about 9.29 g's. The velocity at that point is about 12,000 ft/sec. Nearly a 50% reduction from the nominal velocity. This dramatic point of the trajectory occurs at an altitude of about 120,000 ft. The flight path angle at that altitude is about -5.52°. After the maximum dynamic pressure the vehicle rapidly loses it velocity and the flight path angle approaches -90°. The capsule appears to reach a terminal velocity of about 200 ft/sec and a terminal sensed g's of about 1.02.

In section 2.2 a preliminary estimate of the above values was made. Therefore, a comparison will be made. The maximum sensed deceleration arrived at by use of Chapman's second equation (eq. 2.2.18) is about 10.05 g's, which is an 8.2% difference

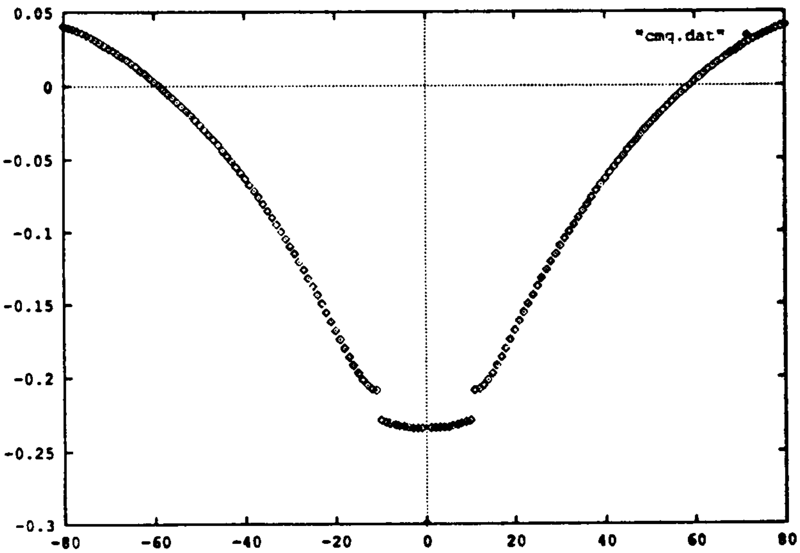

Figure 3-2-5, C_{mq} vs. α (or β, C_{n_r} is equal to - C_{m_q})

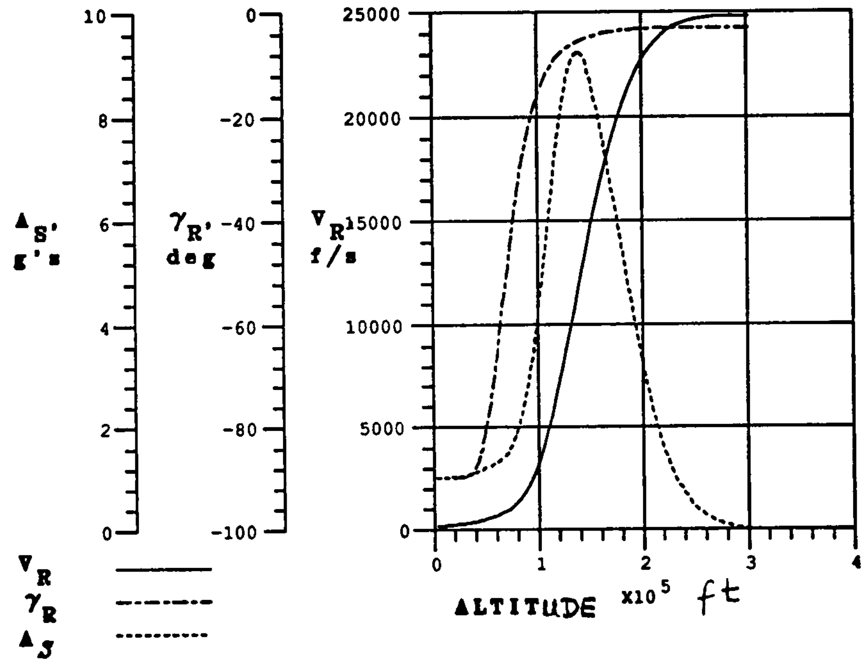

Figure 3-3-1, Sensed g's, Flight path angle & Velocity vs. Altitude (3D).

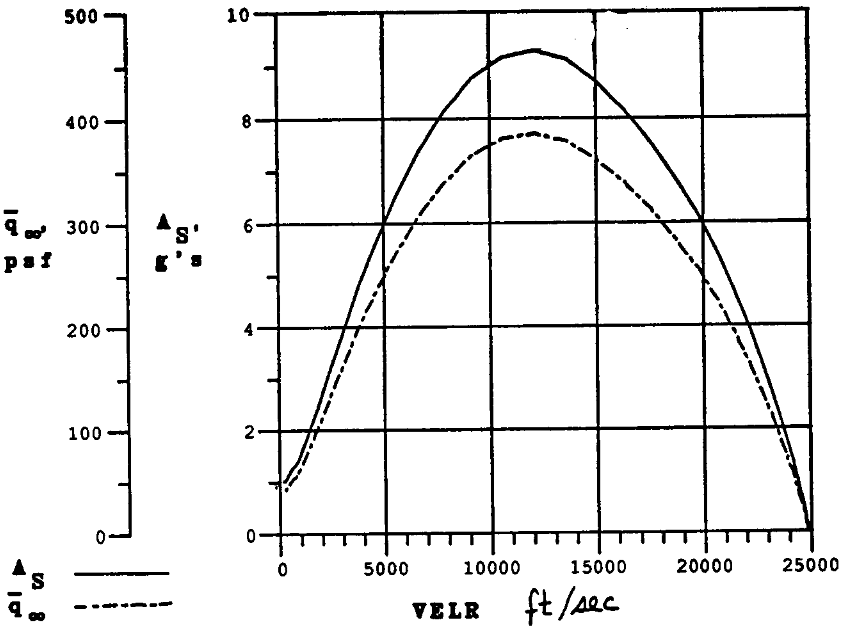

Figure 3-3-2, Dynamic pressure, & Sensed g's vs. Velocity (3D).

from 9.29 g's. A very reasonable estimate for one differential equation. The local flight path angle estimated by Chapman's equation is -4.51°, which is an 18.3% difference.

However, the extremum of the heating rate ensues at an earlier point of the trajectory. If the vehicle cannot withstand the heating rate, the sensed deceleration is irrelevant. In other words, the payload may burn first. The nominal heating rate, $\dot{Q}$, is about 14.43 Btu/(ft^2 sec), and rapidly increases to 123.36 (fig. 3-3-3). This occurs at an altitude of about 188,000 ft. According to section 2.2 the heating rate expected is about 147.014, a 19.2% difference. This is partially due to the fact that Chapman used a different value for C (eq. 2.2.24) in his equation. 3D POST uses a value of 17600 Btu ft$^{-3/2}$ sec^{-1} while Chapman used 17000. The altitude calculated by Chapman's method is about 211,800 ft, a 12.6% discrepancy. The total heat, Q, begins at zero and rapidly approaches an asymptote of about 10418.56 Btu/ft^2. The asymptote begins at an altitude of about 100,000 ft, where the local velocity is about 3,000 ft/sec and the local flight path

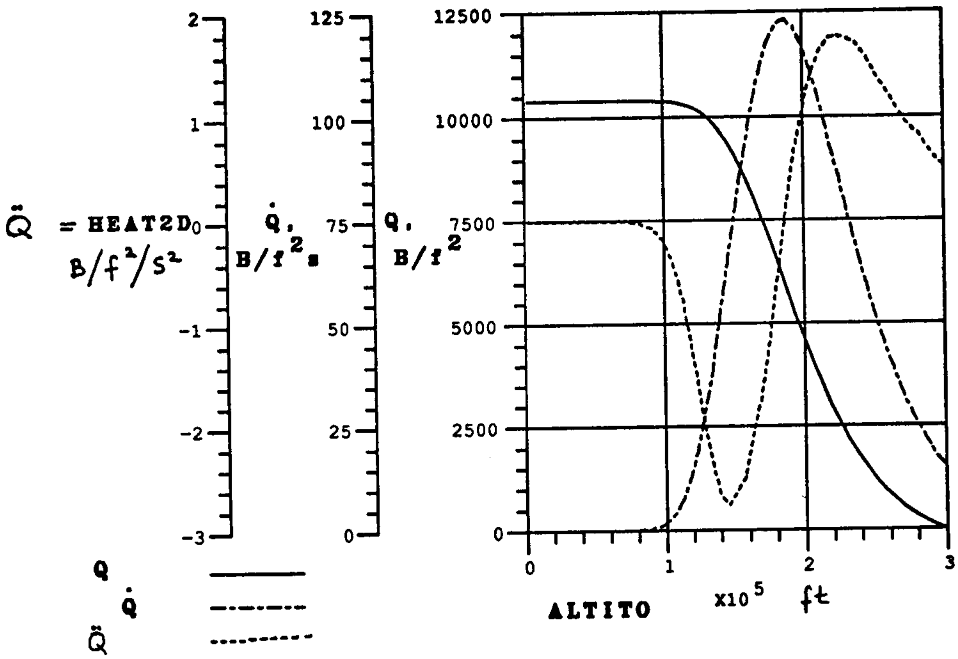

Figure 3-3-3, Total heat, Heating rate, & Heating rate flux vs. Altitude (3D).

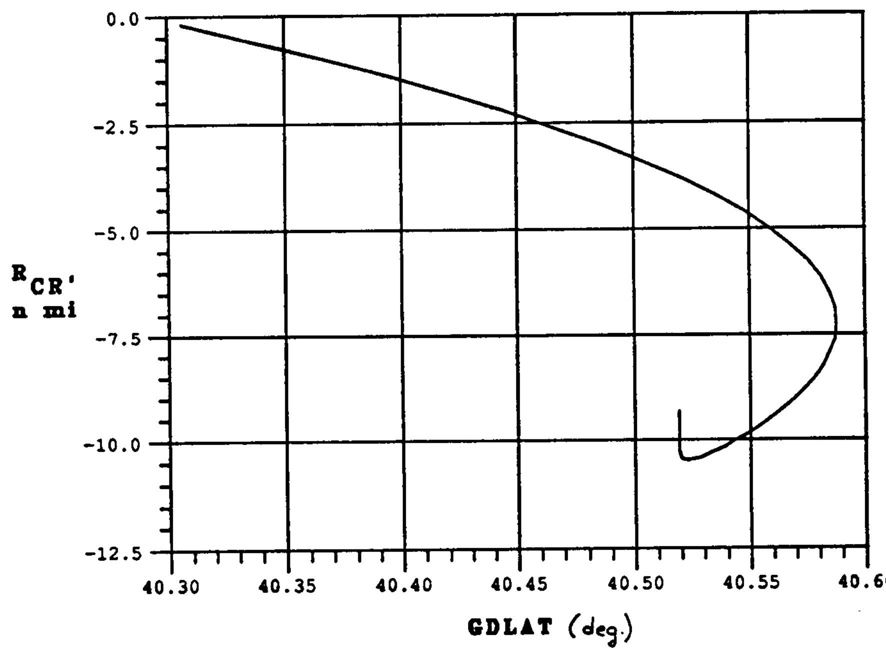

Figure 3-3-4, Crossrange vs. Geodetic Latitude (3D).

angle is about -17°. The vehicle nominally has a -.19 nautical mile crossrange. This tends to increase to a maximum of -10.45 nautical miles (fig. 3-3-4). However, it finally approaches -9.3 nautical miles before touch down. The final earth coordinates of the vehicle (fig. 3-3-5) are 113.59°W, 40.519°N (40.33°N Geocentric) at an altitude of about 3280 ft, which lies in the heart of the Great Salt Lake Desert, Utah.

3.4 Six degrees-of-freedom motion

$$\alpha_{nominal} = -62.651°,\ I_{yy} = I_{zz}$$

The nominal angle of attack, α, is -62.651° (fig. 3-4-1) and the assumption that the two transverse moments of inertia are equal is made. Later the two will be perturbed. This section assumes that the side-slip angle, β, is zero at time zero. The pitching rate and the yawing rate are zero. For these assumptions there are three sections with varying roll rates, p. Comparisons will be made of the effect of spin rates on the dynamical behavior of the vehicle. The simulation of the vehicle "entering" the atmosphere begins at 40.306°N, 124.975°W, , about 200 miles north west of San Francisco. The anticipated touch down location is 40.52°N, 113.6°W, in the Great Salt Lake Desert of Utah (fig. 3-4-2).

p=Rolling rate=2.5 rpm

At this roll rate the maximum total sensed g's encountered is about 9.75 (fig. 3-4-3). This occurs at about 130 sec. into the flight. However, the deceleration oscillates within an envelope. The largest oscillations within this envelope occur between 120 and 135 seconds into the flight. They remain at 9 g's or above for approximately 15 seconds. The Maximum deceleration corresponds to a maximum dynamic pressure, which is about 390 psf. The largest contributor to the deceleration is the axial force (fig. 3-4-4), $A_{x\ body}$, exerted upon the vehicle. This value also oscillates within an envelope, and its maximum value is also about 9.75 g's. The side acceleration has an interesting portrait (fig. 3-4-5).

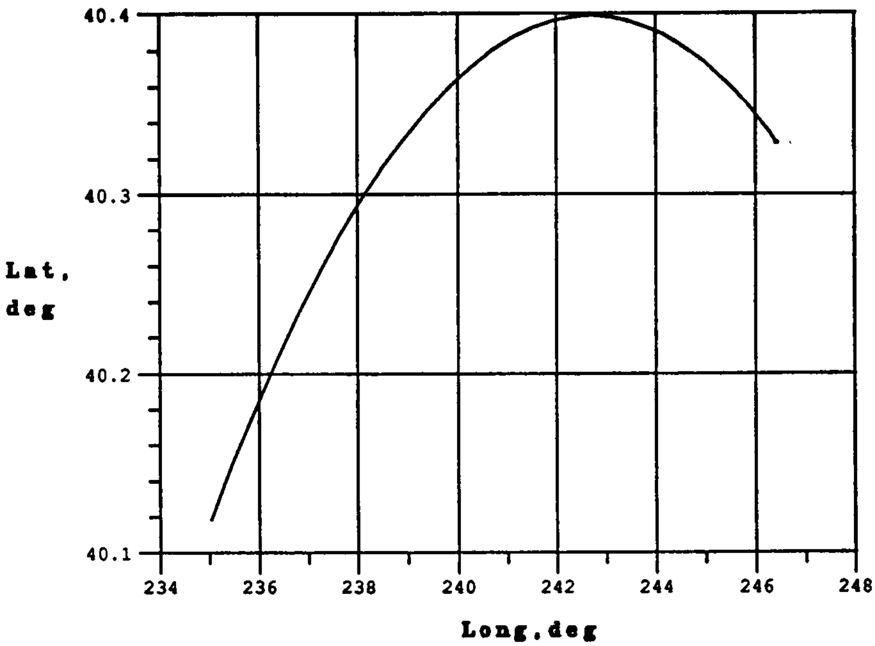

Figure 3-3-5, Geodetic Latitude vs. Longitude of vehicle (3D).

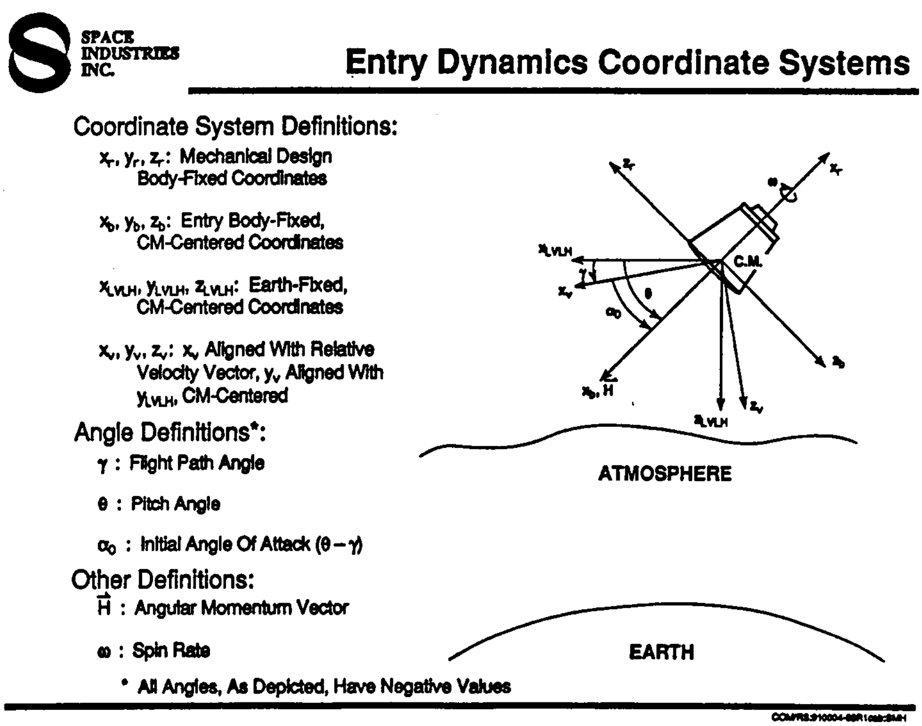

Figure 3-4-1, Orientation of RV as it "enters" atmosphere.
(SII)

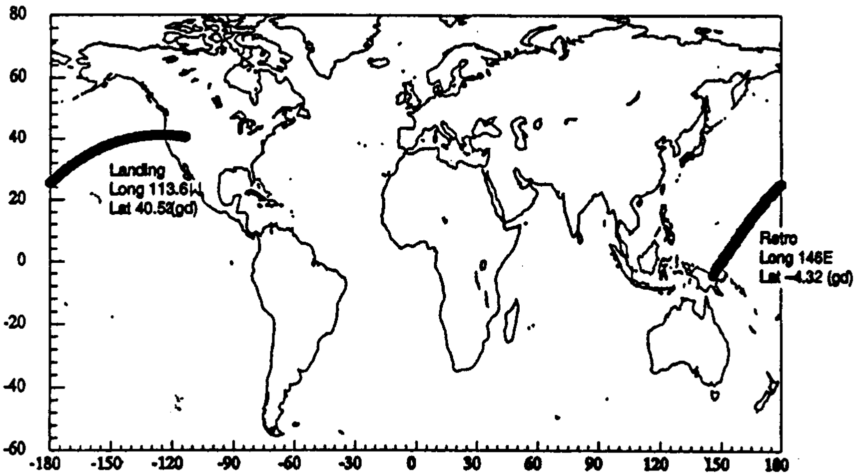

Figure 3-4-2, COMET's RV ground trace.
(CSTAR)

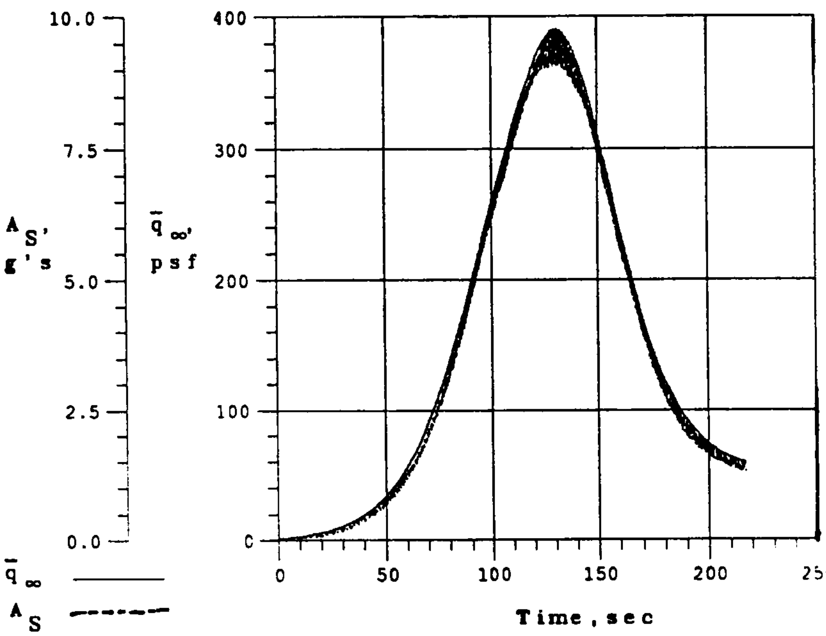

Figure 3-4-3, Sensed acceleration & dynamic pressure vs. Time (2.5 rpm).

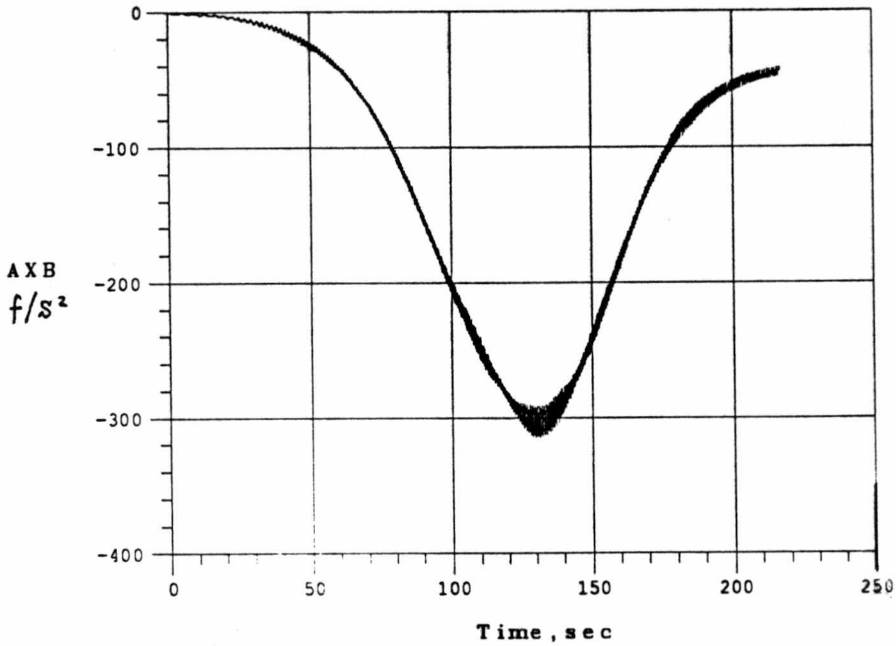

Figure 3-4-4, Body axial acceleration vs. Time (2.5 rpm).

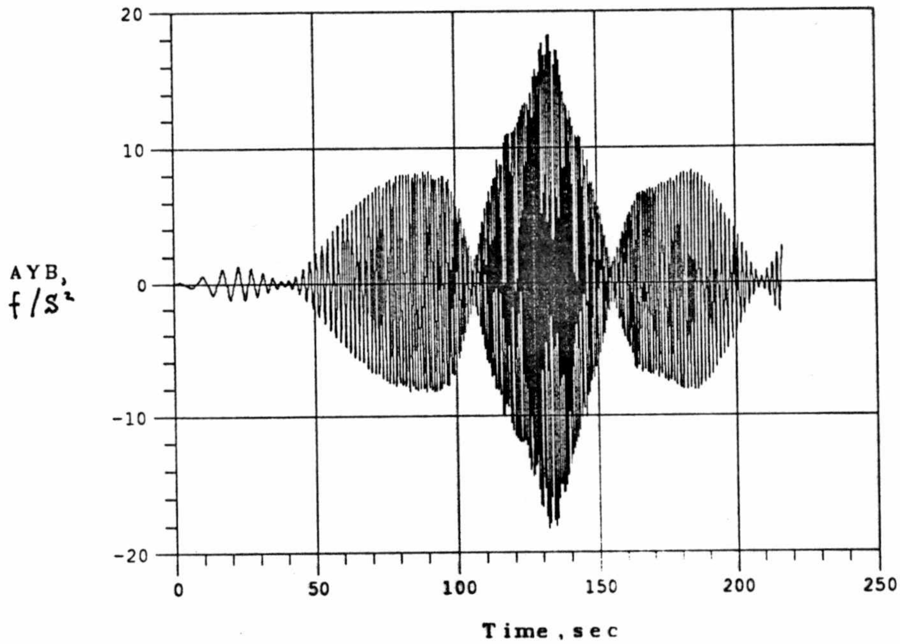

Figure 3-4-5, Sensed side acceleration vs. Time (2.5 rpm).

Nominally it is zero and then proceeds to oscillate until it reaches the first maximum of 0.047 g's at about 20 seconds into the flight. However, convergence begins and the first minimum of virtually zero g's is encountered at about 38 seconds. Then divergence restarts until 0.249 g's is sensed. This ensues at 75 seconds. Then again there is steep convergence in 35 seconds to a second minimum, 0.062 g's. The Aerodynamic forces are becoming significant at this point since the dynamic pressure is in the order of 250 psf. Therefore, the sensed side acceleration envelope diverges to a maximum of .559 g's and then quickly converges to another minimum of 0.062 g's at 155 seconds. However, the envelope diverges again to another maximum of 0.265 g's. This behavior is caused by yawing angular acceleration, $\dot{r}$, which can be seen in fig. 3-4-6. They indicate a very close correlation between the side force and the yawing acceleration.

The force in z direction of the body axes also has a very interesting portrait (fig. 3-4-7). However, the envelope tends to be the reverse of the side force curve. That is, where the side force is a maximum the vertical force, A_z, is a minimum. Therefore, at about 110 seconds into the flight the vertical force is 0.404 g's while A_y is 0.062 g's. A_z quickly reaches a minimum at 130 seconds into the flight. This time period is the point that maximum dynamic pressure is encountered by the vehicle. Since the dynamic pressure is significant the stabilizing moment in pitch, C_m, becomes an extremely powerful restoring moment. Thus the minimization of A_z. In addition, the high correlation between the vertical acceleration and the pitching angular acceleration is clearly evident (fig. 3-4-8).

The pitching rate, q, and the yawing rate, r, both exhibit behaviors similar to their time variants (fig. 3-4-9 & fig. 3-4-10).

From Euler's equations of motion (Greenwood 1988, 392), it can be seen that there is coupling between angular rotations. In other words, a vehicle cannot change its side angle without affecting its angle of attack, and vice versa. This behavior will be

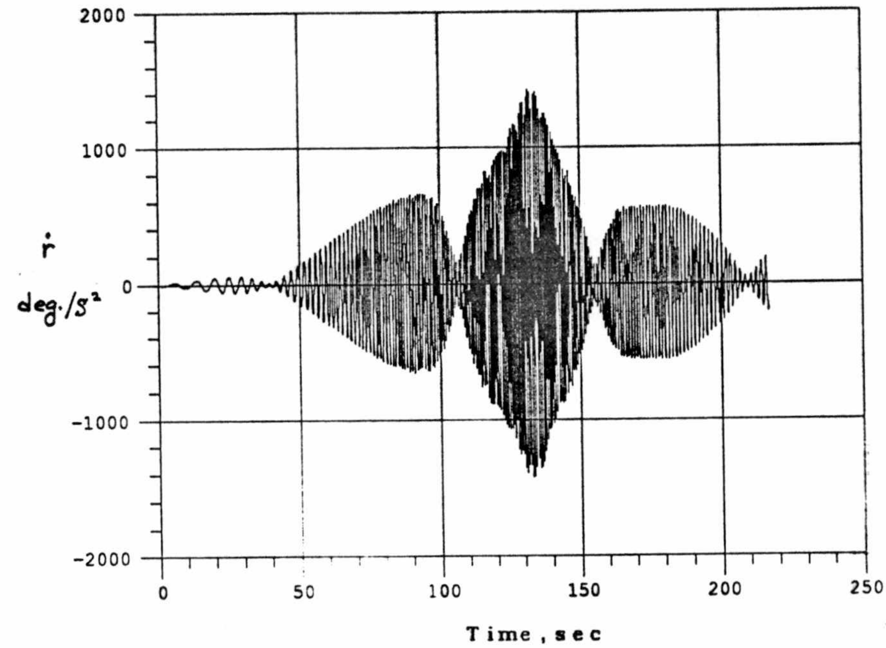

Figure 3-4-6, Yawing angular acceleration vs. Time (2.5 rpm).

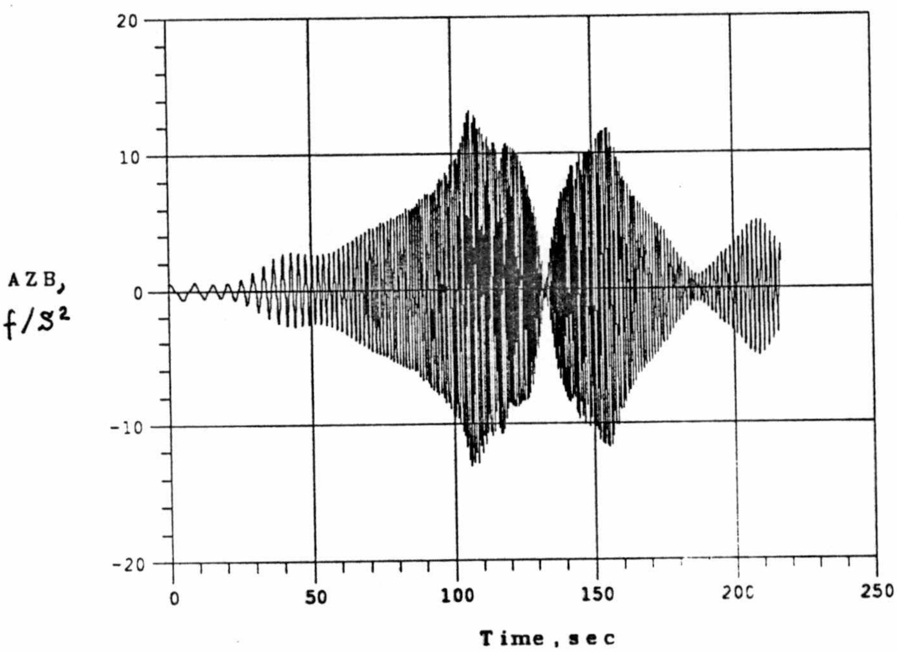

Figure 3-4-7, Vertical sensed body force vs. Time (2.5 rpm).

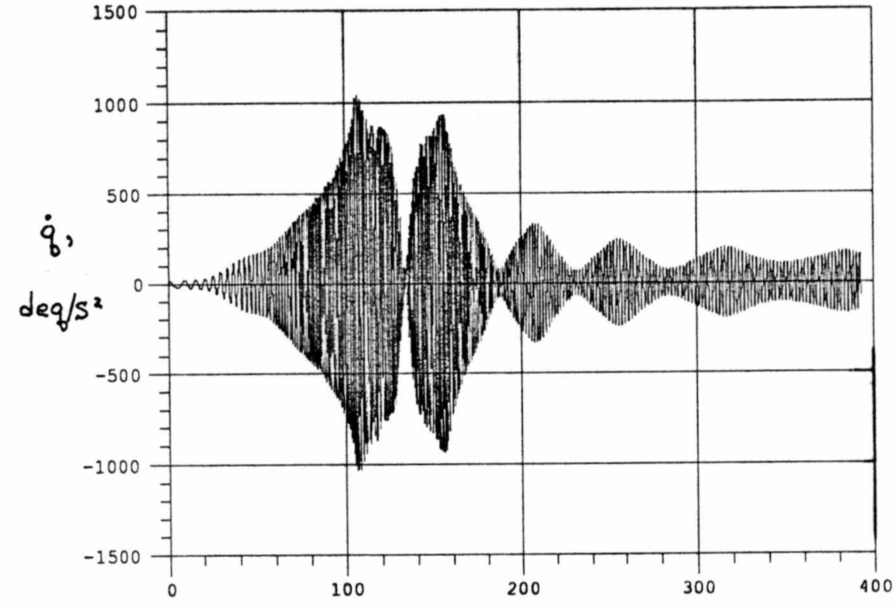

Figure 3-4-8, Pitching angular acceleration vs. Time (2.5 rpm).

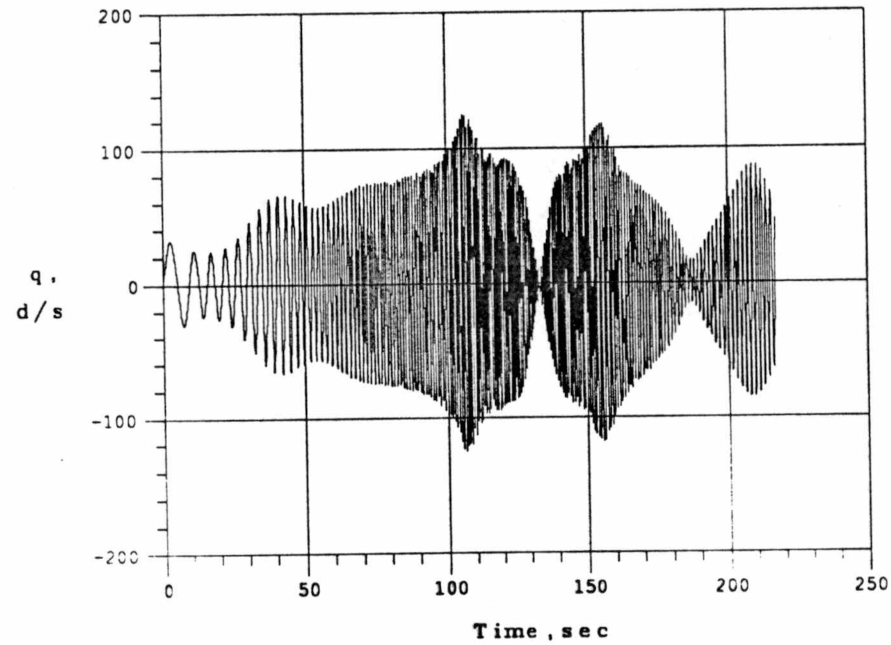

Figure 3-4-9, Pitching rate vs. Time (2.5 rpm).

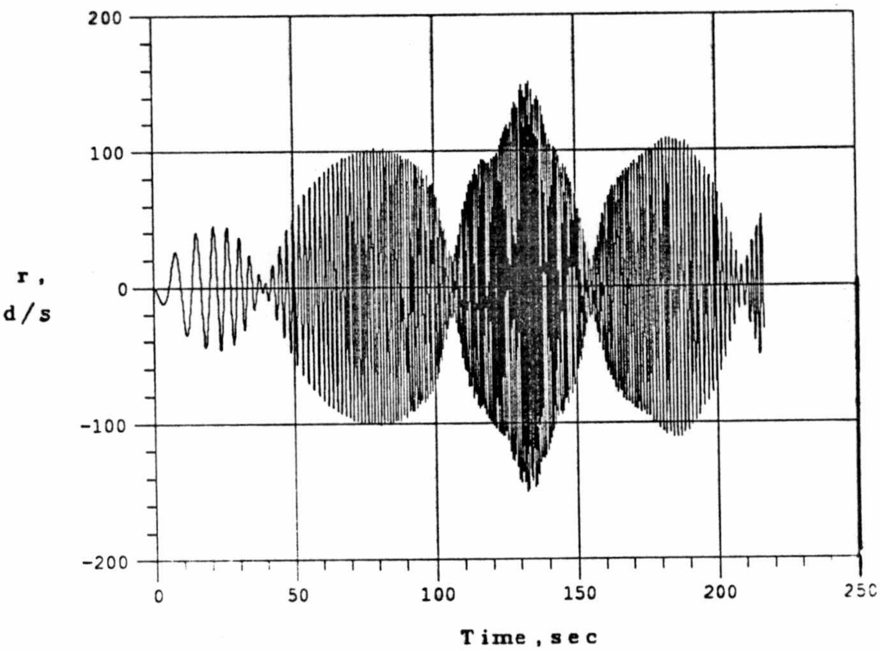

Figure 3-4-10, Yawing rate vs. Time (2.5 rpm).

encountered repeatedly in any rotating vehicles. The rolling rate, p, does not change since frictional effects have been ignored and the moments about the y axis and z axis have been assumed to be equivalent. However, in the case that they are slightly different the rolling rate would oscillate within certain bounds.

As stated earlier the vehicle is nominally at an angle of attack, α, of -62.651° and a side-slip angle, β, 0.0°. However as the vehicle plummets through the atmosphere both angles go through dramatic oscillations (fig. 3-4-11 & fig. 3-4-12). The behavior of coupling can clearly be seen. When α is a minimum, β is a maximum. 130 seconds into the flight and at maximum sensed deceleration, α reaches a minimum of virtually zero degrees. However, due to coupling β has a value of about 15°.

As stated in section 3.3, maximum heating occurs at about 188,000 ft. At this altitude the total angle of attack, α_{total}, is approximately 15° (fig. 3-4-13) and refer to fig. 3-4-14 to illustrate the coupling. This may pose a problem since the half cone angle of

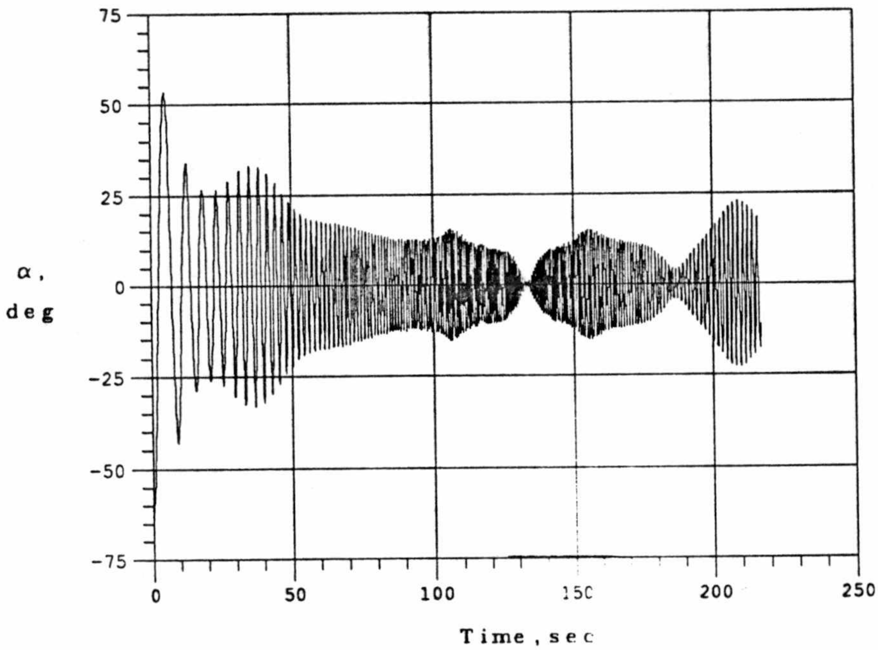

Figure 3-4-11, Angle of Attack vs. Time (2.5 rpm).

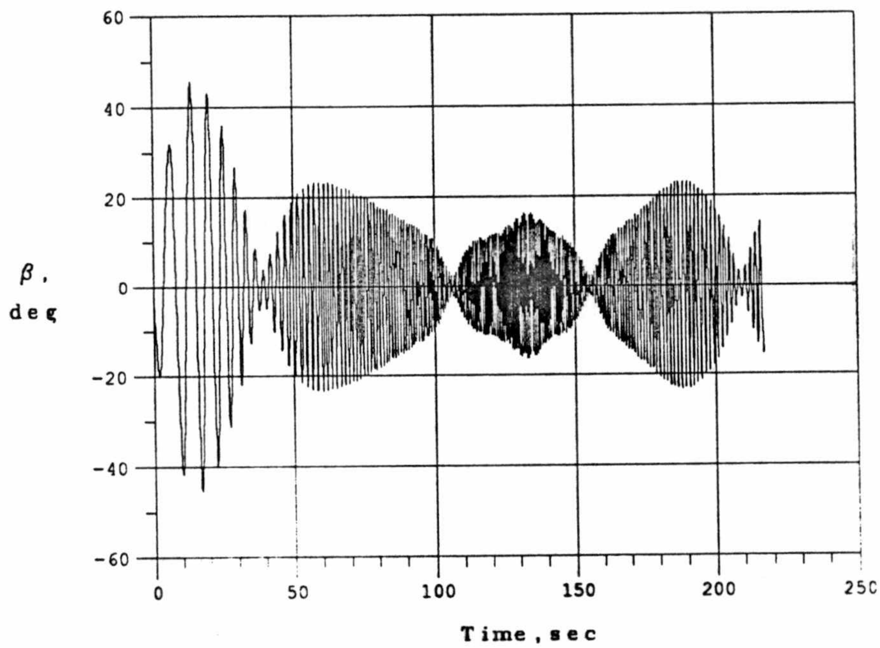

Figure 3-4-12, Side-slip Angle vs. Time (2.5 rpm).

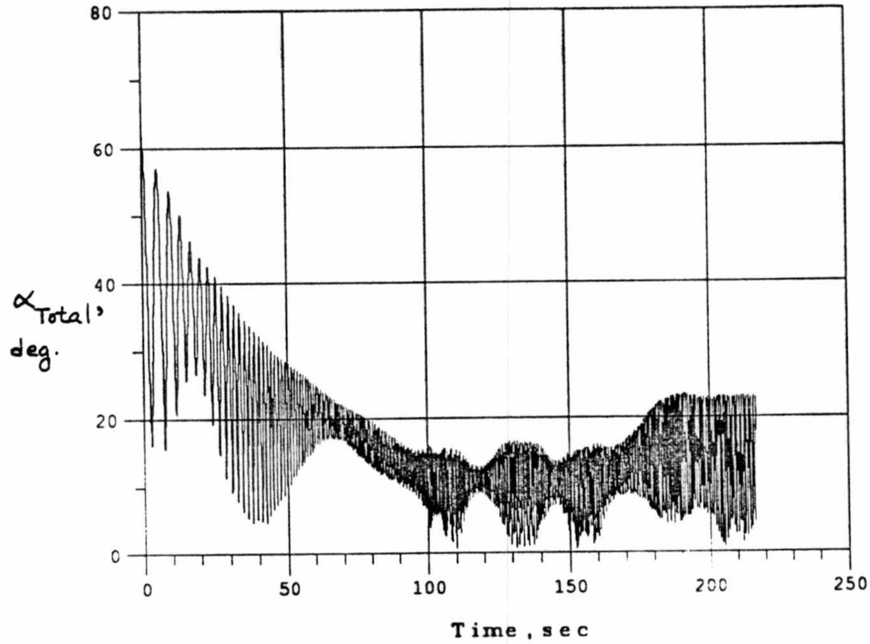

Figure 3-4-13, Total angle of attack vs. Time (2.5 rpm).

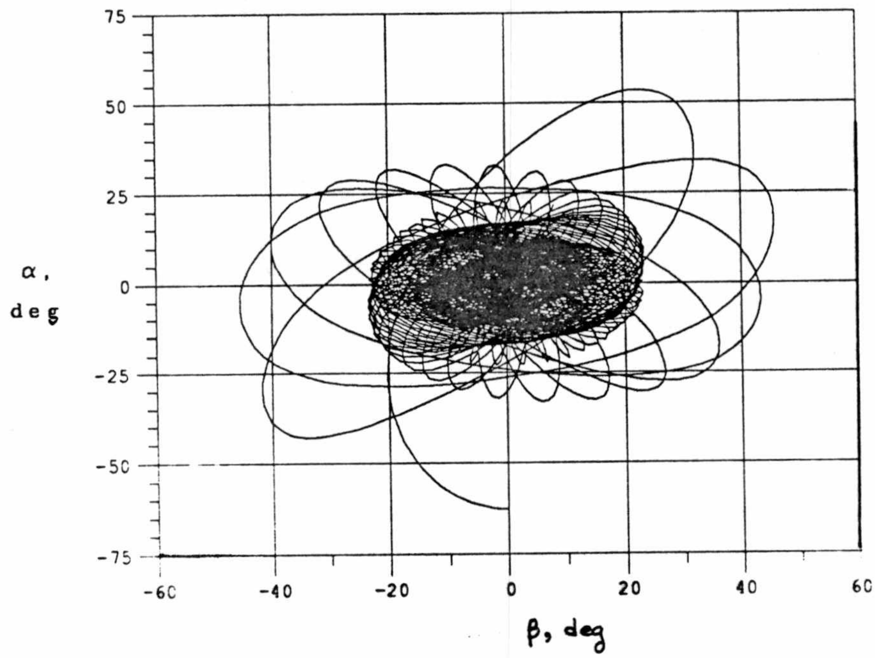

Figure 3-4-14, Angle of Attack vs. Side-slip Angle (2.5 rpm).

the body is about 10° (fig. 3-2-1), and the sides of the vehicle would be exposed to further heating.

The time history of the velocity, the flight path angle and altitude exhibit a close similarity (fig. 3-4-15) to the three degrees-of-freedom. It took the RV about 390 seconds from the nominal altitude to touch down. The flight path angle remains virtually constant for about 100 seconds form the nominal angle. However, after a rapid increase the flight path angle reached a virtually vertical descent in 250 seconds from atmospheric entry. As can be seen from the plot, the vehicle's flight path angle does oscillate somewhat about the asymptote. The vehicle appears to reach a terminal speed of about 200 ft/sec before impact.

The crossrange of vehicle tends to increase until the vehicle has a virtually vertical descend (fig. 3-4-16). The final crossrange before touchdown is about 9.36 nautical miles, and the final longitude is about 246.495°. That gives about a 5.7 nautical mile downrange difference. However, this is still within the Great Salt Lake Desert, Utah.

p=Rolling rate=5.0 rpm

This spin rate has been determined (SII) to be closer to the actual condition at atmospheric entry.

With this different rolling rate and with the same nominal conditions a comparison is made of the different characteristics that are influenced by this different rolling rate.

At 5 rpm (30 deg/sec) the envelope of the sensed acceleration in g's is close to 9.9 (fig. 3-4-17), a 1.52% increase. The envelope of the sensed g's remains above nine for about 25 seconds. However, the g's begin to approach a value of 1.0.

In addition, the maximum dynamic pressure is virtually 400 psf, a 2.5% increase. Both extrema occur at about 130 seconds into the flight. This is the same time as the 2.5 rpm rolling rate. The increase in g's is not very significant. However, a reason behind them is interesting. Due to doubling of the spin rate the vehicle cannot dampen to an

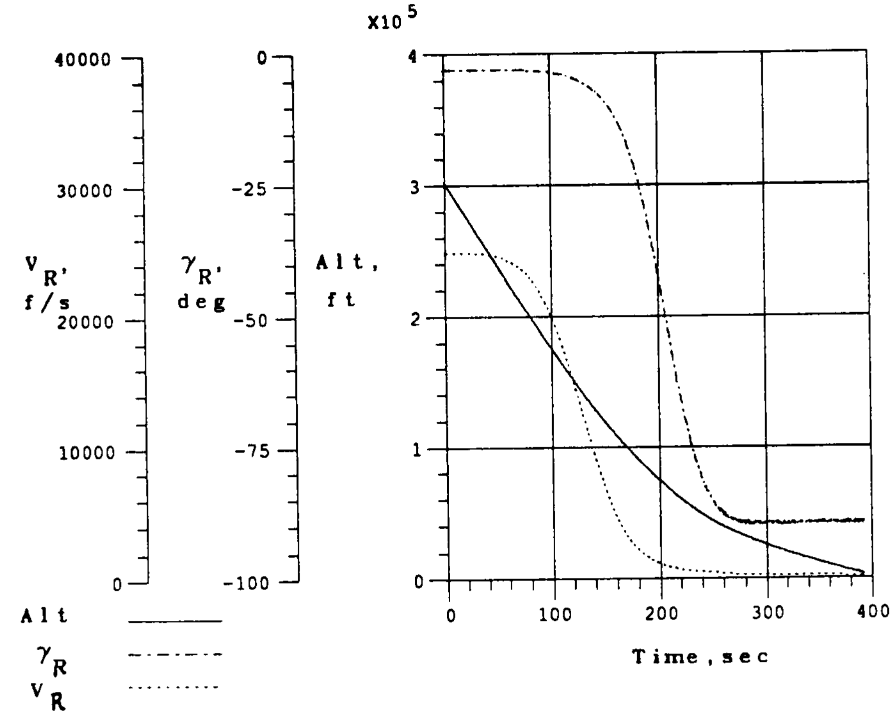

Figure 3-4-15, Velocity, Flight path angle & Altitude vs. Time (2.5 rpm).

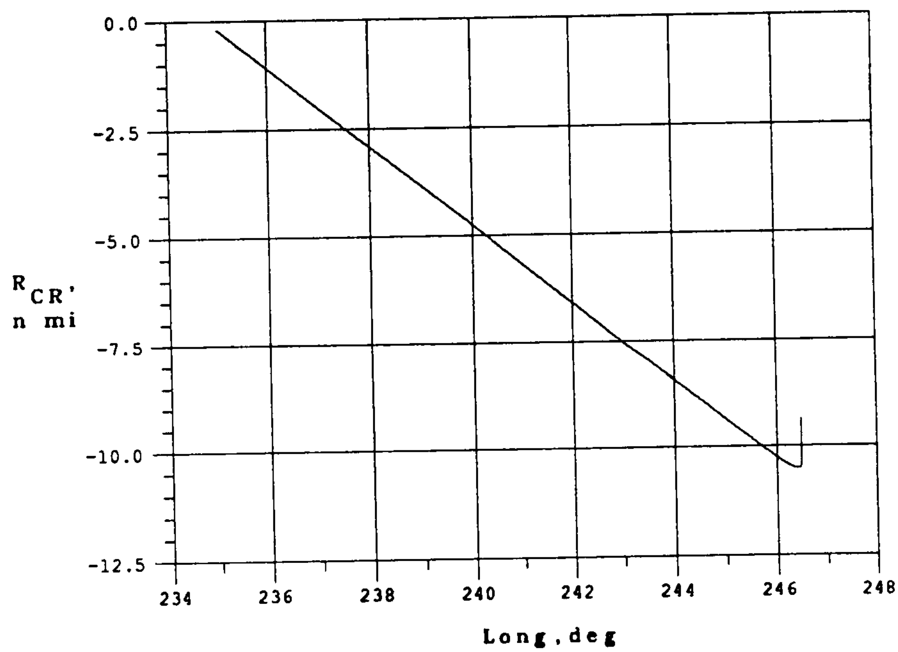

Figure 3-4-16, Crossrange vs. Longitude (2.5 rpm)

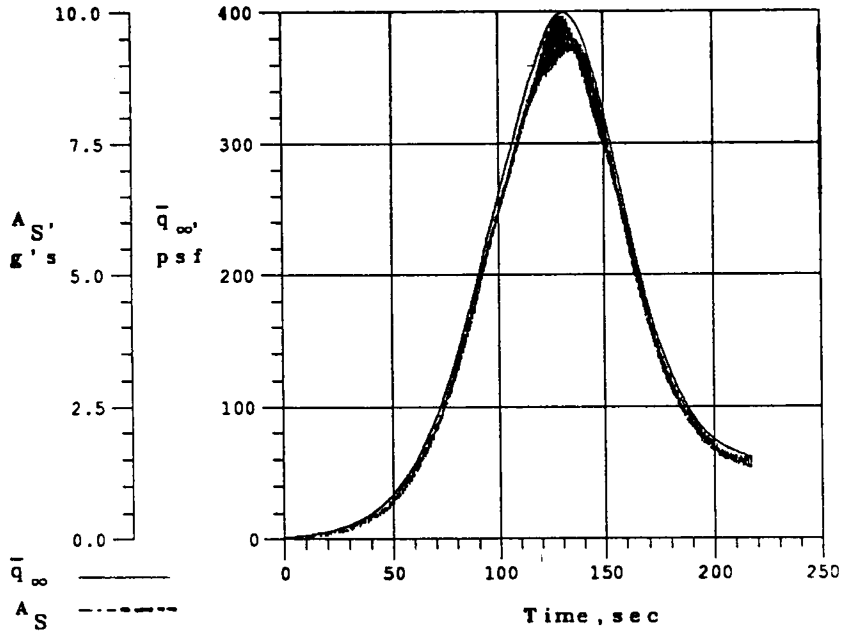

Figure 3-4-17, Sensed g's & Dynamic Pressure (5 rpm).

angle of attack as small as encountered by the 2.5 rpm case. This occurs due to the fact that spinning bodies are gyroscopically rigid; that is, they tend to remain closer to their initial condition as the spin rate is increased. Hence a larger angle, and thus lower drag for this vehicle, which tends to make the vehicle descend faster until it encounters significant dynamic pressure. However, the dynamic pressure will be higher since the vehicle has penetrated the atmosphere further and the local density and velocity is higher.

The sensed g's correlate highly to the axial acceleration of the vehicle. The maximum axial acceleration also occurs at an earlier time (fig. 3-4-18). It has a value very close to 10 g's. After 300 seconds into the flight the vehicle has reached an asymptote, which has a value of about 1.0 g.

The side acceleration (fig. 3-4-19) has also its envelope drastically changed to the doubling of the spin rate. The envelope has a higher frequency of oscillation. The larger amplitudes occur between 100 and 130 seconds into the flight. In this region the dynamic

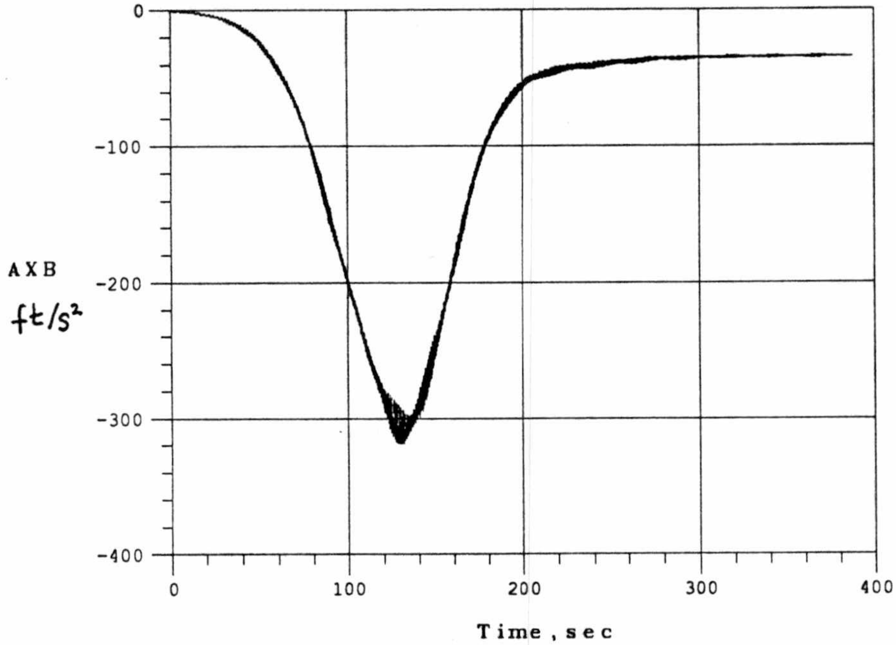

Figure 3-4-18, Axial acceleration vs. Time (5 rpm).

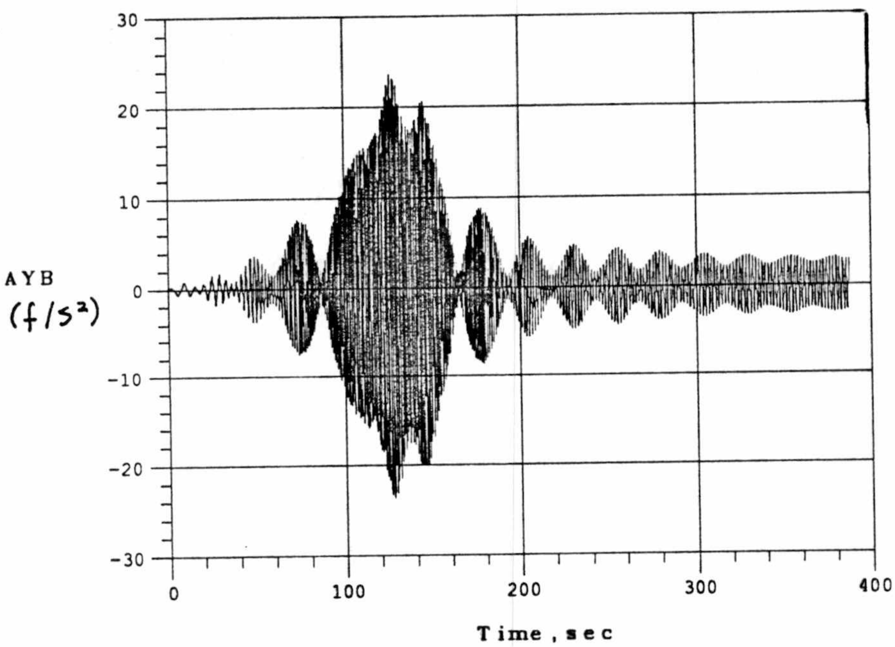

Figure 3-4-19, Side acceleration vs. Time (5 rpm).

pressure has become relatively significant. After 200 seconds the side acceleration has leveled off to about .124 g's. However, the envelope continues to oscillate. The one to one correlation between the yawing angular acceleration (fig. 3-4-20) and the side acceleration is clearly evident.

The vertical acceleration (fig. 3-4-21) has lower g values than the side acceleration but tends to have more oscillations near the maximum dynamic pressure. It also levels to about .11 g's. It also highly correlated to the pitching angular acceleration (fig. 3-4-22). The pitching angular acceleration and the vertical acceleration do not dampen to as a low value as the 2.5 rpm case. This is due to the higher spin rate.

The pitching rate (fig. 3-4-23) and the yawing rate (fig. 3-4-24) exhibit similar behavior similar to the angular accelerations. The pitching rate reaches a maximum of about 130 °/sec at 165 seconds into the flight. The yawing rate reaches a maximum of 180 °/sec at 130 seconds into the flight.

The affect of gyroscopic rigidity, discussed above, can be seen in fig. 3-4-25 when compared to fig. 3-4-11. Clearly the angle of attack's envelope is wider and tends to oscillate more than the case for 2.5 rpm. After 50 seconds of flight, both cases tend to have similar envelope values. However, while the 2.5 rpm case continues to decrease after 50 seconds, the 5 rpm case the increases to just above 25°. The minimum envelope value for the angle of attack does not go below 5°, while for 2.5 rpm the value drops to virtually zero.

To acquire further insight into this angular behavior the side slip angle, β, is investigated. The side slip angle history for the 5 rpm case is significantly different from the 2.5 rpm case (fig. 3-4-26 & fig. 3-4-12). While for the 2.5 rpm case in the 100 to 150 second region there are clear minima, but the 5 rpm case has stabilized to a 15° side slip angle. As can be seen from fig. 3-4-26, the frequency of oscillation of this envelope tends to be higher than the 2.5 rpm case (fig. 3-4-12).

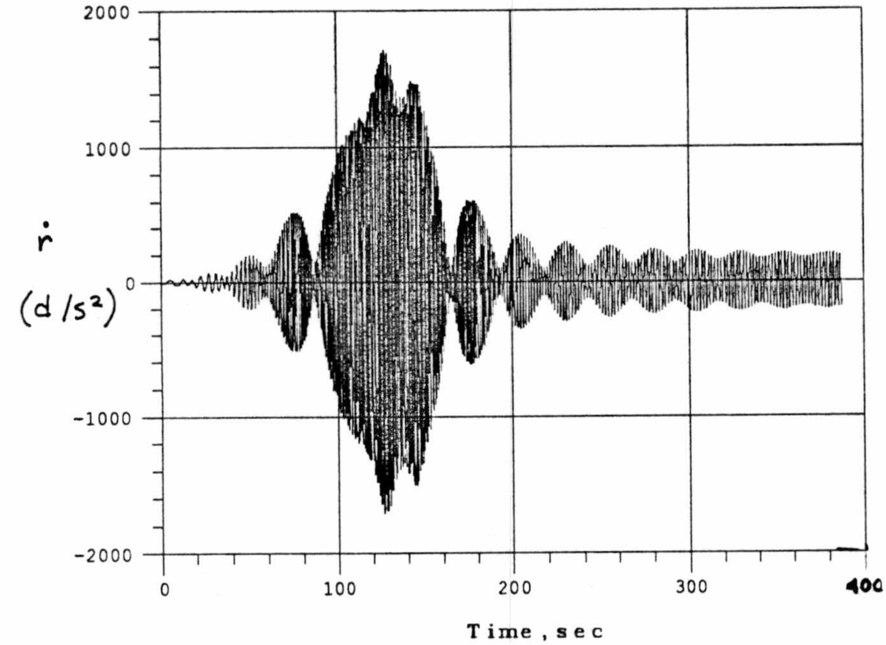

Figure 3-4-20, Yawing angular acceleration vs. Time (5 rpm).

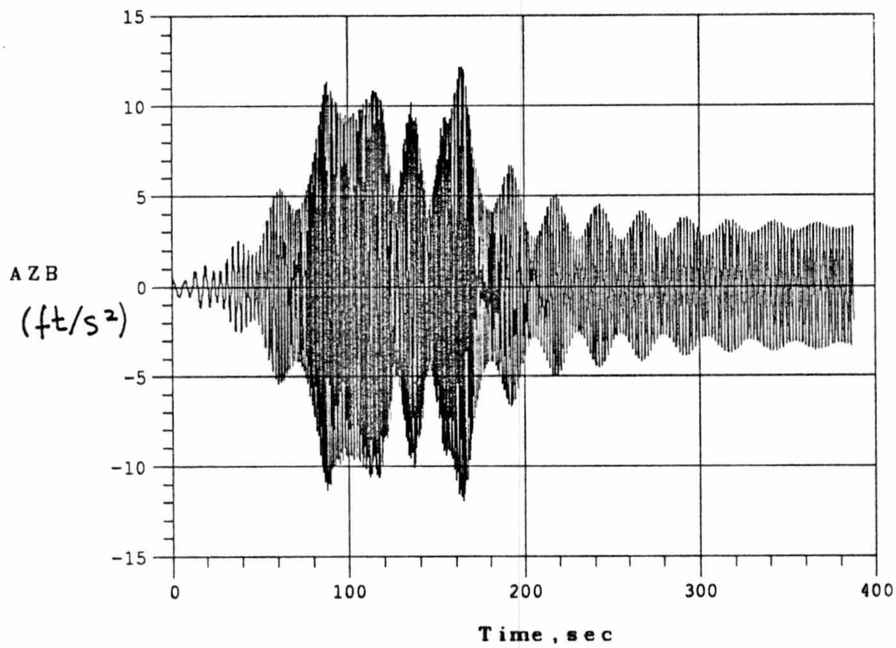

Figure 3-4-21, Vertical acceleration vs. Time (5 rpm).

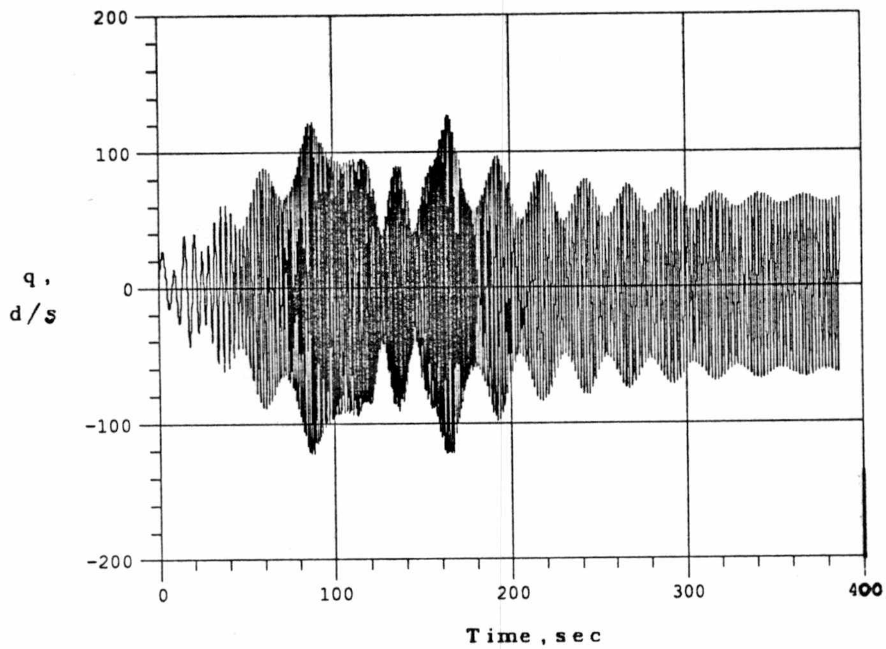

Figure 3-4-22, Pitching angular acceleration vs. Time (5 rpm).

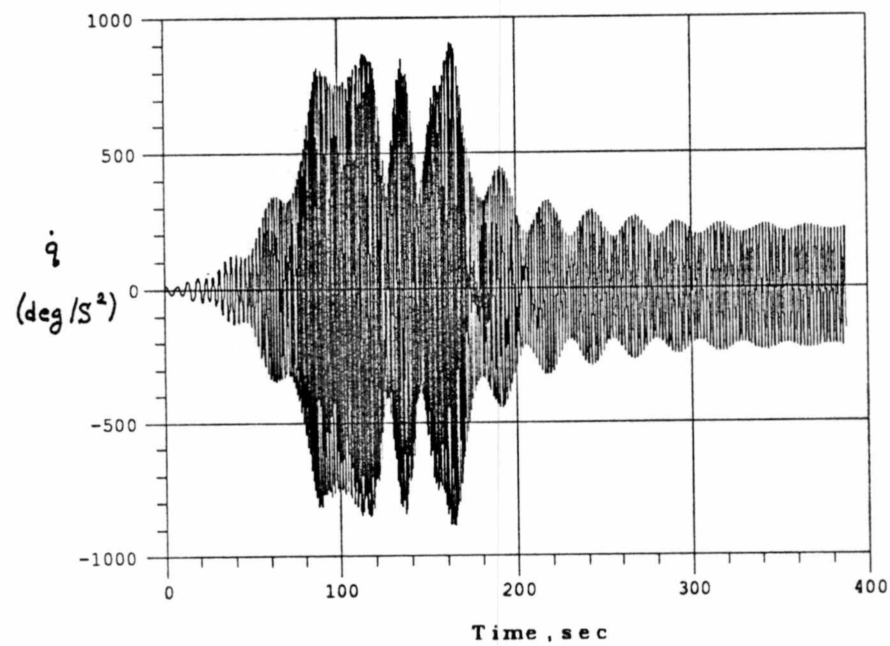

Figure 3-4-23, Pitching rate vs. Time (5 rpm).

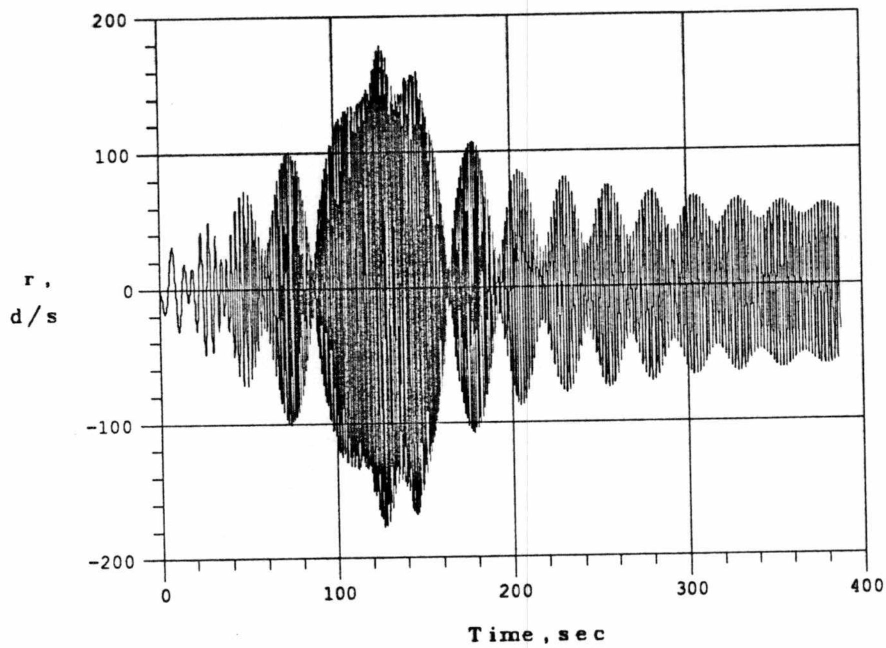

Figure 3-4-24, Yawing rate vs. Time (5 rpm).

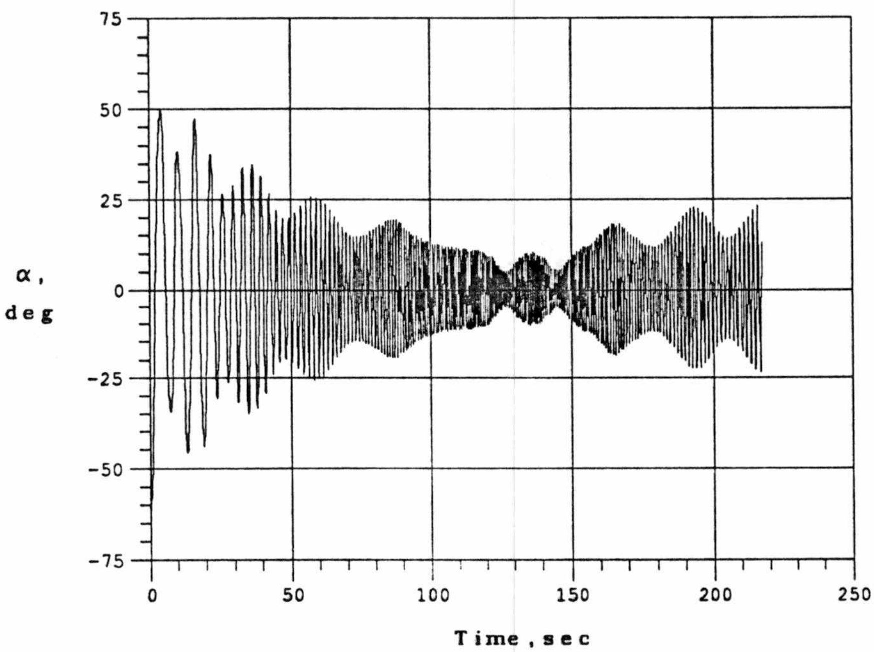

Figure 3-4-25, Angle of Attack vs. Time (5 rpm).

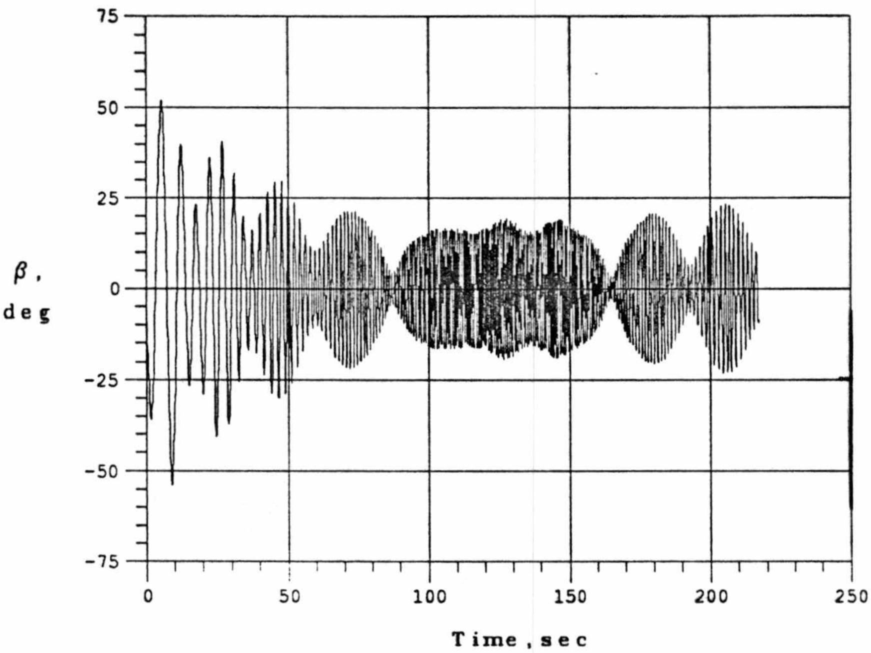

Figure 3-4-26, Side slip angle vs. Time (5 rpm).

The total angle of attack, α_{total} (fig. 3-4-27), for the 5 rpm, also has a envelope with a higher frequency of oscillation than the 2.5 rpm case (fig. 3-4-13). However at the 100 second point the total angle of attack is about 15°. This again would expose the sides of the vehicle to further heating. At the 130 second point, the maximum sensed g's, the angle is again higher then the 2.5 case. The maximum angle of the envelope is close to 19°, while for the 2.5 rpm case it is closer to 15°. This is about a 21% increase.

The profile of the angle of attack versus the side slip angle (fig. 3-4-28) is also significantly different from the 2.5 rpm case (fig. 3-4-14). In the 5 rpm case the vehicle tends to remain closer to the nominal angles for a longer period of time. This is caused, as stated above, by what this author calls gyroscopic rigidity.

The time history of the local velocity, flight path angle, and altitude (fig. 3-4-29) of the 5 rpm case is nearly identical to the 2.5 rpm case (fig. 3-4-15).

Interestingly, the crossrange, 9.408 nautical miles, (fig. 3-4-30) is virtually the

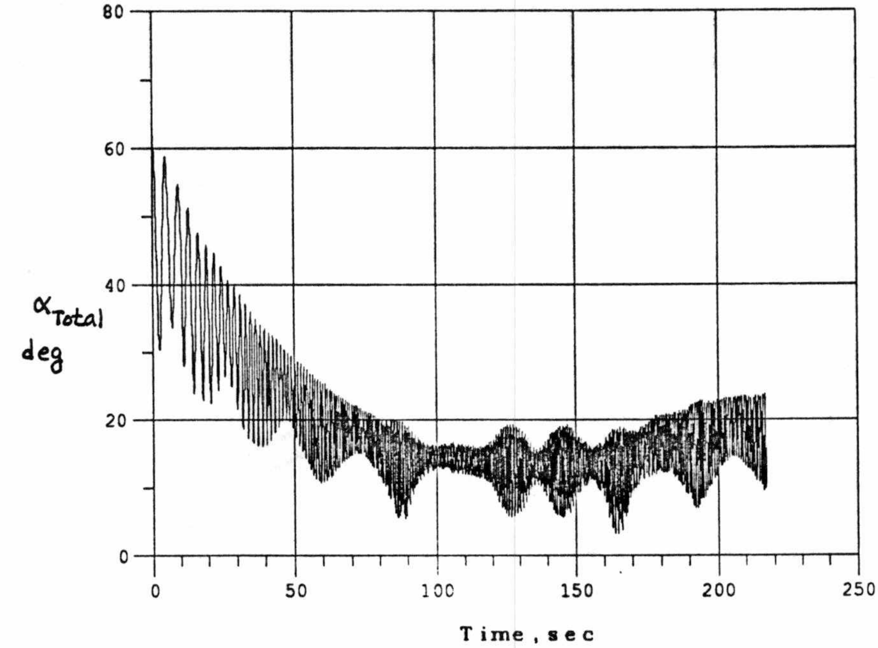

Figure 3-4-27, Total angle of attack vs. Time (5 rpm).

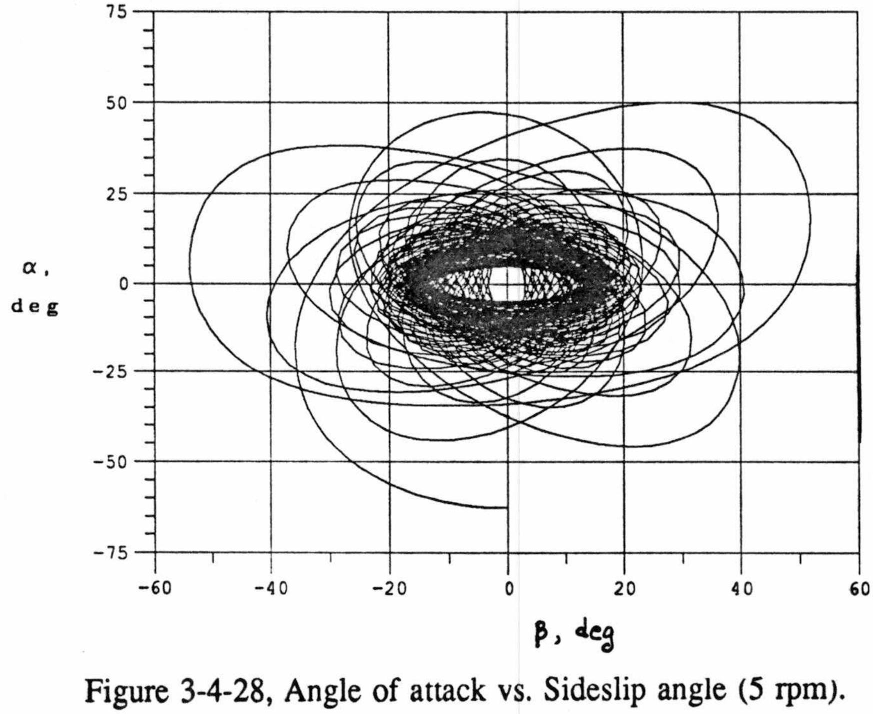

Figure 3-4-28, Angle of attack vs. Sideslip angle (5 rpm).

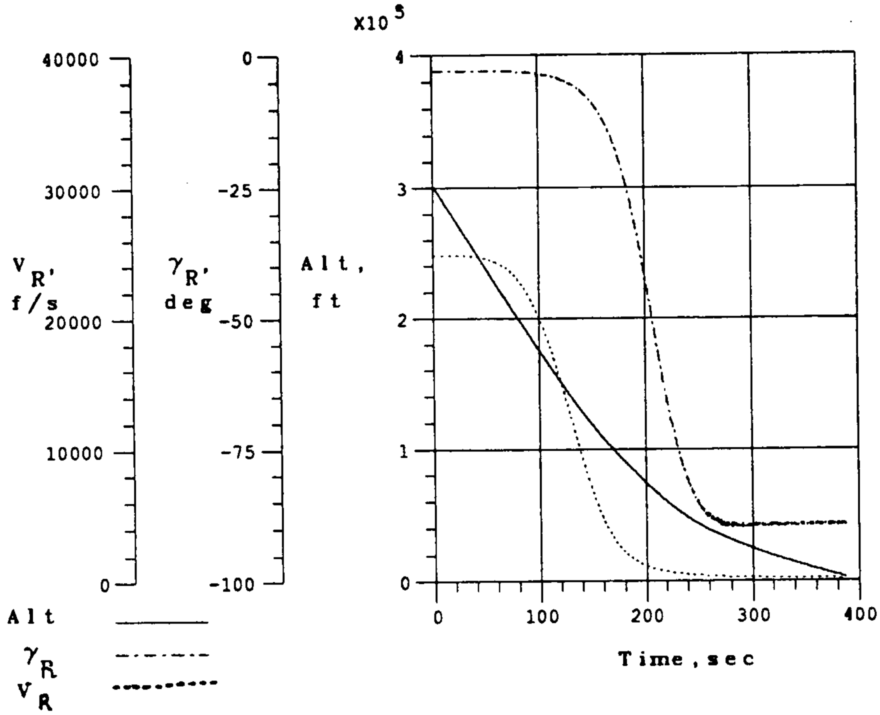

Figure 3-4-29, Velocity, Flight path angle & Altitude vs. Time (5 rpm).

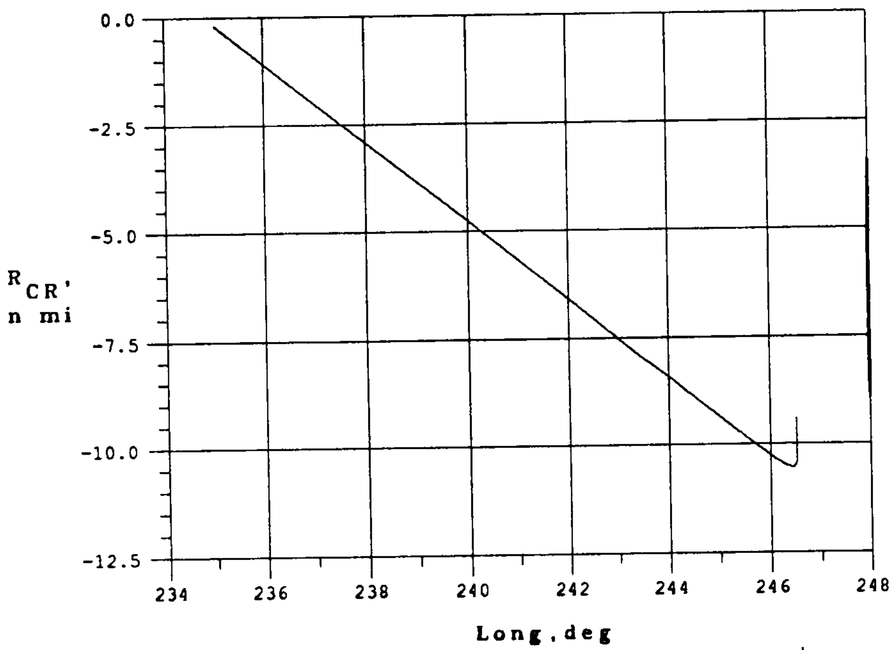

Figure 3-4-30, Crossrange vs. Longitude (5 rpm).

same as the 2.5 rpm case, 9.36 nautical miles; however, the final longitude is slightly more to the east than the 2.5 rpm case. While for the 2.5 rpm case the final longitude is about 246.4955° (113.5045°W) the 5 rpm case's final longitude is about 246.527° (113.473°W). Since the target longitude is 246.4° (113.6°W) there would be a downrange "error". For the 2.5 rpm case the downrange would come out to about 5.73 nautical miles (difference of target and final longitude multiplied by 60, since 1 nautical mile is equivalent to 1 angular minute) and for the 5 rpm case the downrange would be 7.62 nautical miles. This is a 32.98 % increase in the downrange due to the increase in the spin rate! Nevertheless, this remains within the boundaries of the Great Salt Lake Desert. Perhaps the reason is due to the fact that at the 5 rpm case the overall drag is lower, hence the vehicle remains longer in flight.

p=Rolling rate=7.5 rpm

This rolling rate tends to cause the sensed g's to occur at an earlier time into the flight (fig. 3-4-31). The maximum sensed g's is about 9.5, and which occurs at about 125 seconds into the flight, 5 seconds before the other cases. However, the maximum dynamic pressure, 405 psf, occurs at 130 seconds.

The maximum axial acceleration for 7.5 rpm also tends to occur at an earlier time (fig. 3-4-32). In fact the major contributor to the sensed g's is the axial one.

The side acceleration has changed drastically (fig. 3-4-33) from the 2.5 and 5 rpm cases. The frequency of the envelope is also higher than the other cases. The two maxima have a value of about 0.466 g's. The correlation with the yawing acceleration (fig. 3-4-34) is clearly evident. The two maxima here are about 1250 °/sec^2. The maxima tend to have similar value; however, they occur at different times. The vertical acceleration (fig. 3-4-35) also correlates highly with the pitching angular acceleration (fig. 3-4-36). As described above the frequency of oscillation of the envelope has also increased.

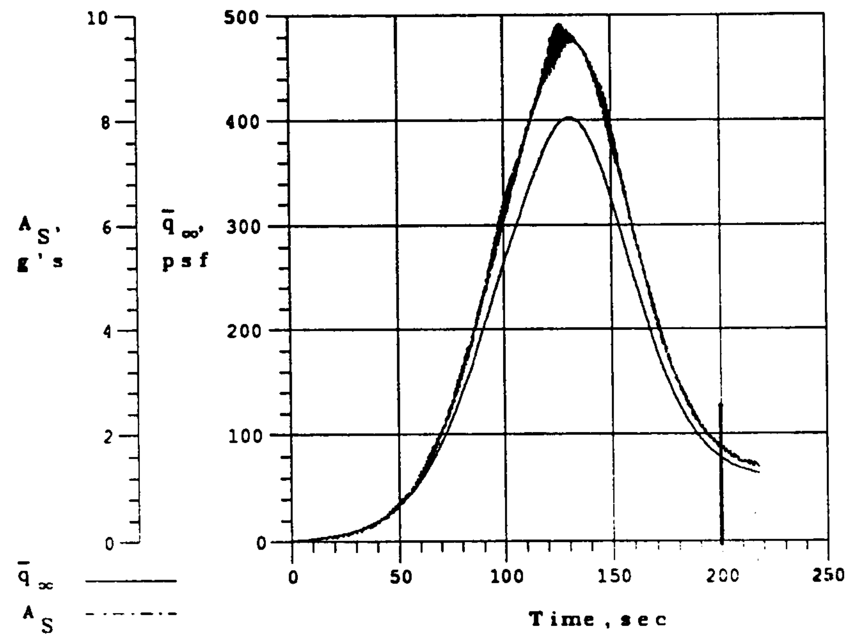

Figure 3-4-31, Sensed g's & Dynamic pressure vs. Time (7.5 rpm).

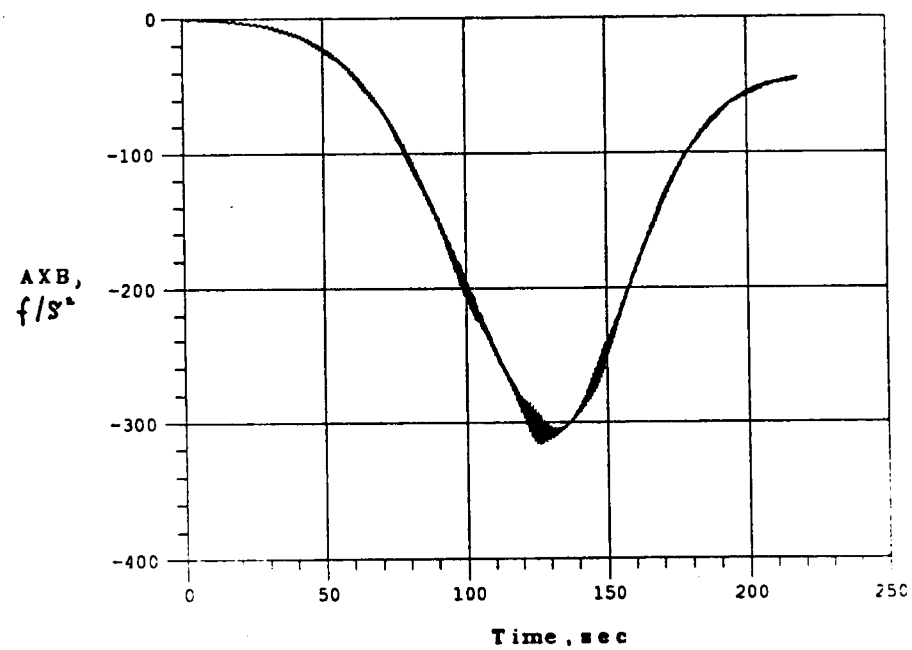

Figure 3-4-32, Axial acceleration vs. Time (7.5 rpm).

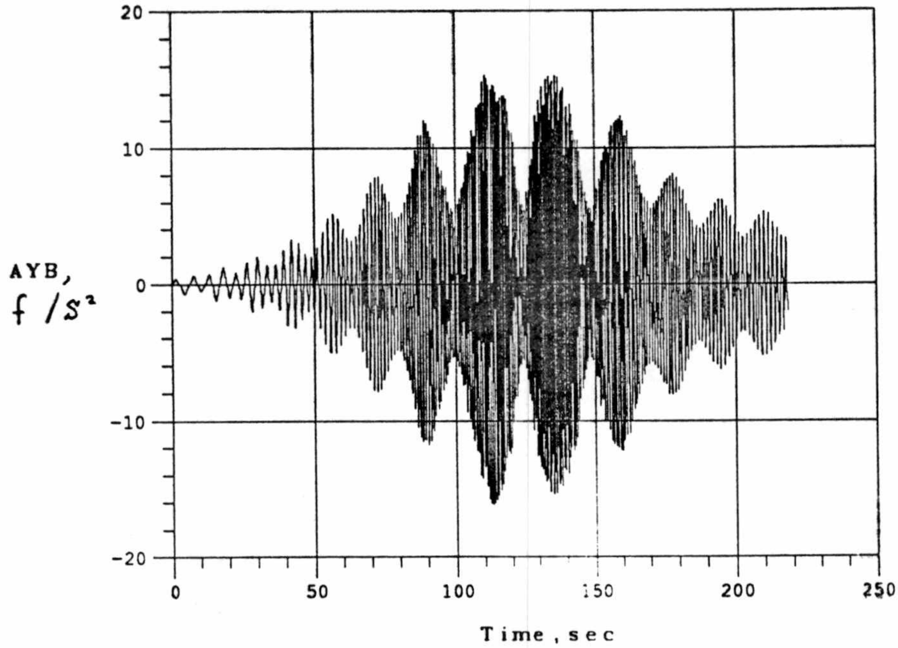

Figure 3-4-33, Side acceleration vs. Time (7.5 rpm).

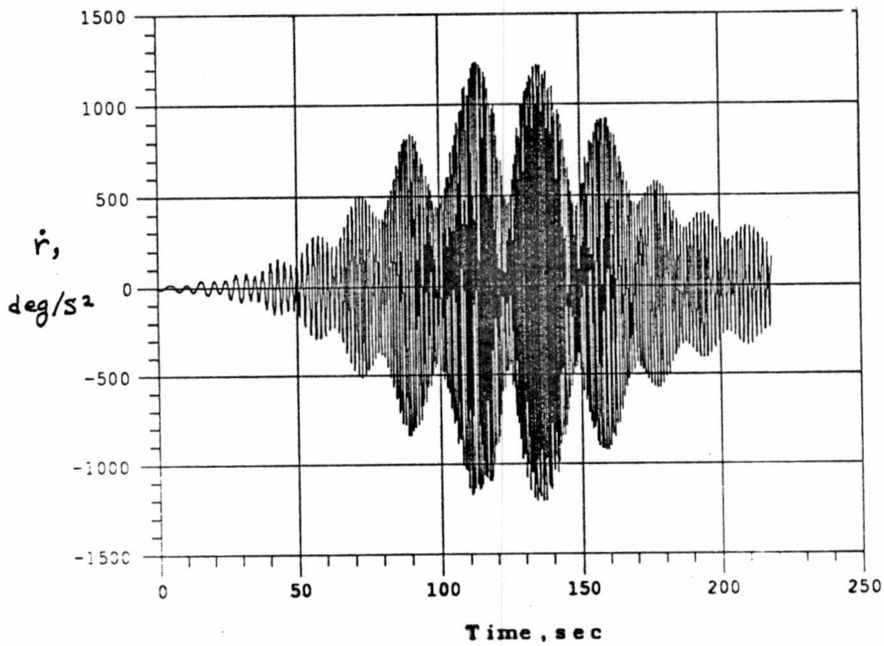

Figure 3-4-34, Yawing angular acceleration vs. Time (7.5 rpm).

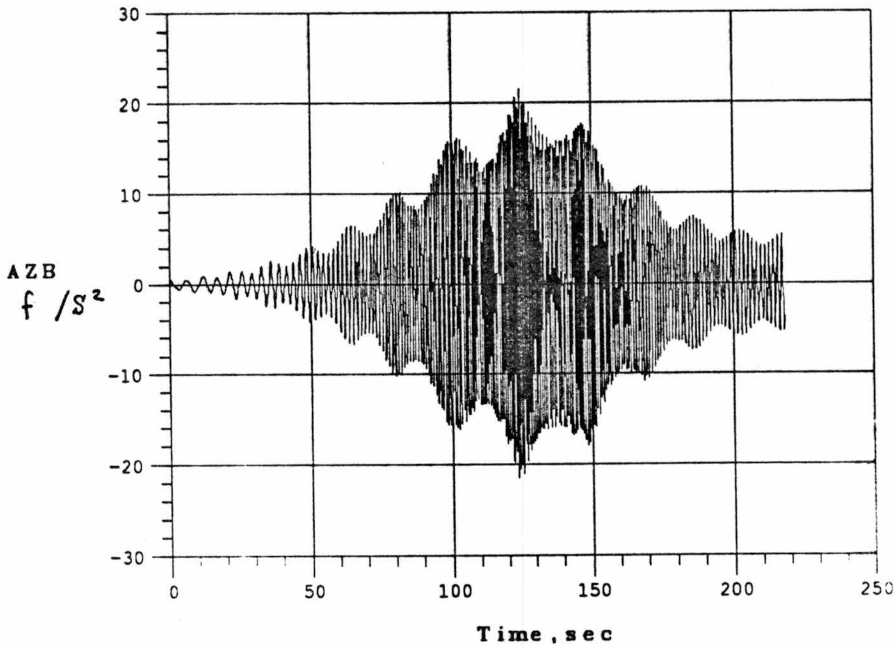

Figure 3-4-35, Vertical acceleration vs. Time (7.5 rpm).

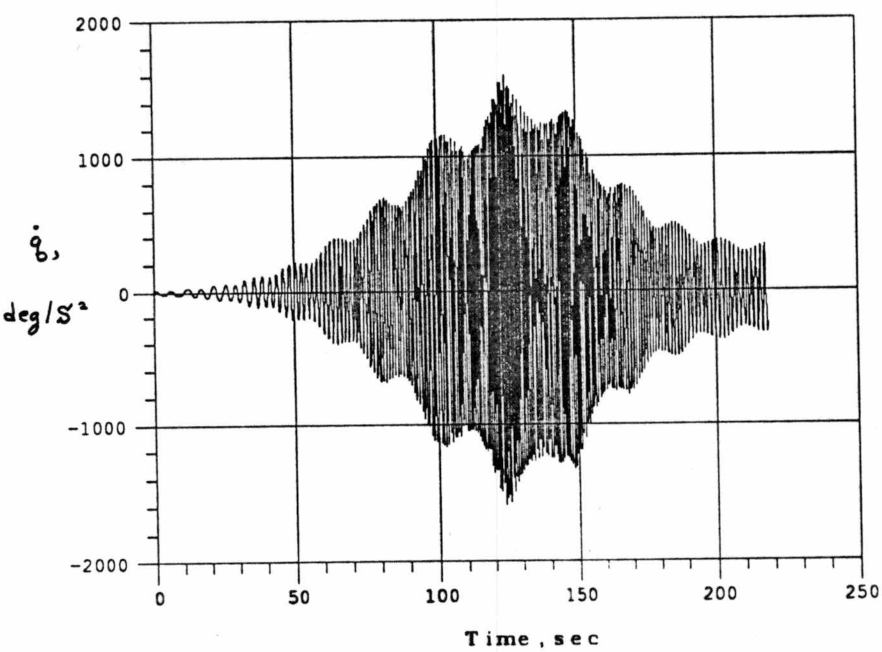

Figure 3-4-36, Pitching angular acceleration vs. Time (7.5 rpm).

The pitching rate (fig. 3-4-37) is also quite different for the two other cases. The increase in the pitching rate envelope appears to be virtually linear until the maximum dynamic pressure is reached, where it linearly begins to decrease. The maximum pitching rate is 150 °/sec at about 125 seconds into the flight.

The maximum of the yawing rate (fig. 3-4-38) is about 125 °/sec which happens at 115 seconds into the flight. After the maximum the envelope of the rate begins to diminish in what appears to be a linear fashion.

The angle of attack time history (fig. 3-4-39) exhibits a behavior quite different from the other two cases. In fact, it exhibits a behavior closer the dynamical analyses done in Chapter 2 (fig. 2-3-2). However, the envelope continues to oscillate. The minimum angle of attack is about 15° at the 130 second point. However, after that point the angle of attack envelope begins to diverge. At about the 80 second point the maximum heating rate is encountered; however, the angle of attack at this point is about 16°. Hence, the sides are exposed to further heating.

The side slip angle time history (fig. 3-4-40) exhibits a similar behavior to the angle of attack. However, it is out of phase with the angle of attack, as in the other cases. The minimum value reached is about 7° at 125 seconds into the flight.

The total angle of attack (fig. 3-4-41), which exhibits the effects of side slip angle and the angle of attack, has similar behavior to the other spin rate cases. However, at the 80 second point, the maximum heating rate, the angle is just above 25°. This is not an unexpected result, since the spin is higher the damping is expected to be lower due to reasons discussed above. The minimum value reached by envelope is very close to 7°. After that point the envelope begins to diverge, as predicted in Chapter 2.

The profile of the angle of attack versus the side slip angle (fig. 3-4-42) is similar to the other case; however, it tends to remain wider than the other cases. In fact, it appears to be more circular. The vehicle would approach a more circular profile as the

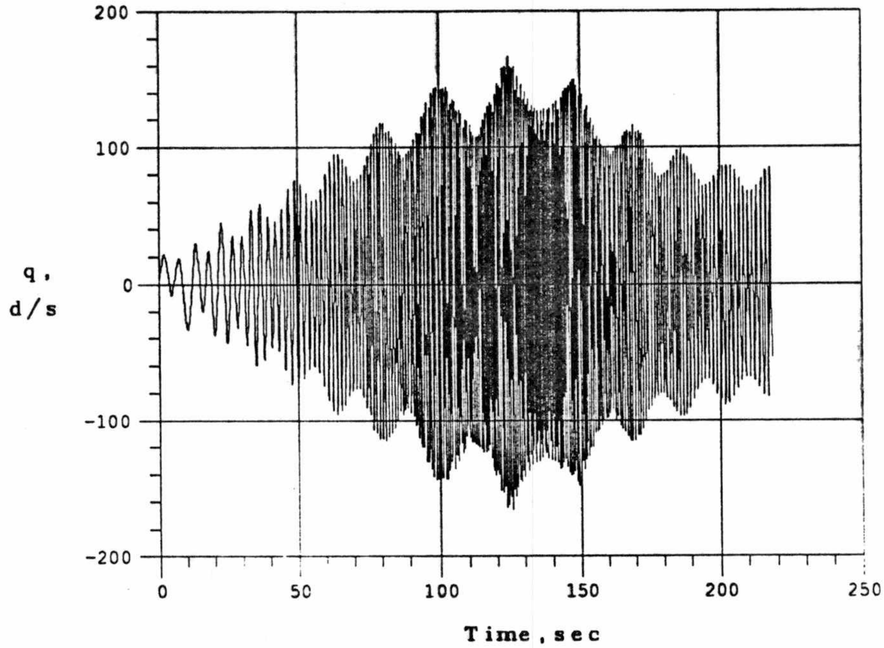

Figure 3-4-37, Pitching rate vs. Time (7.5 rpm).

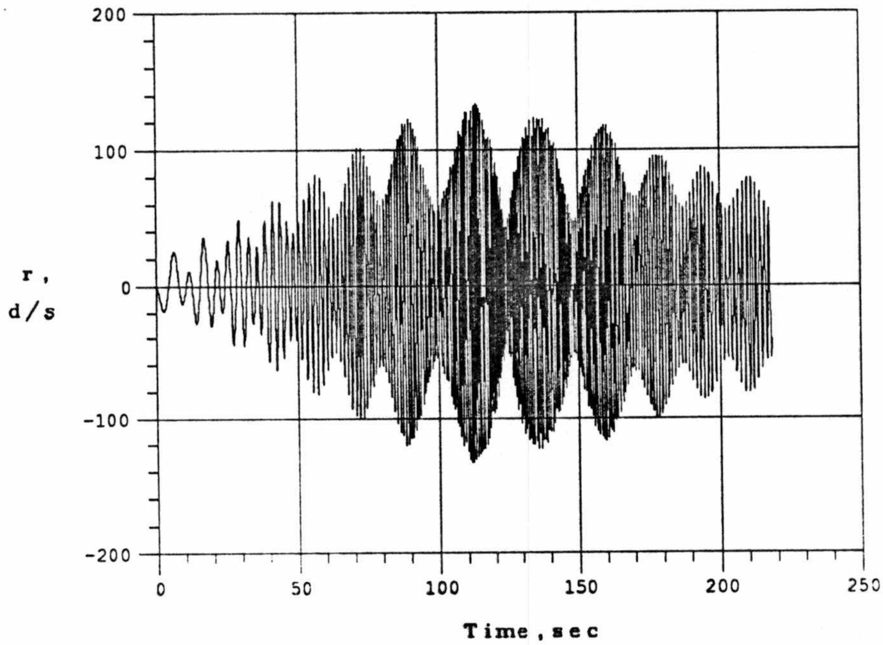

Figure 3-4-38, Yawing rate vs. Time (7.5 rpm).

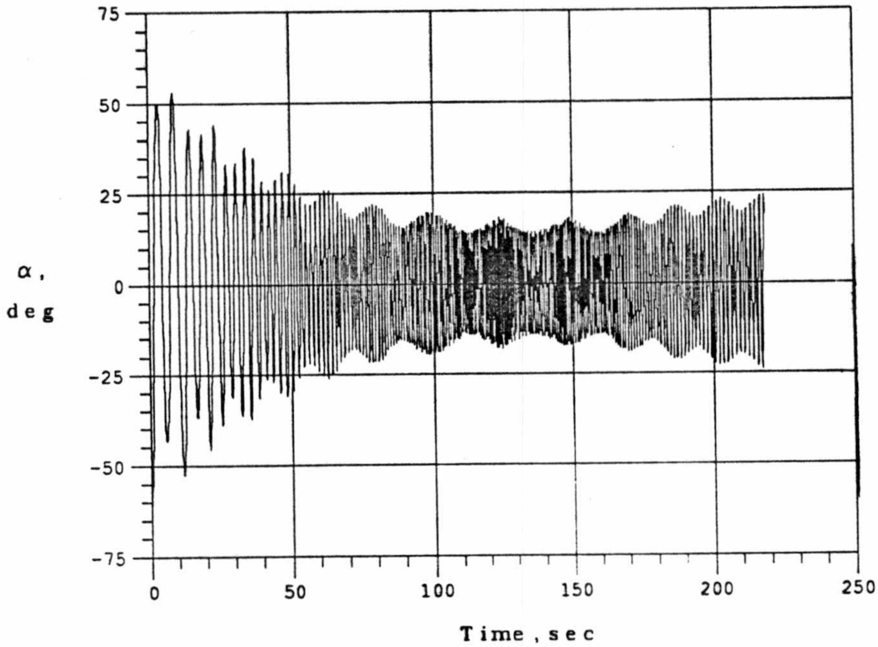

Figure 3-4-39, Angle of Attack vs. Time (7.5 rpm).

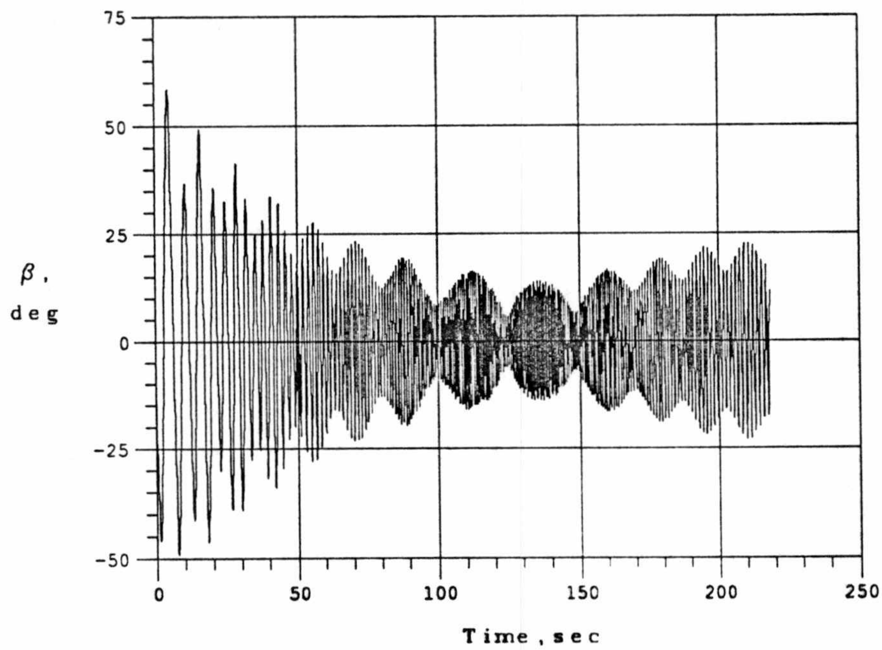

Figure 3-4-40, Side slip angle vs. Time (7.5 rpm).

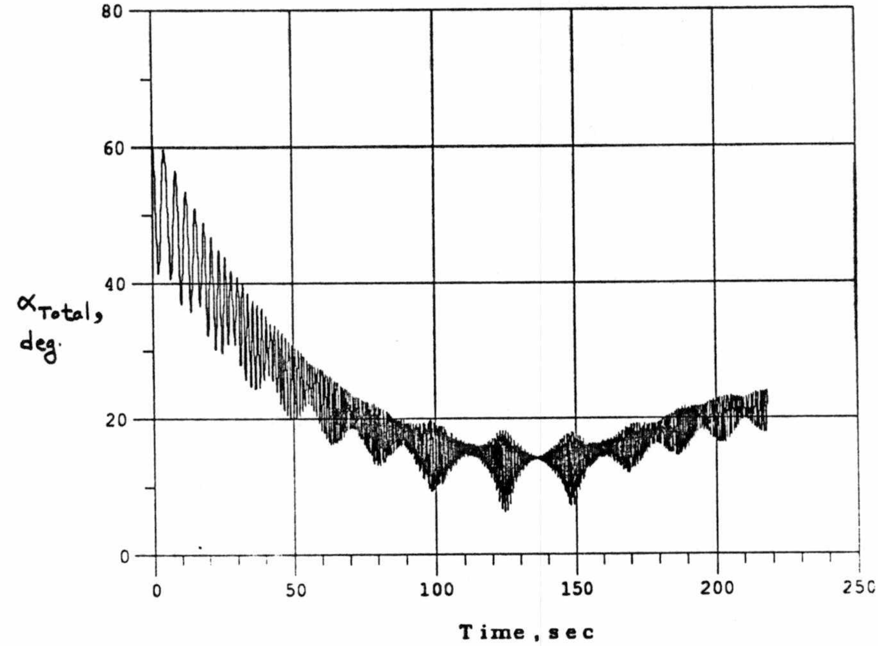

Figure 3-4-41, Total angle of attack vs. Time (7.5 rpm).

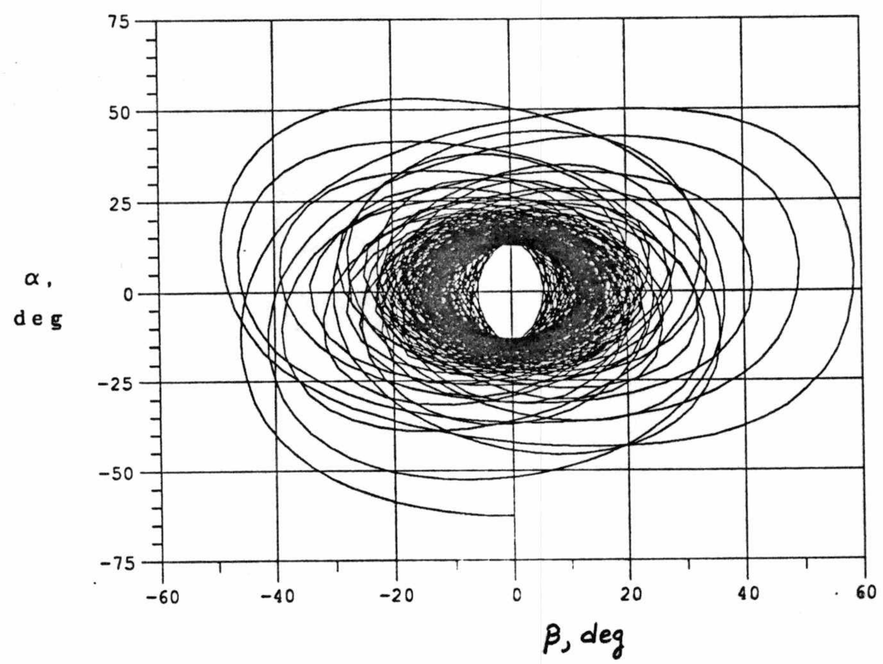

Figure 3-4-42, Angle of Attack vs. Side Slip Angle (7.5 rpm).

spin rate is increased.

The profile of the velocity, flight path angle and the altitude with respect to time (fig. 3-4-43) is virtually identical to the other two spin rates.

However, the final longitude of the vehicle (fig. 3-4-44) is about 246.565° (113.435°W) and the crossrange is 9.46 nautical miles. The final longitude indicates that the final downrange is about 9.9 nautical miles. This is a 29.92% increase from the 5 rpm case and a 72.77% increase from the 2.5 rpm case. It appears that the increase in downrange correlates linearly to the spin rate.

As an illustration of the variation of final longitude to initial roll rate look at figure 3-4-45. The variation of maximum sensed g's and the final longitude with respect to a ±.5° perturbation of the initial flight path angle, γ_R look at figures 3-4-46 and 3-4-47, respectively.

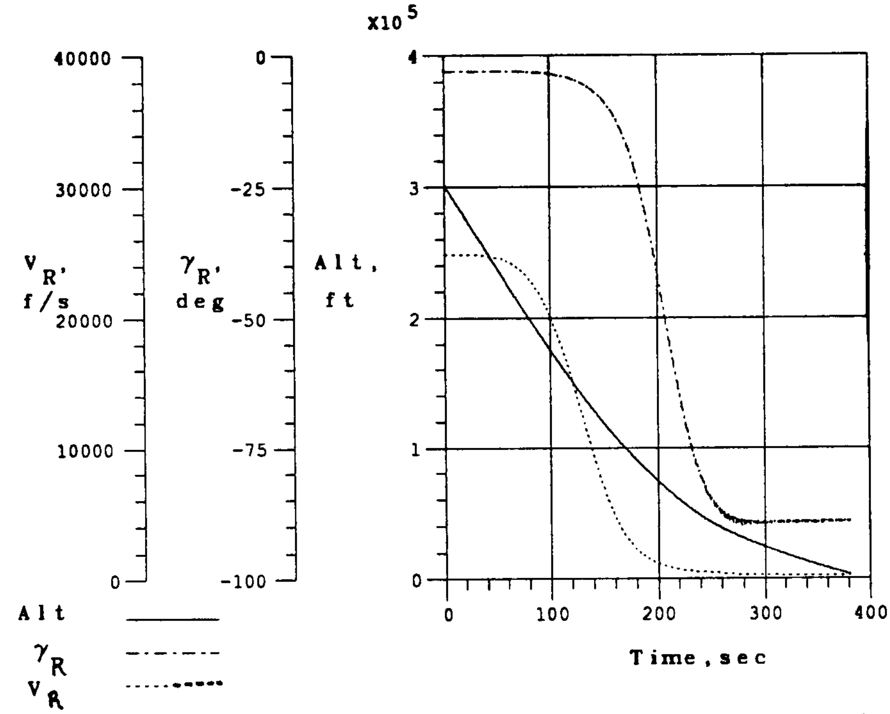

Figure 3-4-43, Velocity, Flight path angle & Altitude vs. Time (7.5 rpm).

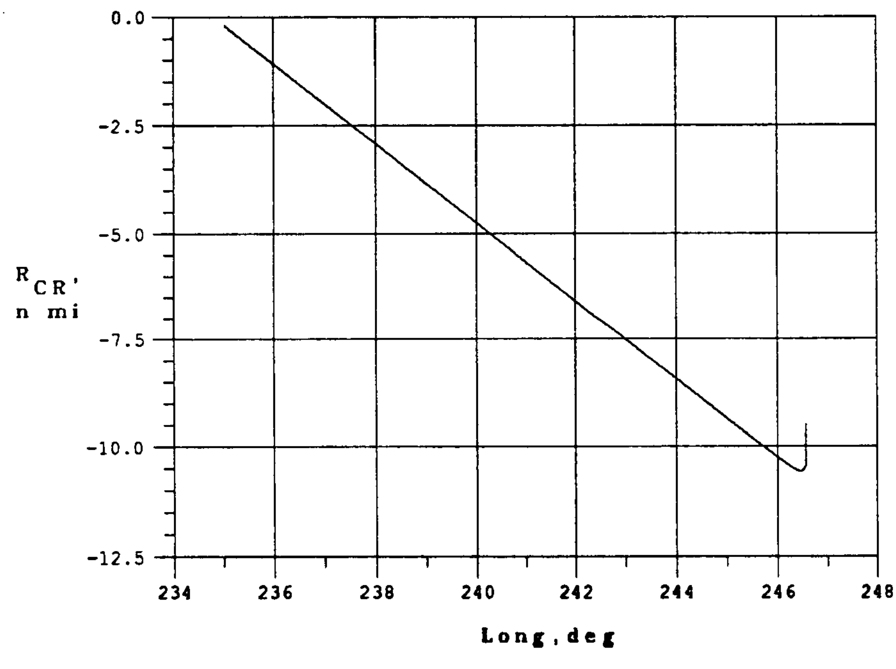

Figure 3-4-44, Crossrange vs. Longitude (7.5 rpm).

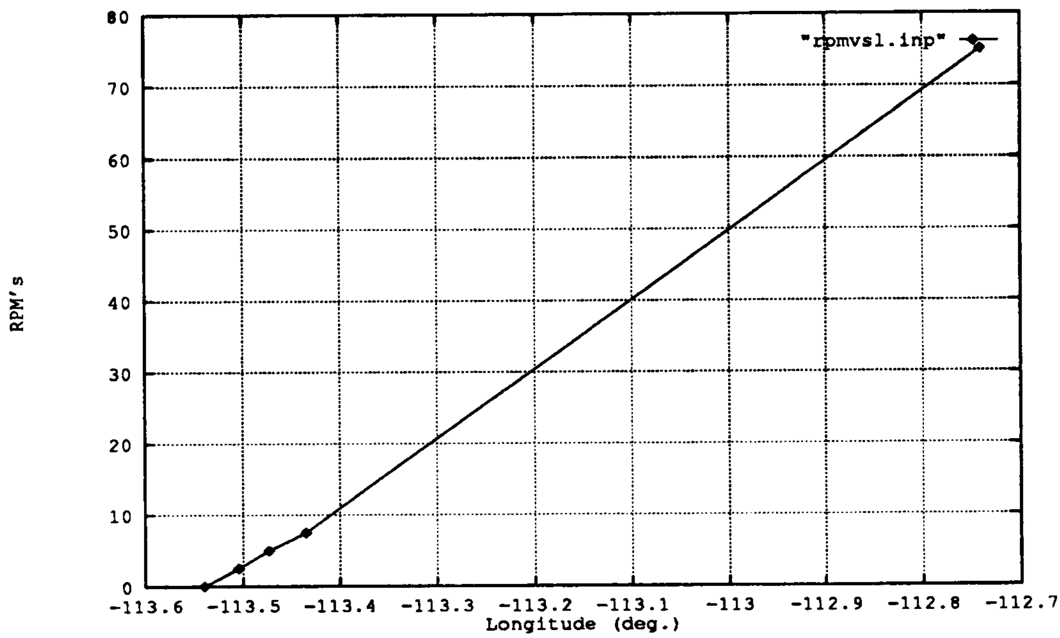

Figure 3-4-45, Final Longitude vs. Initial Roll Rate of RV.

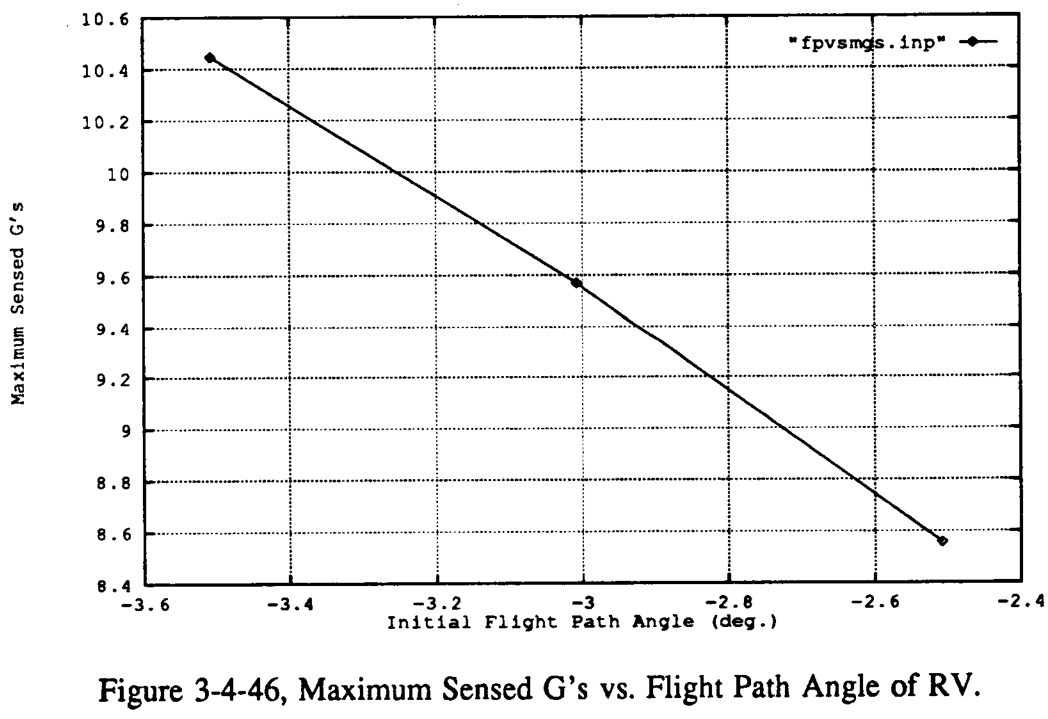

Figure 3-4-46, Maximum Sensed G's vs. Flight Path Angle of RV.

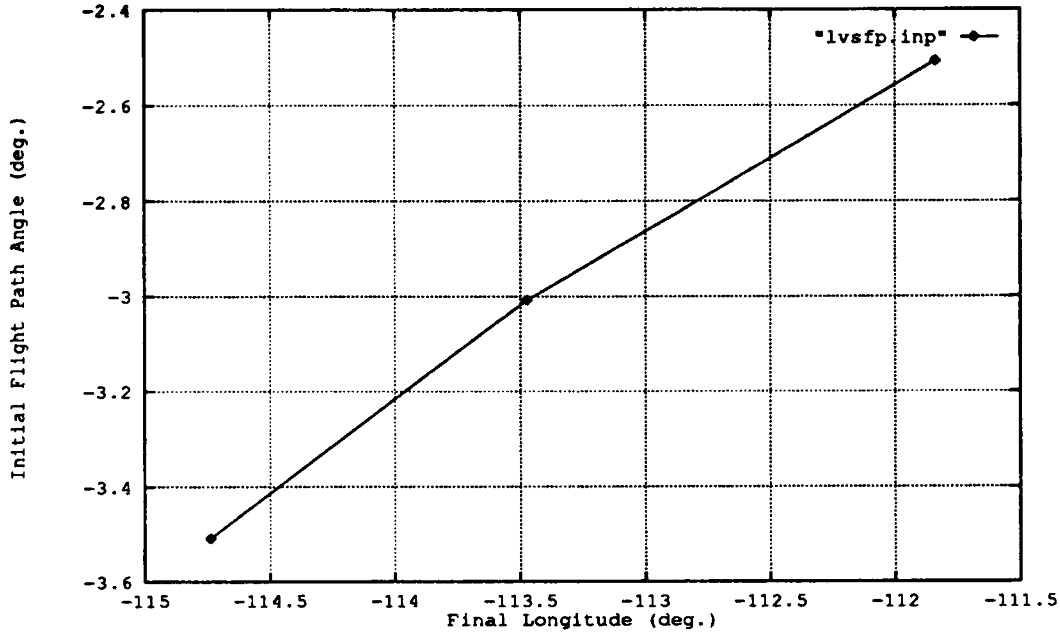

Figure 3-4-47, Final Longitude vs. Initial Flight Path Angle (5 rpm)

CHAPTER 4: CONCLUSIONS

It is evident from the previous chapter that the time history of the angles varies greatly with the spin rates.

The downrange also varies greatly with the spin rates. An increase in the downrange is not critical to the mission, since it remains within the boundaries of the Great Salt Lake Desert.

The three primary orbital elements that strongly effect the sensed g's are the velocity, the altitude and the flight path angle. All are elements that can be controlled; however, for the COMET RV these are constrained by the fact that the vehicle is initially sun synchronous. Therefore, after the RV's separation from the Service Module the RV remains somewhat sun synchronous. Hence, the -62.651° angle of attack at atmospheric entry. The RV, as in all systems, is limited by the energy it can consume. Hence, it is limited by the energy imparted on it by the retro motor, which is itself limited in energy and fuel. Therefore, the above elements cannot be changed without changing the mission.

However, the remaining "uncertainty" is the spin rate. It is proposed by Space Industries Incorporated to despin the RV from 75 rpm to about 5 rpm. In Chapter 3 the spin rate was perturbed from 2.5 to 7.5 rpm to determine the effects on the behavior. Nevertheless, all the spin rates considered produce sensed g's that are larger 9.

Since the primary concerns upon entry are the sensed g's and the heating rate, a consideration of their reduction must be evaluated. Assuming a fixed flight path angle and altitude and velocity upon entry, vehicles entering the atmosphere cannot reduce the sensed acceleration and heating rate, without modulating the lifting and the drag forces. However, this vehicle has very little potential in aerodynamic force modulation, since the drag coefficient remains virtually the same for large angles of deviations, and the lift coefficient remains quite small. Also at zero angle of attack the vehicle has a zero lift to drag ratio. To significantly reduce the sensed g's the vehicle needs to determine the applied acceleration and counter them. In other words, a control system is needed for modulation. However, for effective modulation (Grant 1959, Katzen 1961, Levy 1960-61, and Tobak 1956) the aerodynamics of the vehicle must changed. A change of the aerodynamics is a fundamental change of the vehicle's geometry. Consequently, a lifting body is necessary. A half cone as a vehicle for entry is perhaps a reasonable starting point. Unfortunately, the inclusion of controls will increase the costs of the vehicle. However, it may also increase demand for such a vehicle, since reduced loads may encourage a wider variety of experiments onboard. Hence, a reduction in overall capital cost.

BIBLIOGRAPHY

BIBLIOGRAPHY

Alekseyev, K. B. and G. G. Bebenin, "Problems of Spacecraft Control During Descent in the Atmosphere," NASA TT F-9336, Washington, D.C.: U.S. Government Printing Office, May 1965.

Allen, H. Julian, "Motion of a Ballistic Missile Angularly Misaligned with the Flight Path upon Entering the Atmosphere and its Effect upon Aerodynamic Heating, Aerodynamic Loads and Miss Distance," NACA TN 4048, Washington, D.C.: National Advisory Committee for Aeronautics, October 1957. **pp. 17 to 19.**

Allen, H. Julian, "A Study of the Motion and Aerodynamic Heating of Missiles Entering the Earth's Atmosphere at High Supersonic Speeds," NACA TN 4047, Washington, D.C.: National Advisory Committee for Aeronautics, October, 1957.

Assadourian, Arthur and Donald C. Cheatham, "Longitudinal Range Control During the Atmospheric Phase of a Manned Satellite Reentry," NASA TN D-253, Washington, D.C.: U.S. Government Printing Office, May 1960.

Babister, A. W., *Aircraft Dynamic Stability and Response*, Oxford, England: Pergamon Press, 1980.

Barbara, Frank J., "An Analytical Technique for Studying the Anomalous Roll Behavior of Re-entry Vehicles," *Journal of Spacecraft*, Vol. 6, No. 11 (November 1969): pp. 1279-1284.

Bohachevsky, Ihor O. and Robert E. Mates, "A Direct Method for Calculation of the Flow about an Axisymmetric Blunt Body at Angle of Attack," NASA CR-483, Washington, D.C.: U.S. Government Printing Office, May 1966.

Boltz, Frederick W., "Z-Function Solutions for the Motion and Heating During Atmosphere Entry from Equatorial Orbits of a Rotating Planet," NASA TN D-1555, Washington, D.C.: U.S. Government Printing Office, February 1963.

Brauer, G. L., et al., "Capabilities and Applications of the Program to Optimize Simulated Trajectories (POST): Program Summary Document," NASA CR-2770, Washington, D.C.: U.S. Government Printing Office, February 1977.

Brauer, G. L., et al., "Program to Optimize Simulated Trajectories (POST)," Vol. 1 to 3, Denver, Colorado: Martin Marietta Corporation, September 1987.

Brauer, G. L., et al., "Six-Degree-of-Freedom Program to Optimize Simulated Trajectories (6d POST)," Vol. 1 to 3, Denver, Colorado: Martin Marietta Corporation, September 1987.

Brofman, W., "Aerodynamic Stability of Planetary Entry-Vehicles," JPL TR No. 32-338, Pasadena, CA: Jet Propulsion Laboratory, September 24, 1962.

Center for Space Transportation and Applied Research (CSTAR), *Customer's Operational Guide*, Tullahoma, TN: CSTAR, March 23, 1992.

Chapman, Dean R., "An Analysis of the Corridor and Guidance Requirements for Supercircular Entry Into Planetary Atmospheres," NASA TR R-55, Washington, D.C.: U.S. Government Printing Office, 1960.

Chapman, Dean R., "An Approximate Analytical Method for Studying Entry Into Planetary Atmospheres," NASA TR R-11, Washington, D.C.: U.S. Government Printing Office, 1959.

Chapman, Dean R. and Arline K. Kaapphan, "Table of Z functions for Atmosphere Entry Analysis," NASA TR R-106, Washington, D.C.: U.S. Government Printing Office, 1961.

Charters, A. C., "The Linearized Equations of Motion Underlying the Dynamic Stability of Aircraft, Spinning Projectiles, and Symmetrical Missiles," NACA TN 3350, Washington, D.C.: National Advisory Committee for Aeronautics, January 1955.

The Chicago Manual of Style, Chicago, IL: The University of Chicago Press, 1982.

Chobotov, Vladimir A., *Spacecraft Attitude Dynamics and Control*, Malabar, FL: Krieger Publishing Company, 1991.

Cornelisse, J. W., et al., *Rocket Propulsion and Spacecraft Dynamics*, London: Pitman, 1979.

Duncan, C. D., *Dynamics of Atmospheric Entry*, New York: McGraw-Hill, 1962.

Dunning, Robert Scott, "The Orbital Mechanics of Flight Mechanics," NASA SP-325, Washington, D.C.: U.S. Government Printing Office, 1973.

East, R. A., "Hypersonic Static and Dynamic Stability," *Hypersonic Aerothermodynamics*, Lecture Series 1984-01, Paper presented at the Von Karman Institute for Fluid Dynamics, Belgium, February 6-10, 1984.

Eggers, Alfred J., ed., "Atmosphere Entry," AIAA Selected Reprint Series, Vol. 1, New York, New York: American Institute of Aeronautics and Astronautics.

Eggers, A. J., et al., "Stagnation-Point Heat Transfer to Blunt Shapes in Hypersonic Flight, Including Effects of Yaw," NACA TN 4229, Washington, D.C.: U.S. Government Printing Office, April 1958.

Eggleston, John M. and John W. Young, "Trajectory Control for Vehicles Entering the Earth's Atmosphere at Small Flight-Path Angles," NASA TR R-89, Washington, D.C.: U.S. Government Printing Office, 1961.

Everhart, Philip E., "Measurements of the Surface Flows, Heat Transfer, Pressure Distribution, and Longitudinal Stability of a Mercury Capsule Model at Mach Numbers of 6.9 and 9.6," NASA TM X-458, Washington, D.C.: U.S. Government Printing Office, April 1961.

Faget, Maxime A., et al., "Preliminary Studies of Manned Satellites Wingless Configuration: Nonlifting," NASA TN D-1254, Washington, D.C.: U.S. Government Printing Office, March 1962.

Faget, Maxime A., et al., "Space Capsule," Patent Number 3,093,346, United States Patent Office,, June 11, 1963.

Fine, J. H., "Stability of Flight Paths of Lifting Vehicles During Entry into Planetary Atmospheres," UTIA TN No. 48, AFOSR 1488, Toronto, Ontario, Canada: M. A. Sc. Thesis, University of Toronto, July 1961.

Fiedenthal, M. J., "Control of Re-entry From Orbit," Transactions of the Seventh Symposium on Ballistic Missile and Space Technology, Vol. II, Held at the United States Air Force Academy, 13-16 August 1962.

Garber, T. B., "On the Rotational Motion of a Body Re-entering the Atmosphere," *Journal of the Aero/Space Science*, (July 1959): pp. 443-449.

Gazley, Carl, Jr., "Deceleration and Heating of a Body Entering a Planetary Atmosphere from Space," Rand Paper P-955, Paper presented at the Convair-OSR Astronautics Symposium, San Diego, February 18-20, 1957.

Glover, Louis S., "Effects on Roll Rate of Mass and Aerodynamic Asymmetries for Ballistic Re-entry Bodies," *Journal of Spacecraft*, Vol.2, No. 2 (March-April 1965): pp. 220-225.

Goldstein, Herbert, *Classical Mechanics*, Reading, MA: Addison-Wesley Publishing Company, 1980.

Grant, Frederick C., "Importance of the Variation of Drag with Lift in Minimization of Satellite Entry Acceleration," NASA TN D-120, Washington, D.C.: U.S. Government Printing Office, October 1959.

Greenwood, Donald T., *Principles of Dynamics*. Englewood Cliffs, NJ: Prentice-Hall, 1988.

Griffin, Michael D. and James R. French, *Space Vehicle Design*. New York: AIAA, 1991.

Griffith, B. J. and D. E. Boylan, "Reynolds and Mach Number Simulation of Apollo and Gemini Re-entry and Comparison with Flight," AGARD Conference Proceedings No. 30, *Hypersonic Boundary Layers and Flow Fields*, Paper presented at a Specialists's Meeting of the Fluid Dynamics Panel of AGARD, Royal Aeronautical Society, London, 1-3 May 1968.

Hillje, Ernest R., "Entry Flight Aerodynamics From Apollo Mission AS-202," NASA TN D-4185, Washington, D.C.: U.S. Government Printing Office, October 1967.

Horiuchi, F. Y., "A Parametric Study of the Dynamic Motion of a Spinning and Non-Spinning Re-entry Vehicle with Non-linear Aerodynamic Characteristics," Paper presented at the Sixth Symposium on Ballistic Missile and Aerospace Technology.

Horstman, C. C. and M. I. Kussoy, "Free-flight Measurements of Aerodynamic Viscous Effects on Lifting Reentry Bodies," AIAA Paper No. 67-165, AIAA 5th Aerospace Sciences Meeting, New York, New York, January 23-26, 1967.

Intrieri, Peter F., "Effects of Transverse Center-of-Gravity Displacement, Afterbody Geometry, and Front-Face Curvature on the Aerodynamic Characteristics of Mercury-Type Models," NASA TM X-569, Washington, D.C.: U.S. Government Printing Office, June 1961.

James, Robert L., Jr., "A Three-Dimensional Trajectory Simulation Using Six Degrees of Freedom with Arbitrary Wind," NASA TN D-641, Washington, D.C.: U.S. Government Printing Office, March 1961.

Jensen, Jorgen, *et al., Design Guide to Orbital Flight*, New York: McGraw-Hill Book Company, 1962.

Johnston, Patrick and Curtis D. Snyder, "Static Longitudinal Stability and Performance of Several Ballistic Spacecraft Configurations in Helium at a Mach Number of 24.5," NASA TN D-1379, Washington, D.C.: U.S. Government Printing Office, August 1962.

Kaplan, Marshall H., *Modern Spacecraft Dynamics & Control.* New York: John Wiley & Sons, 1976.

Katzen, Elliott D. and Lionel L. Levy, Jr., "Atmosphere Entries with Vehicle Lift-Drag Ratio Modulated to Limit Deceleration and Rate of Deceleration-Vehicles with Maximum Lift-Drag Ratio of 0.5," NASA TN D-1145, Washington, D.C.: U.S. Government Printing Office, December 1961.

Koppenwallner, G., "Fundamentals of Hypersonics: Aerodynamics and Heat Transfer," *Hypersonic Aerothermodynamics*, Lecture Series 1984-01,Paper presented at the Von Karman Institute for Fluid Dynamics, Belgium, February 6-10, 1984.

Lees, Lester, "Ablation in Hypersonic Flows," *Reprint from the Seventh Anglo-American Aeronautical Conference*, (1960): pp. 254-267.

Leon, Herman I., "Angle of Attack Convergence of a Spinning Missile Descending Through the Atmosphere," *Journal of Aero/Space Science*, (August 1958): pp. 480-484.

Levy, Lionel L., "An Approximate Analytical Method for Studying Atmosphere Entry of Vehicles with Modulated Aerodynamic Forces," NASA TN D-319, Washington, D.C.: U.S. Government Printing Office, October 1960.

Levy, Lionel L., Jr., "The Use of Drag Modulation to Limit the Rate at which Deceleration Increases During Nonlifting Entry," NASA TN D-1037, Washington, D.C.: U.S. Government Printing Office, September 1961.

Lichtenstein, Jacob H., "Analytical Investigation of the Dynamic Behavior of a Nonlifting Manned Reentry Vehicle," NASA TN D-416, Washington, D.C.: U.S. Government Printing Office,, September 1960.

Loh, W. H. T., *Dynamics and Thermodynamics of Planetary Entry*, Englewood Cliffs, NJ: Prentice-Hall, Inc., 1963.

Loh, W. H. T., ed., *Re-entry and Planetary Entry Physics and Technology*, Pt. 1 & 2, Applied Physics and Engineering, an International Series, Vol.2 & 3, New York: Springer-Verlag, 1968.

Lovelace, Uriel M., et al., "Analysis of the Trajectory and Large-Amplitude Motions of a Scout Vehicle During Fourth-Stage Reentry Flight," NASA TN D-2309, Washington, D.C.: U.S. Government Printing Office, June 1964.

Low, George M., "Nearly Circular Transfer Trajectories for descending Satellites," NASA TR R-3, Washington, D.C.: U.S. Government Printing Office, 1959.

Luidens, Roger W., "Approximate Analysis of Atmospheric Entry Corridors and Angles," NASA TN D-590, Washington, D.C.: U.S. Government Printing Office, January 1961.

Luidens, Roger W., "Flight-Path Characteristics for Decelerating from Supercircular Speed," NASA TN D-1091, Washington, D.C.: U.S. Government Printing Office, December 1961.

Martin, John J., *Atmospheric Reentry: An introduction to its Science and Engineering*. Englewood Cliffs, NJ: Prentice-Hall, Inc., 1966.

Mayhue, Robert J., "Determination of Trajectory and Angles of Attack of A Scout Heat-Transfer Spacecraft During Reentry Flight in the Atmosphere," NASA TN D-2776, Washington, D.C.: U.S. Government Printing Office, May 1965.

Moseley, William C., Jr., et al., "Stability Characteristics of the Apollo Command Module," NASA TN D-3890, Washington, D.C.: U.S. Government Printing Office, March 1967.

Moss, Steven W., "Determination of Reentry Parameters During Descent from Low Earth Orbit," Master of Science Thesis, University of Tennessee, Knoxville, Tennessee, May 1991.

Moul, Martin T., et al., "Dynamic Stability and Control Problems of Piloted Reentry From Lunar Missions," NASA TN D-986, Washington, D.C.: U.S. Government Printing Office, November 1961.

National Aeronautics and Space Administration. "Apollo: Final Report, Aerodynamics," NASA CR-136719, Washington, D.C.: U.S. Government Printing Office, June 1961. **pp. v1 to v4 and B-20.**

National Aeronautics and Space Administration. *U.S. Standard Atmosphere, 1976*. Washington, D.C.: U.S. Government Printing Office,, October 1976.

Nielsen, Jack N., et al., "Three-Dimensional Orbits of Earth Satellites, Including Effects of Earth Oblateness and Atmospheric Rotation," NASA Memo 12-4-58A, Washington, D.C.: U.S. Government Printing Office, December 1958.

Nelson, Robert L., "The Motions of Rolling Symmetrical Missiles Referred to a Body-Axis System," NACA TN 3737, Washington, D.C.: National Advisory Committee for Aeronautics, November 1956.

Pearson, Albin O., "Wind-tunnel Investigation of the Static Longitudinal Aerodynamic Characteristics of Models of Reentry and Atmospheric-Abort

Configurations of a Proposed Apollo Spacecraft at Mach Numbers from 0.30 to 1.20," NASA TM X-604, Washington, D.C.: U.S. Government Printing Office, September 1961.

Peterson, Victor L., "Motions of a Short 10 deg. Blunted Cone Entering a Martian Atmosphere at Arbitrary Angles of Attack and Arbitrary Pitching Rates," NASA TN D-1326, Washington, D.C.: U.S. Government Printing Office, May 1962. pp. 10 to 12.

Pettus, Joseph J., "Persistent Re-entry Vehicle Roll Resonance," AIAA Paper No. 66-49, AIAA 3rd Aerospace Sciences Meeting, New York, New York, January 24-26, 1966.

Platus, D. H., "Ballistic Re-entry Vehicle Flight Dynamics," *Journal of Guidance*, Vol. 5, No. 1 (Jan.-Feb. 1982): pp. 4-16.

Platus, D. H., "Roll Resonance Control of Angle of Attack for Reentry Vehicle Drag Modulation," AIAA Paper No. 80-1574, 1980.

Platus, D. H., "A Simple Analysis of Reentry Vehicle Roll Resonance," Air Force Report No. SST-TR-67-25, Los Angeles, CA: U.S. Air Force, January 1967.

Price, D. A. and L. E. Ericsson, "A New Treatment of Roll-Pitch Coupling for Ballistic Re-entry Vehicles," *AIAA Journal*, Vol.8, No. 9 (September 1970): pp. 1608-1615.

Redd, Bass, et al., "Relationship Between the Aerodynamic Damping Derivatives Measured as a Function of Instantaneous Angular Displacement and the Aerodynamic Damping Derivatives Measured as a Function of Oscillation Amplitude," NASA TN D-2855, Washington, D.C.: U.S. Government Printing Office, June 1965.

Regan, Frank J., *Re-entry Vehicle Dynamics*. New York: AIAA, 1984.

Roberts, Leonard, "An Analysis of Ablation-Shield Requirements for Manned Reentry Vehicles," NASA TR R-62, Washington, D.C.: U.S. Government Printing Office, 1960.

Sammonds, Robert I., "Forces and Moments on an Apollo Model in Air at Mach Numbers to 35 and Effects of Changing Face and Corner Radii," NASA TM X-1086, Washington, D.C.: U.S. Government Printing Office, April 1965.

Seiff, Alvin and Michael E. Tauber, "Minimization of the Total Heat Input for Manned Vehicles Entering the Earth's Atmosphere at Hyperbolic Speeds," NASA TR R-236, Washington, D.C.: U.S. Government Printing Office, May 1966.

Slye, Robert E., "An Analytical Method for Studying the Lateral Motion of Atmosphere Entry Vehicles," NASA TN D-325, Washington, D.C.: U.S. Government Printing Office, September 1960.

Steketee, F.D., "Dynamic Stability of Space Vehicles.: Volume XI-Entry Disturbance and Control," NASA CR-945, Washington, D.C.: U.S. Government Printing Office, November 1967.

Stern, R. G. and S. T. Chu, "Landing Site Coverage for Orbital Lifting Re-entry Vehicles," SSD-TDR-63-97, Inglewood, CA: Commander Space Systems Division, United States Air Force, 1 April 1963.

Suttles, John T. and Lucille C. Coltrane, "A Study of Ballistic Reentry Trajectories at a Velocity of 50,000 Feet Per Second (15240 Meters Per Second)," NASA TN D-4011, Washington, D.C.: U.S. Government Printing Office, June 1961.

Thomson, William Tyrrell, *Introduction to Space Dynamics*, New York: Dover Publications, Inc., 1986.

Tobak, Murray and H. Julian Allan, "Dynamic Stability of Vehicles Traversing Ascending or Descending Paths through the Atmosphere," NACA TN 4275, Washington, D.C.: National Advisory Committee for Aeronautics, July 1958.

Tobak, Murray and Victor L. Peterson, "Analytical Study of the Tumbling Motions of Vehicles Entering Planetary Atmospheres," NASA TN D-1549, Washington, D.C.: U.S. Government Printing Office, October 1962.

Tobak, Murray and Victor L. Peterson, "Angle-of-Attack Convergence of Spinning Bodies Entering Planetary Atmospheres at Large Inclination to the Flight Path," NASA TR R-210, Washington, D.C.: U.S. Government Printing Office, October 1964.

Tobak, Murray and Victor L. Peterson, "Theory of Tumbling Bodies Entering Planetary Atmospheres with Applications to Probe Vehicles and the Australian Tektites," NASA TR R-203, Washington, D.C.: U.S. Government Printing Office, July 1964.

Tobak, Murray and William R. Wehrend, "Stability Derivatives of Cones at Supersonic Speeds," NACA TN 3788, Washington, D.C.: U.S. Government Printing Office, September 1956.

Tucker, Maurice, "Spacecraft Entry and Landing in Planetary Atmospheres," *Advances in Space Science and Technology*, Vol. 4, New York: Academic Press, 1962.

Vincze, John, "Gemini Spacecraft Parachute Landing System," NASA TN D-3496, Washington, D.C.: U.S. Government Printing Office, July 1966.

Vinh, Nguyen X., et al., *Hypersonic and Planetary Entry Flight Mechanics*. Ann Arbor, MI: The University of Michigan Press, 1980.

Vinh, Nguyen X. and Arthur J. Dobrzelecki, "Non-linear Longitudinal Dynamics of an Orbital Lifting Vehicle," NASA CR-1449, Washington, D.C.: U.S. Government Printing Office, October 1969.

Vinh, Nguyen X., *Optimal Trajectories in Atmospheric Flight*. Amsterdam, The Netherlands: Elsevier Scientific Publishing Company, 1981.

Wingrove, Rodney C., "Piloted Simulator Tests for a Guidance System which can continuously Predict Landing Point of a Low L/D Vehicle During Atmosphere Re-entry," NASA TN D-787, Washington, D.C.: U.S. Government Printing Office, March 1961.

Whitlock, Charles H., "Approximation of Reentry Angles of Attack for a Spinning Body from Rate-Gyro and Accelerometer Data," NASA TN D-3492, Washington, D.C.: U.S. Government Printing Office, July 1966.

Wiesel, William E., *Spaceflight Dynamics*, New York: McGraw-Hill Book Co., 1989.

Williams, Thomas, and Colin Kelley, *Gnuplot: An Interactive Plotting Program*. Version 2.0, Cambridge, MA: Free Software Foundation, Inc.

Wolverton, Raymond W., ed., *Flight Performance Handbook for Orbital Operations*, New York: John Wiley and Sons, 1963.

Wright, Bruce R. and Robert A. Kilgore, "Aerodynamic Damping and Oscillatory Stability in Pitch and Yaw of Gemini Configurations at Mach Numbers from 0.50 to 4.63," NASA TN D-3334, Washington, D.C.: U.S. Government Printing Office, March 1966.

Yaroshevskii, V. A., "The Approximate Calculation of Trajectories of Entry into the Atmosphere.I," Translated from *Космические Исследования* (*Kosmicheskie Issledovaniya*) Vol.2, No.4 (July-August, 1964): pp. 507-531.

Yaroshevskii, V. A., "The Approximate Calculation of the Trajectories of Entry into the Atmosphere.II," Translated from *Космические Исследования* (*Kosmicheskie Issledovaniya*) Vol.2, No.5 (September-October, 1964): pp. 679-697.

APPENDIXES

APPENDIX A: POST'S SIMULATION MODELS*

The Program to Optimize Simulated Trajectories (POST) (Brauer September 1987) has a tremendously detailed formulation of all the coordinate transformations, planet models, vehicle models, and trajectory simulations. In the present chapter only the necessary elements will be presented.

COORDINATE SYSTEMS (Brauer September 1987, 6D POST V.1 pp. (3-1)-(3-6))

Earth-Centered Inertial (ECI) Axes (x_I, y_I, z_I). This system is an Earth-centered Cartesian system with z_I coincident with the North Pole, x_I coincident with the Greenwich Meridian at time zero and in the equatorial plane, and y_I completing a right-hand system. The translational equations of motion are solved in the system (fig. A-1).

Earth-Centered Rotating (ECR) Axes (x_R, y_R, z_R). This system is an Earth-Centered Cartesian system with z_R coincident with the North Pole, x_R, coincident with the Greenwich Meridian at all times and in the equatorial plane, and y_R completing a right-hand system. This system is similar to the ECI system except that it rotates with the earth (fig. A-1).

Earth Position Coordinates (ϕ_g, θ, h). These are the familiar latitude, longitude and altitude designators. Latitude is positive in the Northern Hemisphere and negative in the Southern Hemisphere. Longitude is measured positive east of Greenwich. Altitude is measured positive above the surface of the planet (fig. A-1).

*This appendix has been essentially taken from Brauer September 1987, 6D POST V.1. In no way does the author of this thesis imply that the text is his own, except for minor modifications and additions specific to this research.

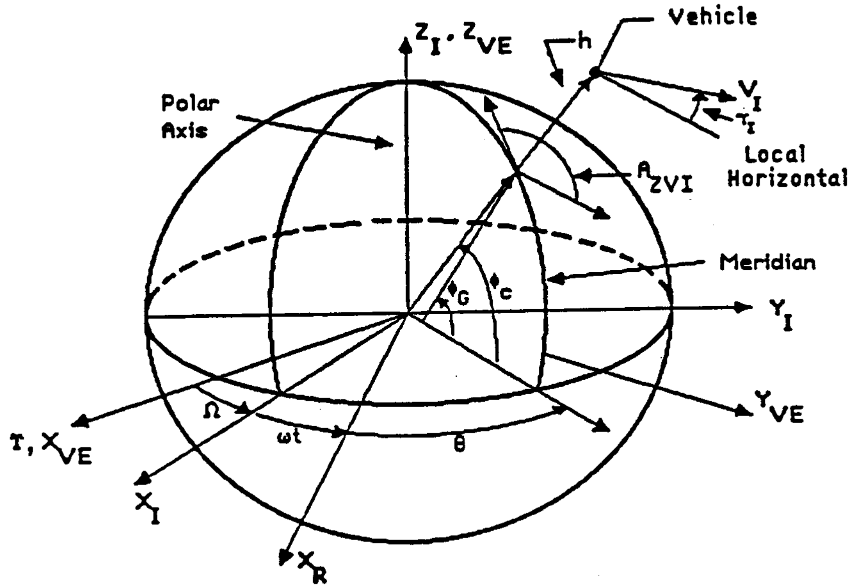

Figure A-1, Coordinate Systems (Brauer September 1987)

Geographic (G) Axes (x_G, y_G, z_G). This system is located at the surface of the planet at the present geocentric latitude and longitude of the vehicle. The x_G axis is in the local horizontal plane and points north, the y_G, axis is in the local horizontal plane and points east, and z_G completes a right-hand system. This system is used to calculate parameters associated with the azimuth and elevation angles (fig. A-1).

Inertial Launch (L) Axes (x_L, y_L, z_L). This is an inertial Cartesian system that is used as an inertial reference system from which the inertial attitude angles of the vehicle are measured. This coordinate system is automatically located at the geodetic latitude and inertial longitude of the vehicle at the beginning of the simulation. The orientation of this system is such that x_L is along the positive radius vector if the L-frame origin latitude, ϕ_L, is input as the geocentric latitude. z_L is in the local horizontal or tangent plane and is directed along the azimuth A_{ZL}, and y_L completes a right-hand system. The inertial angles, (ϕ_I, ψ_I, θ_I), are always measured with respect to this system (fig. A-2).

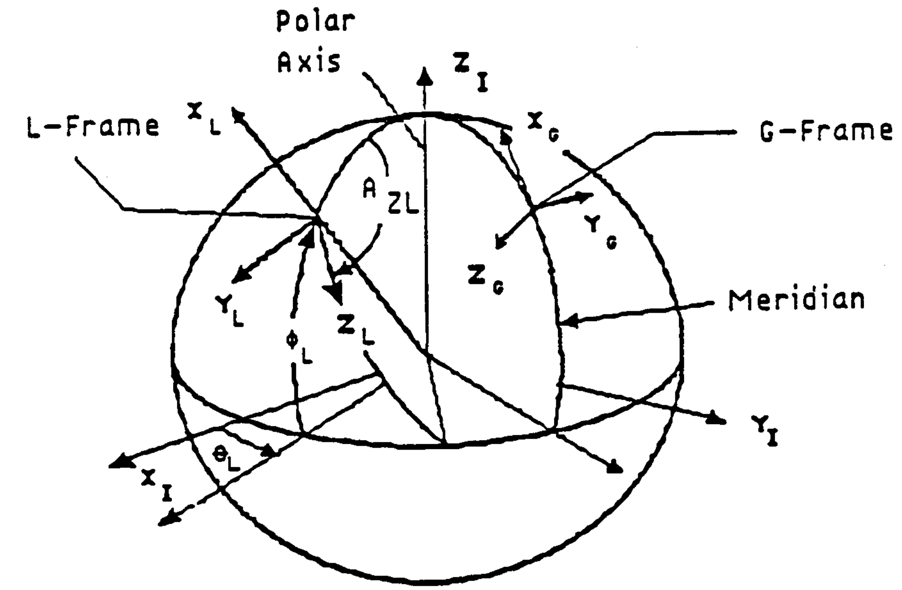

Figure A-2, Launch Frame (Brauer September 1987)

Body (B) Axes (x_B, y_B, z_B). The body axes form a right-hand Cartesian system aligned with the axes of the vehicle and centered at the vehicle's center of gravity. The x_B axis is directed forward along the longitudinal axis of the vehicle. The y_B axis is directed along the right wing and z_B is directed downward through the vehicle, completing a right-hand system. All aerodynamic and thrust forces are calculated in the body system. These forces are then transformed to the inertial (I) system where they are combined with the gravitational forces (fig A-3).

ATTITUDE ANGLES (Brauer September 1987, 6D POST V.1 pp. (3-5)-(3-6))

Inertial Euler angles (fig. A-4):

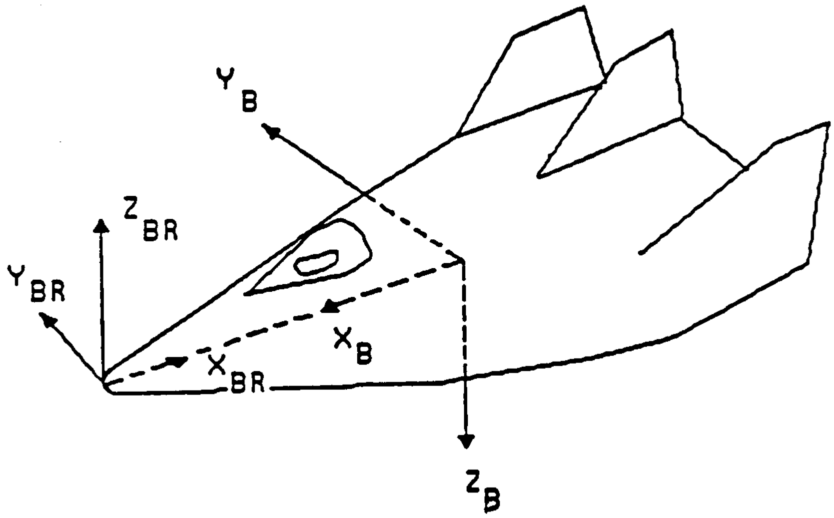

Figure A-3, Body Frame (Brauer September 1987)

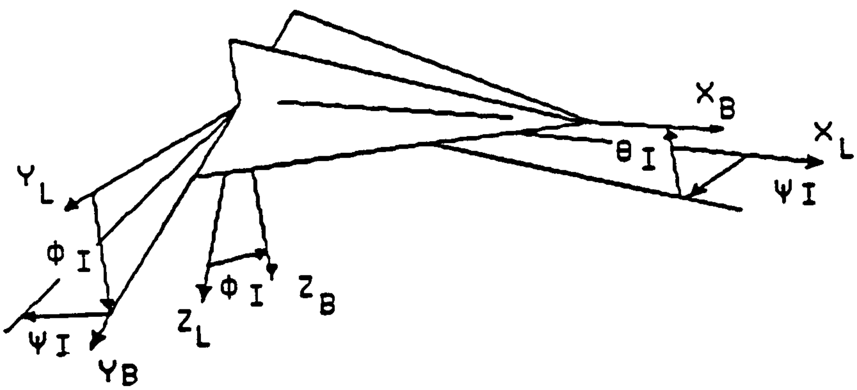

Figure A-4, Inertial Euler Angles (Brauer September 1987)

ϕ_I-Inertial roll angle. The roll angle with respect to the L-frame (first rotation)

ψ_I-Inertial yaw angle. The yaw angle with respect to the L-frame (second rotation).

θ_I-Inertial pitch angle. The pitch angle with respect to the L-frame (third rotation).

Relative Euler angles (fig. A-5):

ψ_R-Relative yaw angle. The yaw angle with respect to the G-frame (first rotation). This is the azimuth angle of the x_B axis measured clockwise from the yaw reference direction.

θ_R-Relative pitch angle. The pitch angle with respect to the G-frame (second rotation). This is the elevation angle of the x_B axis measured positive above the local horizontal plane.

ϕ_R-Relative roll angle. The roll angle with respect to the G-frame (third rotation). This is the roll angle about the x_B axis measured positive in the right-hand sense.

Aerodynamic angles (fig. A-6):

σ-Bank angle. Positive σ is a positive rotation about the atmosphere relative velocity vector (first rotation).

β-Sideslip angle. Positive β is nose-left (negative) rotation when flying the vehicle upright (second rotation).

α-Angle of attack. Positive α is nose-up (positive) rotation when flying the vehicle upright (third rotation).

COORDINATE TRANSFORMATIONS (Brauer September 1987, 6D POST V.1 pp. (3-7)-(3-10))

Many matrix transformations are required to transform data between the coordinate

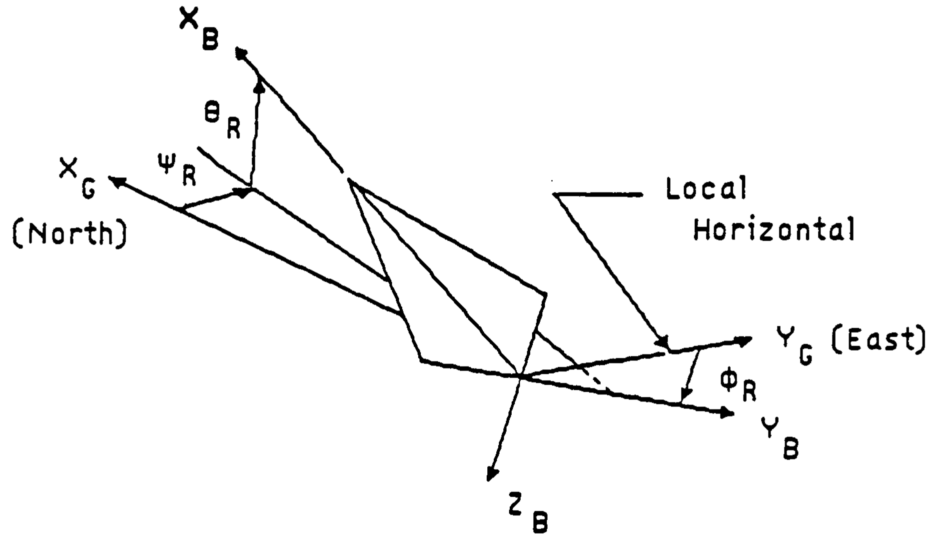

Figure A-5, Relative Euler Angles (Brauer September 1987)

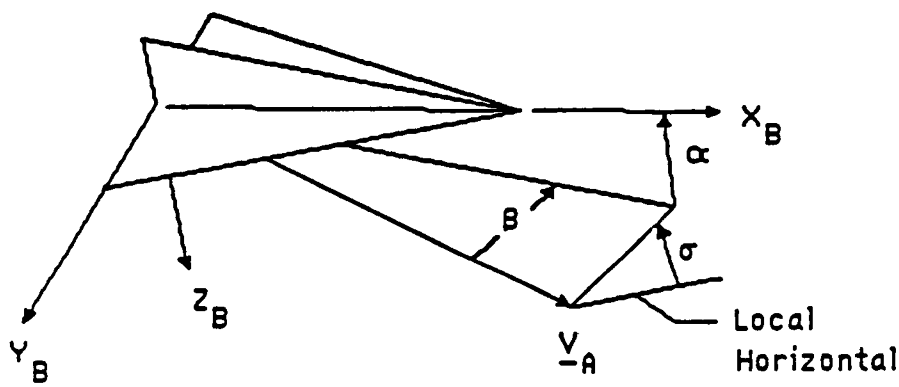

Figure A-6, Aerodynamic Angles (Brauer September 1987) systems (Brauer September 1987, 6D POST V.1 pp. 3-7). The most important of these transformations is the [IB] matrix. The inverse of this matrix is used to transform accelerations in the body frame to the planet-centered inertial frame. The remaining transformations are generally used to either compute [IB] or to transform auxiliary data into some convenient output coordinate system. The [IB] matrix is essentially dependent on the attitude of the vehicle. The following matrix equations are used to compute the [IB] matrix.

[IB] = [LB] [IL], (body rates or inertial Euler angles)

[IB] = [GB] [IG], (relative Euler angles)

[IB] = [AB] [GA] [IG], (aerodynamic angles)

The POST manual (Brauer September 1987, 6D POST V.1 pp. 3-8) gives a very understandable sketch of the transformations and their relations to each other (fig. A-7). POST summarizes these matrices below. The symbols s and c denote sine and cosine, respectively.

[IL] Inertial to Launch. The [IL] matrix depends on ϕ_L, θ_L, A_{ZL}, and is given by

$$[IL] = \begin{bmatrix} c\phi_L c\theta_L & c\phi_L s\theta_L & s\phi_L \\ s\phi_L c\theta_L sA_{ZL} - cA_{ZL} s\theta_L & sA_{ZL} s\phi_L s\theta_L + cA_{ZL} c\theta_L & -sA_{ZL} c\phi_L \\ -s\phi_L c\theta_L cA_{ZL} - sA_{ZL} s\theta_L & -cA_{ZL} s\phi_L s\theta_L + sA_{ZL} c\theta_L & cA_{ZL} c\phi_L \end{bmatrix} \qquad \textbf{A-1}$$

$$\begin{bmatrix} \dot{e}_0 \\ \dot{e}_1 \\ \dot{e}_2 \\ \dot{e}_3 \end{bmatrix} = \begin{bmatrix} -e_1 & e_2 & e_3 \\ e_0 & e_2 & -e_3 \\ e_0 & -e_1 & e_3 \\ e_0 & e_1 & -e_2 \end{bmatrix} \begin{bmatrix} \omega_x \\ \omega_y \\ \omega_z \end{bmatrix} \qquad \textbf{A-2}$$

where, $[\omega_x, \omega_y, \omega_z]^T = [p, q, r]^T$.

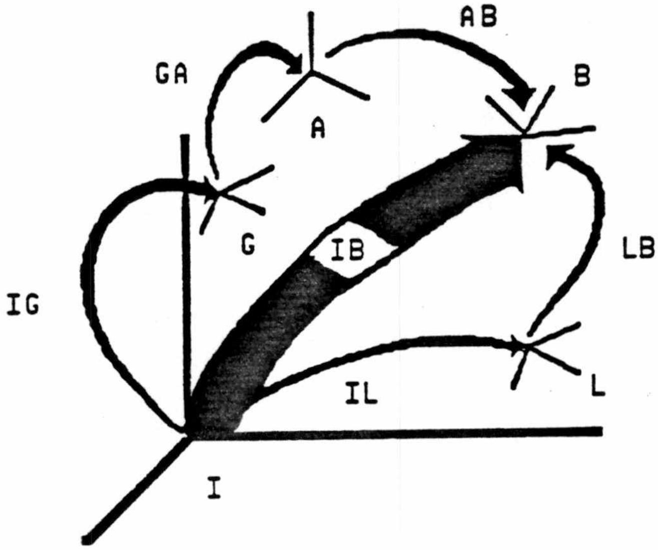

Figure A-7, Matrix Transformations (Brauer September 1987)

Equation A-2 is integrated to compute the [LB] matrix, which is given by,

$$[LB] = \begin{bmatrix} e_0^2+e_1^2-e_2^2-e_3^2 & 2(e_1e_2+e_0e_3) & 2(e_1e_3-e_0e_2) \\ 2(e_1e_2-e_0e_3) & e_0^2-e_1^2+e_2^2-e_3^2 & 2(e_0e_1+e_2e_3) \\ 2(e_1e_3+e_0e_2) & 2(e_2e_3-e_0e_1) & e_0^2-e_1^2-e_2^2+e_3^2 \end{bmatrix} \qquad \textbf{A-3}$$

When the inertial Euler angle is used, [LB] is computed directly as

$$[LB] = \begin{bmatrix} c\psi_I c\theta_I & c\phi_I s\psi_I c\theta_I + s\phi_I s\theta_I & s\phi_I s\psi_I c\theta_I - c\phi_I s\theta_I \\ -s\psi_I & c\phi_I c\psi_I & s\phi_I c\psi_I \\ c\psi_I s\theta_I & c\phi_I s\psi_I s\theta_I - s\phi_I c\theta_I & s\phi_I s\psi_I s\theta_I + c\phi_I c\theta_I \end{bmatrix} \qquad \textbf{A-4}$$

[IG], Inertial to Geographic. The [IG] matrix depends on the geocentric latitude and the inertial longitude, and is given by

$$[IG] = \begin{bmatrix} -s\phi_c c\theta_I & -s\phi_c s\theta_I & c\phi_c \\ -s\phi_I & c\theta_I & 0 \\ -c\phi_c c\theta_I & -\phi_c s\theta_I & s\phi_c \end{bmatrix} \qquad \textbf{A-5}$$

[GB], Geographic to Body. The [GB] matrix depends on the relative Euler angles and is given by

$$[GB] = \begin{bmatrix} c\theta_R c\psi_r & c\theta_R s\psi_R & -s\theta_R \\ s\phi_R s\theta_R c\psi_R - c\phi_r s\psi_R & s\phi_R s\theta_R s\psi_R + c\phi_R c\psi_R & s\phi_R c\theta_R \\ c\phi_R s\theta_R c\psi_R + s\phi_R s\psi_R & c\phi_R s\theta_R s\psi_R - s\phi_R c\psi_R & s\phi_R c\theta_R \end{bmatrix} \qquad \textbf{A-6}$$

[GA], Geographic to Atmospheric Relative Velocity System (ARVS). The [GA] matrix depends on the atmospheric relative flight azimuth and flight path angles and is given by

$$[GA] = \begin{bmatrix} c\gamma_A c\lambda_A & c\gamma_A s\lambda_A & -s\gamma_A \\ -s\lambda_A & c\lambda_A & 0 \\ s\gamma_A c\lambda_A & s\gamma_A s\lambda_A & c\gamma_A \end{bmatrix} \qquad \textbf{A-7}$$

[AB], AVRS to Body. The [AB] matrix depends on the aerodynamics angles, and is given by

$$[AB] = \begin{bmatrix} c\alpha c\beta & -c\alpha s\beta c\sigma + s\alpha s\sigma & -c\alpha s\beta s\sigma - s\alpha s\sigma \\ s\beta & c\beta c\sigma & c\beta s\sigma \\ s\alpha c\beta & -s\alpha s\beta c\sigma - c\alpha s\sigma & -s\alpha s\beta s\sigma + c\alpha c\sigma \end{bmatrix} \qquad \textbf{A-8}$$

PLANET MODEL (Brauer September 1987, 6D POST V.1 pp. 4-1)

Oblate Spheroid

The Smithsonian Earth model has been used in this research. The constants used are

R_E = 2.092566237 x 10^7 ft (Equatorial Radius),

R_P = 2.085550242 x 10^7 ft (Polar Radius),

Ω_P = 7.292115150 x 10^{-5} radians/sec (Earth's spin rate),

μ = 1.407645794 x 10^{16} ft^3 / sec^2, (Earth's gravitational constant, GM),

J_2 = 1.082639 x 10^{-3},

J_3 = -2.565 x 10^{-6},

J_4 = -1.608 x 10^{-6},

where the J's represent the harmonics in the gravity potential. The potential for this the Smithsonian model is

$$U = -\mu\left(\frac{1}{r} - \frac{J_2}{2}R_E^2\left(\frac{3z^2}{r^5} - \frac{1}{r^3}\right) - \frac{J_3}{2}R_E^3\left(\frac{5z^3}{r^7} - \frac{3z}{r^5}\right)\right) - \mu\left(-\frac{J_4}{8}R_E^4\left(\frac{35z^4}{r^9} - \frac{30z^2}{r^7} - \frac{3}{r^5}\right)\right) \tag{A-9}$$

From eq. A-9 one can calculate the gravitational accelerations

$$G_{XI} = -\frac{\partial U}{\partial x_I}$$
$$G_{YI} = -\frac{\partial U}{\partial y_I} \tag{A-10}$$
$$G_{ZI} = -\frac{\partial U}{\partial z_I}$$

where $r = (x_I^2+y_I^2+z_I^2)^{1/2}$. The geometry of the spheroid is illustrated in figure A-8. The other equations related to this model are

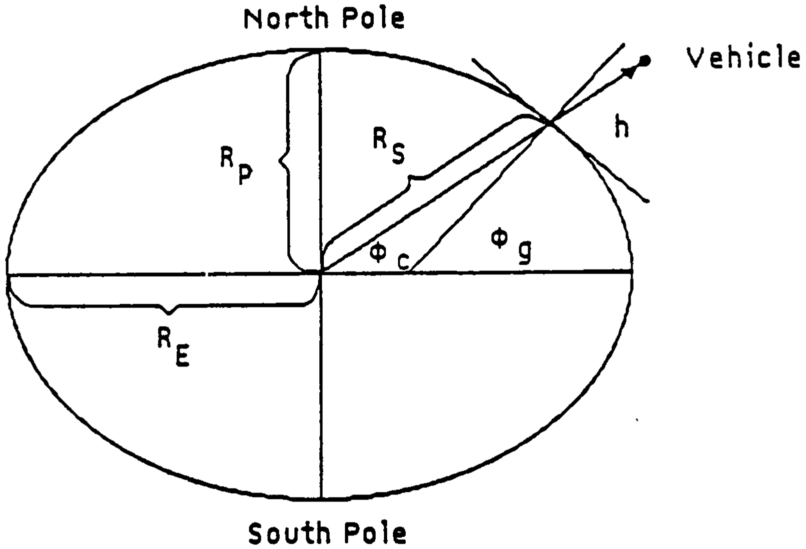

Figure A-8, Oblate Planet (Brauer September 1987)

$$\phi_c = \sin^{-1}\left(\frac{z_I}{r_I}\right)$$

$$\phi_g = \tan^{-1}(k\tan\phi_c), \quad k = \left(\frac{R_E}{R_P}\right)^2 \qquad \textbf{A-11}$$

$$R_s = R_E\left(1 + (k-1)\sin^2\phi_c\right)^{-1/2}$$

$$h = r_I - R_s \qquad \textbf{A-12}$$

where ϕ_c is the geocentric latitude, ϕ_g is the geodetic latitude, r_I is the distance from the center of the planet to the planet surface, and h is the distance from the planet surface to the vehicle.

Atmosphere Model.

The 1976 U.S. Standard Atmosphere model has been chosen for this research. The model is an idealized, steady-state representation of the Earth's atmosphere from the surface to 1000 km. For heights from the surface to 51 geopotential kilometers, the table of this standard are identical with those of the 1962 U.S. Standard Atmosphere and are based on traditional definitions (fig. A-9).

VEHICLE MODEL (Brauer September 1987, v.1 pp. 5-9)

Mass Properties Model

The moments and products of inertia are defined as the integrals

$$
\begin{aligned}
I_{xx} &= \int y^2 + z^2 \, dv, & I_{xy} &= \int xy \, dv, \\
I_{yy} &= \int x^2 + z^2 \, dv, & I_{xz} &= \int xz \, dv, \\
I_{zz} &= \int x^2 + y^2 \, dv, & I_{yz} &= \int yz \, dv,
\end{aligned}
$$

The inertia matrix is then

$$
[I] = \begin{bmatrix} I_{xx} & -I_{xy} & -I_{xz} \\ -I_{xy} & I_{yy} & -I_{yz} \\ -I_{xz} & -I_{yz} & I_{zz} \end{bmatrix}
$$

In POST [I] is generally input as a function of the weight of the vehicle. In this research [I] has been assumed to be constant, however. That is a reasonable assumption for the COMET's recovery vehicle since it lacks propulsion units. The shield ablates but the invariancy of [I] is still relatively small.

The center of gravity is referenced with respect to the vehicle reference frame (fig. A-3), and the components (x_{cg}, y_{cg}, z_{cg}) are input, in POST, as a function of vehicle weight. However, the location of the center of gravity has been assumed to be constant due to the argument above.

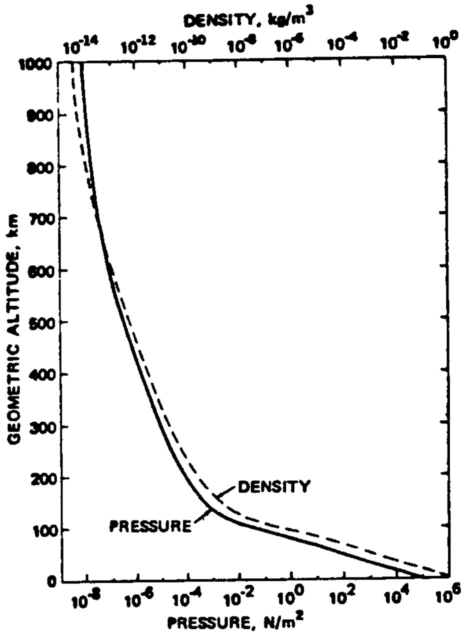

Figure A-9, Pressure and density vs. geometric altitude (U.S. Standard Atmosphere, 1976)

<u>Aerodynamic Calculations</u>

The aerodynamic force coefficients can be expressed in terms of lift, drag and side-force coefficients C_L, C_D, and C_Y or in terms of the axial force, normal force, and side force (C_A, C_N, and C_Y, respectively). C_L and C_D are directed normal to and coincident with the atmospheric relative velocity projection in the x_B - z_B plane and C_A and C_N produce forces that act in the $-x_B$ and $-z_B$ directions (fig. A-10). Axial and Normal force coefficients are transformed to lift and drag force coefficients as follows:

$$\begin{pmatrix} C_D \\ C_L \end{pmatrix} = \begin{bmatrix} \cos\alpha & \sin\alpha \\ -\sin\alpha & \cos\alpha \end{bmatrix} \begin{pmatrix} C_A \\ C_N \end{pmatrix} \qquad \textbf{A-13}$$

where α is the angle of attack.

If each aerodynamic coefficient is given as a table then POST would compute the coefficient by interpolating the values in the table. In general, POST, these tables can be dependent on up to three variables. In this research all the coefficients were assumed to

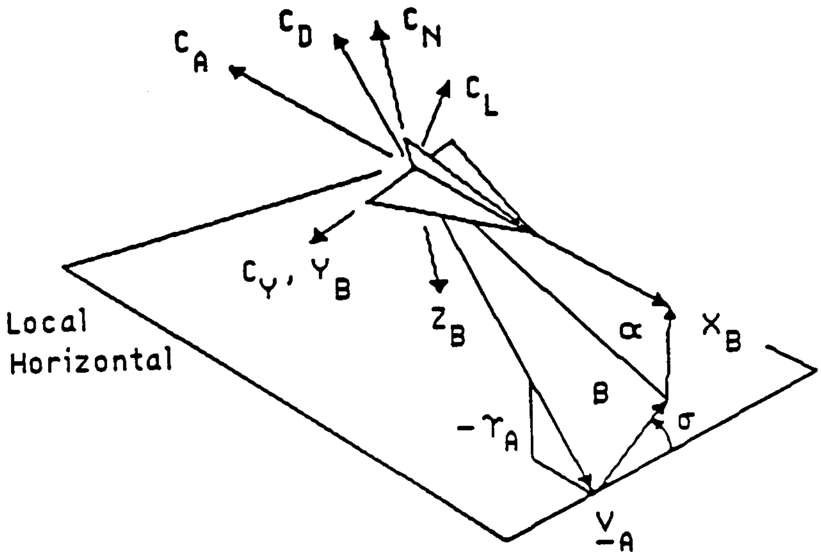

Figure A-10, Aerodynamic Angles (Brauer September 1987)

be functions of only α, however. Note that C_A was assumed to be a function of α_{total} since the COMET RV is an axisymmetric vehicle. That had to be assumed since $C_A(|\alpha|>0,|\beta|=0)\neq C_A(|\alpha|=0,|\beta|>0)$. The aerodynamic force coefficients are given by:

$$C_A = C_{A_0} + C_A(\alpha_T) \qquad \textbf{A-14}$$

$$C_N = C_{N_0} + C_N(\alpha) \qquad \textbf{A-15}$$

and

$$C_Y = C_{Y_0} + C_Y(\beta) \qquad \textbf{A-16}$$

The aerodynamic moment coefficients are given by:

$$C_l = C_{l_0} + C_l(\alpha) + C_{l_{r'}} r' + C_{l_{p'}} p' \qquad \textbf{A-17}$$

and

$$
\begin{aligned}
p' &= pd_R/2V_A = \omega_x d_R/2V_A \\
q' &= qd_P/2V_A = \omega_y d_P/2V_A \\
r' &= rd_Y/2V_A = \omega_z d_y/2V_A
\end{aligned}
\qquad \textbf{A-18}
$$

Aeroheating Calculations

Chapman's heating equation is used,

$$
\dot{Q} = \frac{17600}{\sqrt{R_N}}\left(\frac{\rho}{\rho_{SL}}\right)^{1/2}\left(\frac{V_A}{26000}\right)^{3.15} \qquad \textbf{A-19}
$$

where R_N is the nose radius, and ρ is the atmospheric density.

TRAJECTORY SIMULATION (Brauer September 1987, 6D POST V.1 6-1 to 6-11)

Translational Equations

The translational equations of motion are numerically solved in the planet-centered inertial coordinate system. These equations are

$$
\dot{\underline{r}}_I = \underline{V}_I \qquad \textbf{A-20}
$$

$$
\dot{\underline{V}}_I = [IB]^{-1}\left(\underline{A}_{AB}\right) + \underline{G}_I \qquad \textbf{A-21}
$$

$\underline{A}_{AB}$ is the aerodynamic acceleration in the body frame, and $\underline{G}_I$ is the gravitational acceleration in the ECI frame (The thrust acceleration has been dropped from eq. A-21).

For this research only one of the five options for the initializing the velocity vector and one for the position vector has been used.

Earth-Relative Local Horizontal (V_R, γ_R, A_{ZR}). The Earth-relative velocity components in the horizontal frame are first transformed to the geographic frame as

$$\underline{V}_{RG} = V_R \begin{pmatrix} \cos\gamma_r \cos A_{ZR} \\ \cos\gamma_R \sin A_{ZR} \\ -\sin\gamma_R \end{pmatrix} \qquad \textbf{A-22}$$

and then POST transforms it to the ECI frame by

$$\underline{V}_I = [IG]^{-1}\, \underline{V}_{RG} + \underline{\Omega}_p \times \underline{r}_I \qquad \textbf{A-23}$$

where

$$\underline{r}_I = r_I \begin{pmatrix} \cos\phi_c \cos\theta_I \\ \cos\phi_c \sin\theta_I \\ \sin\phi_c \end{pmatrix}$$

and ϕ_c is the geocentric latitude and θ_I is the inertial longitude.

Rotational Equations

The rotational equations of motion are solved in the body-centered coordinate system. These equations are

$$\underline{\dot{e}} = \frac{1}{2}[E]\underline{\omega}_B \qquad \textbf{A-24}$$

$$\underline{\dot{\omega}}_B = [I]^{-1}\left(\underline{M}_{AB} - [\dot{I}]\underline{\omega}_B - \underline{\omega}_B \times [I]\underline{\omega}_B\right) \qquad \textbf{A-25}$$

where $\underline{e}$ is a four-dimensional vector of quaternion parameters, [E] is the quaternion matrix defined above, $\underline{\omega}_B$ is the inertial angular velocity expressed in the body frame; $\underline{M}_{AB}$ is the moment caused by aerodynamic forces, and [I] is the inertia matrix given above.

APPENDIX B: THREE DEGREES-OF-FREEDOM INPUT FILE

```
P$SEARCH
C*********************************************************************
C  STARTED INPUTTING ON OCT. 1991, AT UT-CALSPAN CENTER FOR SPACE    *
C             TRANSPORTATION AND APPLIED RESEARCH                    *
C                                IN                                  *
C                      TULLAHOMA,  TENNESSEE                         *
C                                BY                                  *
C                         HAISAM K. IDO                              *
C*********************************************************************
 $
P$GENDAT
C TITLE(1)  = 19hCOMET ENTRY CAPSULE,
C********************************************************************
C                                3 DoF
C********************************************************************
 PRNC       =5,
 EVENT      = 1.,
 FESN       = 10.,
 NPC(2)     = 1,
 DT         = .05,
 MAXTIM     = 2500.,
 ALTMIN     =3280.,
 TIME       = 0.0,
 TIMRF(1)   = 1507.793,
C-------BELOW ARE THE INITIAL CONDITIONS OF THE VEHICLE---------
C NPC(4)=2, NPC(3)=4 INPUT PLANET-RELATIVE VELOCITY IN SPHERICAL
C COORDINATES.
C
 NPC(3)     = 4,
 NPC(4)     = 2,
C---------------------INITIAL CONDITIONS------------------------
C INITIAL ALTITude
 ALTITO     = 301830.438,
C GEODETIC LATITUDE IN DEG.
 GDLAT      = 40.306,
C LONGITUDE IN DEG.,INITIALLY
 LONG       = -124.975,
C RELATIVE VELOCITY (FT/SEC)
 VELR       =24816.715,
C INITIAL FLIGHT. PATH ANGLE,DEG.
 GAMMAR     = -3.008,
C INITIAL AZIMUTH ANGLE OF RELATIVE VELOCITY VECTOR, DEG.
 AZVELR     = 84.532,
C
C-------------------------------------------------------------
C-------------------------------------------------------------
C       ATMOSPHERE
C----NPC(5)=5 FLAG SELECTS THE 1976 U.S. STANDARD ATMOSPHERE----
 NPC(5)=5,
```

```
C---NPC(8)=2 FLAG SELECTS LIFT AND DRAG COEFFICIENTS.------------
 NPC(8)=2,
 NPC(10)=1,
C       AERODYNAMIC REFERENCES (POST6D,V.2,PG.6.A.1-4)
C FT**2
 SREF      =14.74803219,
C In FT taken from COMET
 LREF      =4.3333333,
C Lbs
 WGTSG     =926.,
C
C AEROHEATING CALCULATIONS (POST3D,V.2,PG.6.A.2-3)
C CALCULATE HEATRT AS THE MAXIMUM CENTERLINE HEAT RATE. (BTU/FT^2/s)
 NPC(15)   =1,
 RN        =2.6531666667,
C FT,NOSE RADIUS USED IN COMPUTING CHAPMAN HEATING RATE, USED IF
C NPC(15)=1,3,5
 NPC(26)   =0,
C CALCULATE ONLY STAGNATION POINT (AHI) ) (FT-LB/FT^2)AND DISPERSED
C STAG. PT. (AHIP) (FT-LB/FT^2)
C---------------------------------------------------------------
C       SMITHSONIAN EARTH MODEL (FROM POST3D,V.2,PG.8.C.1-5)
C---------------------------------------------------------------
C-----NPC(16)=0 USES THE GRAVITY MODEL FOR AN OBLATE PLANET,----
C---------------TAKEN FROM POST3D V.2,6.A.10-1------------------
 NPC(16)  =0,
C CONVERSION FACTOR FROM SLUGS TO LBM (LBM/SLUG)
 GO       =32.174,
C 2ND ZONAL HARMONIC COEFFICIENT IN EARTH POTENTIAL FUNCTION (ND)
 J2       =.001082639,
C NEWTONIAN GRAVITATIONAL CONSTANT (FT**3/SEC**2)
 MU       =1.407645794E+16,
C 3RD ZONAL HARMONIC COEFFICIENT (ND)
 J3       =-2.564E-06,
C 4TH ZONAL HARMONIC COEFFICIENT
 J4       =-1.608E-06,
C EARTH ROTATIONAL RATE (RAD/SEC)
 OMEGA    =7.292115146E-05,
C EARTH EQUATORIAL RADIUS (FT)
 RE       =20925662.73,
C EARTH POLAR RADIUS (FT)
 RP       =20855502.42,
C       PROPULSION,  NONE
C       RANGE CALCULATION
 NPC(12)  = 2,
 LATREF   = 40.52,
C (UTAH, UTTR)
 LONREF   = -113.6,
 AZREF    = -88.9322,
C       GUIDANCE (NONE)
 IGUID(14)=0,
```

```
C       INITIALIZE QUATERNIONS
 IGUID(12)=1
 ALPHA=-62.651,
 BETA=0.0,
 BNKANG=0.0,
C       PARACHUTE DRAG OPTION

C       PRINTOUT
 PINC     =5.0,
 PRNT(1)  =  4HTIME   ,6HALTITO,4HVELR   ,6HGAMMAR,4HMACH   ,6HAZVELR,
             5HGDLAT  ,4HLONG   ,6HDWNRNG,5HCRRNG  ,4HDENS   ,5HREYNO ,
             5HROLBD  ,5HPITBD  ,5HYAWBD  ,5HALPHA  ,4HBETA   ,6HBNKANG,
             4HASMG   ,3HAXB    ,3HAYB    ,3HAZB    ,4HDYNP   ,6HALPTOT,
             2HCD     ,2HCL     ,2HCA     ,2HCY     ,2HCN     ,2HCM    ,
             2HCW     ,6HTLHEAT,6HHEATRT,6HHEAT2D,5HHTURB  ,6HHTURBD,
 PRNT(37)= 5HPSTOP
C////////////////////THE TABLES SECTION//////////////////////
C-----------------------------------------------------------------
C       AERODYNAMIC INPUTS
C
 $
P$TBLMLT
 $
P$TAB
 TABLE     = 3HCDT, 0, 1.51,
 $
P$TAB
 TABLE     = 3HCLT, 0, 0.0,
  $
C-----------------------------------------------------------------
C       INPUT THE SIDE FORCE COEFFICIENT TABLES, CYOT AND CYBT
P$TAB
 TABLE     = 4HCYBT, 0, 0.0,
 $
P$TAB
 TABLE     = 4HCMAT, 0, 0.0,
 $
C Yaw moment coefficient
P$TAB
 TABLE     = 4HCWBT, 0, 0.0,
 $
C-----------------------------------------------------------------
C       CENTER OF GRAVITY LOCATIONS
P$TAB
 TABLE     = 4HXCGT, 0,0.801666667,
 $
P$TAB
 TABLE     = 4HYCGT, 0, 0.0,
 $
P$TAB
 TABLE     = 4HZCGT, 0, 0.0,
```

```
 ENDPHS     = 1,
 $
P$GENDAT
 EVENT      = 10.,
 CRITR      = 6HTIMRF1,
 VALUE      = 2500.,
 MDL        = 1,
 ENDPHS     = 1,
 ENDPRB     = 1,
 ENDJOB     = 1,
 $
```

APPENDIX C: SIX DEGREES-OF-FREEDOM INPUT FILE

```
P$SEARCH
C*******************************************************************
C  STARTED INPUTTING ON OCT. 1991, AT UT-CALSPAN CENTER FOR SPACE   *
C              TRANSPORTATION AND APPLIED RESEARCH                  *
C                                IN                                 *
C                       TULLAHOMA,  TENNESSEE                       *
C                                BY                                 *
C                          HAISAM K. IDO                            *
C*******************************************************************
 $
P$GENDAT
C TITLE(1)  =  19hCOMET ENTRY CAPSULE,
C******************************************************************
C              6 DoF 5 RPM, initial alpha=-62.651 DEG.              *
C*******************************************************************
 PRNC      = .1,
 EVENT     = 1.,
 FESN      = 10.,
 NPC(2)    = 1,
 DT        = .05,
 MAXTIM    = 500.,
 ALTMIN    =3280.,
 TIME      = 0.0,
C*********************************************************************
C NPC(4)=2, NPC(3)=4 INPUT PLANET-RELATIVE VELOCITY IN SPHERICAL
C COORDINATES.
 NPC(3)    = 4,
 NPC(4)    = 2,
C*********************************************************************
C         BELOW ARE THE INITIAL CONDITIONS OF THE VEHICLE
C INITIAL ALTITUDE
 ALTITO    = 301830.438,
C GEODETIC LATITUDE IN DEG.
 GDLAT     = 40.306,
C LONGITUDE IN DEG.,INITIALLY
 LONG      = -124.975,
C RELATIVE VELOCITY (FT/SEC)
 VELR      =24816.715,
C INITIAL FLIGHT. PATH ANGLE,DEG.
 GAMMAR    = -3.008,
C INITIAL AZIMUTH ANGLE OF RELATIVE VELOCITY VECTOR, DEG.
 AZVELR    = 84.532,
 AZL       = 84.532,
C*********************************************************************
C IAEROM=0 FLAG MEANS A SINGLE CENTER OF PRESSURE LOCATION
 IAEROM    = 1,
C*********************************************************************
C       ATMOSPHERE
C----NPC(5)=5 FLAG SELECTS THE 1976 U.S. STANDARD ATMOSPHERE----
```

```
 NPC(5)=5,
C---NPC(8)=1 FLAG SELECTS AXIAL,NORMAL AND SIDE FORCE COEFF.--
 NPC(8)=1,
 NPC(10)=1,
C**********************************************************************
C      AERODYNAMIC REFERENCES (POST6D,V.2,PG.6.A.1-4)
C FT**2
 SREF      =14.74803219,
C In FT taken from COMET
 DREFR     =4.3333333333,
 DREFP     =4.3333333333,
 DREFY     =4.3333333333,
 LREF      =4.3333333333,
C Lbs
 WGTSG     =926.,
C**********************************************************************
C       AEROHEATING CALCULATIONS (POST3D,V.2,PG.6.A.2-3)
C CALCULATE HEATRT AS THE MAXIMUM CENTERLINE HEAT RATE. (BTU/FT^2/s)
 NPC(15)   =1,
 RN        =2.1666666667,
C FT,NOSE RADIUS USED IN COMPUTING CHAPMAN HEATING RATE, USED IF
C NPC(15)=1,3,5
 NPC(26)   =0,
C CALCULATE ONLY STAGNATION POINT (AHI) ) (FT-LB/FT^2)AND DISPERSED
C STAG. PT. (AHIP) (FT-LB/FT^2)
C**********************************************************************
C      SMITHSONIAN EARTH MODEL (FROM POST3D,V.2,PG.8.C.1-5)
C-----NPC(16)=0 USES THE GRAVITY MODEL FOR AN OBLATE PLANET,----
C---------------TAKEN FROM POST3D V.2,6.A.10-1-----------------
 NPC(16)  =0,
C CONVERSION FACTOR FROM SLUGS TO LBM (LBM/SLUG)
 GO       =32.174,
C 2ND ZONAL HARMONIC COEFFICIENT IN EARTH POTENTIAL FUNCTION (ND)
 J2       =.001082639,
C NEWTONIAN GRAVITATIONAL CONSTANT (FT**3/SEC**2)
 MU       =1.407645794E+16,
C 3RD ZONAL HARMONIC COEFFICIENT (ND)
 J3       =-2.564E-06,
C 4TH ZONAL HARMONIC COEFFICIENT
 J4       =-1.608E-06,
C EARTH ROTATIONAL RATE (RAD/SEC)
 OMEGA    =7.292115146E-05,
C EARTH EQUATORIAL RADIUS (FT)
 RE       =20925662.73,
C EARTH POLAR RADIUS (FT)
 RP       =20855502.42,
C**********************************************************************
C      PROPULSION, NONE
C**********************************************************************
C      RANGE CALCULATION
 NPC(12)  = 2,
```

```
 LATREF   = 40.52,
C (UTAH)
 LONREF   = -113.6,
 AZREF    = -88.9322,
C*********************************************************************
C       GUIDANCE (NONE)
 IGUID(14)=0,
C*********************************************************************
C       INITIALIZE QUATERNIONS
 IGUID(12)=3
C RELATIVE YAW ANGLE,DEFINED AS THE AZIMUTH ANGLE OF THE
C XB AXIS, MEASURED CLOCKWISE FROM G_FRAME (POST3D,V.2,6.B.4-1)
 YAWR     =84.532,
 PITR     =-65.659,
 ROLR     =0.0,
C       ANGULAR RATES
C ABOUT THE XB AXIS IN DEG/SEC, 540=90 rpm, 75 rpm=450 deg/sec
 ROLBD    =30.,
 PITBD    =0.0,
C ABOUT THE ZB-AXIS IN DEG/SEC
 YAWBD    =0.0,
C*********************************************************************
C       PARACHUTE DRAG OPTION / NONE
C*********************************************************************
C       PRINT OUT
 PINC     = 5.,
 PRNT(1)  =  4HTIME   ,6HALTITO,4HVELR   ,6HGAMMAR,4HMACH   ,6HAZVELR,
             5HGDLAT  ,5HGCLAT  ,4HLONG   ,6HDWNRNG,5HCRRNG  ,4HDENS   ,
             5HROLBD  ,5HPITBD  ,5HYAWBD  ,6HROLBDD,6HPITBDD,6HYAWBDD,
             4HROLR   ,4HPITR   ,4HYAWR   ,5HALPHA  ,4HBETA   ,6HALPTOT,
             5HYAWRD  ,5HPITRD  ,5HROLRD  ,3HAXB    ,3HAYB    ,3HAZB    ,
             4HDYNP   ,4HASMG   ,4HDRAG   ,4HLIFT   ,4HFAYB   ,4HAMYB   ,
             4HAMZB   ,3HCMQ    ,3HCWR    ,
 PRNT(40)= 5HPSTOP
C////////////////////THE TABLES SECTION////////////////////////////////
 $
P$TBLMLT
 $
C*********************************************************************
C                           AERODYNAMIC INPUTS
C*********************************************************************
C                   STATIC AERODYNAMIC COEFFICIENTS
C                 TAKEN FROM SII'S NEWTONIAN ESTIMATES
C*********************************************************************
C                              NPC(8)=1
C       INPUT THE AXIAL FORCE COEF. TABLES, CAOT AND CAT
C       INPUT THE NORMAL FORCE COEF. TABLES, CNOT AND CNAT
P$TAB
 TABLE     = 3HCAT, 1,6HALPTOT,161,1,1,1,
             -80,0.03250,-79,0.04370,-78,0.05570,-77,0.06870,-76,0.08250,
             -75,0.09710,-74,0.11260,-73,0.12880,-72,0.14580,-71,0.16360,
```

```
         -70,0.18220,-69,0.20140,-68,0.20140,-67,0.24200,-66,0.26320,
         -65,0.28510,-64,0.30760,-63,0.33060,-62,0.35420,-61,0.37820,
         -60,0.40280,-59,0.42780,-58,0.45320,-57,0.47900,-56,0.50510,
         -55,0.53160,-54,0.55840,-53,0.58540,-52,0.61270,-51,0.64010,
         -50,0.66770,-49,0.69540,-48,0.72320,-47,0.75110,-46,0.77900,
         -45,0.80690,-44,0.83470,-43,0.86250,-42,0.89010,-41,0.91760,
         -40,0.94500,-39,0.97210,-38,0.99890,-37, 1.0255,-36, 1.0518,
         -35, 1.0777,-34, 1.1033,-33, 1.1284,-32, 1.1531,-31, 1.1774,
         -30, 1.2011,-29, 1.2243,-28, 1.2470,-27, 1.2691,-26, 1.2906,
         -25, 1.3114,-24, 1.3316,-23, 1.3511,-22, 1.3699,-21, 1.3880,
         -20, 1.4053,-19, 1.4218,-18, 1.4376,-17, 1.4525,-16, 1.4666,
         -15, 1.4799,-14, 1.4922,-13, 1.5037,-12, 1.5144,-11, 1.5241,
         -10, 1.5351, -9, 1.5433, -8, 1.5507, -7, 1.5572, -6, 1.5628,
          -5, 1.5676, -4, 1.5716, -3, 1.5747, -2, 1.5768, -1, 1.5782,
           0, 1.5786,
           1, 1.5782,  2, 1.5768,  3, 1.5747,  4, 1.5716,  5, 1.5676,
           6, 1.5628,  7, 1.5572,  8, 1.5507,  9, 1.5433, 10, 1.5351,
          11, 1.5241, 12, 1.5144, 13, 1.5037, 14, 1.4922, 15, 1.4799,
          16, 1.4666, 17, 1.4525, 18, 1.4376, 19, 1.4218, 20, 1.4053,
          21, 1.3880, 22, 1.3699, 23, 1.3511, 24, 1.3316, 25, 1.3114,
          26, 1.2906, 27, 1.2691, 28, 1.2470, 29, 1.2243, 30, 1.2011,
          31, 1.1774, 32, 1.1531, 33, 1.1284, 34, 1.1033, 35, 1.0777,
          36, 1.0518, 37, 1.0255, 38,0.99890, 39,0.97210, 40,0.94500,
          41,0.91760, 42,0.89010, 43,0.86250, 44,0.83470, 45,0.80690,
          46,0.77900, 47,0.75110, 48,0.72320, 49,0.69540, 50,0.66770,
          51,0.64010, 52,0.61270, 53,0.58540, 54,0.55840, 55,0.53160,
          56,0.50510, 57,0.47900, 58,0.45320, 59,0.42780, 60,0.40280,
          61,0.37820, 62,0.35420, 63,0.33060, 64,0.30760, 65,0.28510,
          66,0.26320, 67,0.24200, 68,0.22140, 69,0.20140, 70,0.18220,
          71,0.16360, 72,0.14580, 73,0.12880, 74,0.11260, 75,0.09710,
          76,0.08250, 77,0.06870, 78,0.05570, 79,0.04370, 80,0.03250,
$
P$TAB
 TABLE   = 4HCNAT, 1, 5HALPHA,161,1,1,1,
         -80,-.8967,-79,-.8902,-78,-.8831,-77,-.8756,-76,-.8677,
         -75,-.8592,-74,-.8503,-73,-.8410,-72,-.8312,-71,-.8210,
         -70,-.8104,-69,-.7993,-68,-.7880,-67,-.7762,-66,-.7641,
         -65,-.7516,-64,-.7388,-63,-.7257,-62,-.7124,-61,-.6987,
         -60,-.6848,-59,-.6706,-58,-.6562,-57,-.6416,-56,-.6268,
         -55,-.6119,-54,-.5968,-53,-.5815,-52,-.5661,-51,-.5507,
         -50,-.5351,-49,-.5195,-48,-.5039,-47,-.4882,-46,-.4725,
         -45,-.4568,-44,-.4412,-43,-.4256,-42,-.4101,-41,-.3947,
         -40,-.3794,-39,-.3643,-38,-.3492,-37,-.3344,-36,-.3197,
         -35,-.3052,-34,-.2910,-33,-.2770,-32,-.2632,-31,-.2497,
         -30,-.2365,-29,-.2236,-28,-.2110,-27,-.1987,-26,-.1868,
         -25,-.1753,-24,-.1641,-23,-.1534,-22,-.1430,-21,-.1330,
         -20,-.1235,-19,-.1144,-18,-.1058,-17,-.0977,-16,-.0900,
         -15,-.0827,-14,-.0760,-13,-.0698,-12,-.0641,-11,-.0589,
         -10,-.0464, -9,-.0419, -8,-.0374, -7,-.0328, -6,-.0282,
          -5,-.0236, -4,-.0189, -3,-.0142, -2,-.0095, -1,-.0047,
         0.0,0.0000,
```

```
             1,0.0047,  2,0.0095,  3,0.0142,  4,0.0189,  5,0.0236,
             6,0.0282,  7,0.0328,  8,0.0374,  9,0.0419, 10,0.0464,
            11,0.0589, 12,0.0641, 13,0.0698, 14,0.0760, 15,0.0827,
            16,0.0900, 17,0.0977, 18,0.1058, 19,0.1144, 20,0.1235,
            21,0.1330, 22,0.1430, 23,0.1534, 24,0.1641, 25,0.1753,
            26,0.1868, 27,0.1987, 28,0.2110, 29,0.2236, 30,0.2365,
            31,0.2497, 32,0.2632, 33,0.2770, 34,0.2910, 35,0.3052,
            36,0.3197, 37,0.3344, 38,0.3492, 39,0.3643, 40,0.3794,
            41,0.3947, 42,0.4101, 43,0.4256, 44,0.4412, 45,0.4568,
            46,0.4725, 47,0.4882, 48,0.5039, 49,0.5195, 50,0.5351,
            51,0.5507, 52,0.5661, 53,0.5815, 54,0.5968, 55,0.6119,
            56,0.6268, 57,0.6416, 58,0.6562, 59,0.6706, 60,0.6848,
            61,0.6987, 62,0.7124, 63,0.7257, 64,0.7388, 65,0.7516,
            66,0.7641, 67,0.7762, 68,0.7880, 69,0.7993, 70,0.8104,
            71,0.8210, 72,0.8312, 73,0.8410, 74,0.8503, 75,0.8592,
            76,0.8677, 77,0.8756, 78,0.8831, 79,0.8902, 80,0.8967,
 $
C        INPUT THE SIDE FORCE COEFFICIENT TABLES, CYOT AND CYBT
P$TAB
 TABLE      = 4HCYBT, 1, 4HBETA,161,1,1,1,
            -80,0.8967,-79,0.8902,-78,0.8831,-77,0.8756,-76,0.8677,
            -75,0.8592,-74,0.8503,-73,0.8410,-72,0.8312,-71,0.8210,
            -70,0.8104,-69,0.7993,-68,0.7880,-67,0.7762,-66,0.7641,
            -65,0.7516,-64,0.7388,-63,0.7257,-62,0.7124,-61,0.6987,
            -60,0.6848,-59,0.6706,-58,0.6562,-57,0.6416,-56,0.6268,
            -55,0.6119,-54,0.5968,-53,0.5815,-52,0.5661,-51,0.5507,
            -50,0.5351,-49,0.5195,-48,0.5039,-47,0.4882,-46,0.4725,
            -45,0.4568,-44,0.4412,-43,0.4256,-42,0.4101,-41,0.3947,
            -40,0.3794,-39,0.3643,-38,0.3492,-37,0.3344,-36,0.3197,
            -35,0.3052,-34,0.2910,-33,0.2770,-32,0.2632,-31,0.2497,
            -30,0.2365,-29,0.2236,-28,0.2110,-27,0.1987,-26,0.1868,
            -25,0.1753,-24,0.1641,-23,0.1534,-22,0.1430,-21,0.1330,
            -20,0.1235,-19,0.1144,-18,0.1058,-17,0.0977,-16,0.0900,
            -15,0.0827,-14,0.0760,-13,0.0698,-12,0.0641,-11,0.0589,
            -10,0.0464, -9,0.0419, -8,0.0374, -7,0.0328, -6,0.0282,
             -5,0.0236, -4,0.0189, -3,0.0142, -2,0.0095, -1,0.0047,
             0,0.0000,
             1,-.0047,  2,-.0095,  3,-.0142,  4,-.0189,  5,-.0236,
             6,-.0282,  7,-.0328,  8,-.0374,  9,-.0419, 10,-.0464,
            11,-.0589, 12,-.0641, 13,-.0698, 14,-.0760, 15,-.0827,
            16,-.0900, 17,-.0977, 18,-.1058, 19,-.1144, 20,-.1235,
            21,-.1330, 22,-.1430, 23,-.1534, 24,-.1641, 25,-.1753,
            26,-.1868, 27,-.1987, 28,-.2110, 29,-.2236, 30,-.2365,
            31,-.2497, 32,-.2632, 33,-.2770, 34,-.2910, 35,-.3052,
            36,-.3197, 37,-.3344, 38,-.3492, 39,-.3643, 40,-.3794,
            41,-.3947, 42,-.4101, 43,-.4256, 44,-.4412, 45,-.4568,
            46,-.4725, 47,-.4882, 48,-.5039, 49,-.5195, 50,-.5351,
            51,-.5507, 52,-.5661, 53,-.5815, 54,-.5968, 55,-.6119,
            56,-.6268, 57,-.6416, 58,-.6562, 59,-.6706, 60,-.6848,
            61,-.6987, 62,-.7124, 63,-.7257, 64,-.7388, 65,-.7516,
            66,-.7641, 67,-.7762, 68,-.7880, 69,-.7993, 70,-.8104,
```

```
            71,-.8210, 72,-.8312, 73,-.8410, 74,-.8503, 75,-.8592,
            76,-.8677, 77,-.8756, 78,-.8831, 79,-.8902, 80,-.8967,
 $
C       INPUT THE MOMENT COEFFICIENT ABOUT C.G.
P$TAB
 TABLE     = 4HCMAT, 1, 5HALPHA,161,1,1,1,
           -80,0.0991,-79,0.1011,-78,0.1031,-77,0.1051,-76,0.1069,
           -75,0.1087,-74,0.1103,-73,0.1119,-72,0.1134,-71,0.1148,
           -70,0.1161,-69,0.1173,-68,0.1184,-67,0.1194,-66,0.1203,
           -65,0.1211,-64,0.1219,-63,0.1225,-62,0.1230,-61,0.1234,
           -60,0.1234,-59,0.1238,-58,0.1239,-57,0.1239,-56,0.1238,
           -55,0.1236,-54,0.1232,-53,0.1228,-52,0.1222,-51,0.1216,
           -50,0.1208,-49,0.1200,-48,0.1190,-47,0.1180,-46,0.1168,
           -45,0.1156,-44,0.1142,-43,0.1128,-42,0.1113,-41,0.1097,
           -40,0.1080,-39,0.1062,-38,0.1043,-37,0.1023,-36,0.1003,
           -35,0.0982,-34,0.0960,-33,0.0938,-32,0.0914,-31,0.0890,
           -30,0.0866,-29,0.0841,-28,0.0815,-27,0.0789,-26,0.0762,
           -25,0.0735,-24,0.0707,-23,0.0679,-22,0.0651,-21,0.0622,
           -20,0.0593,-19,0.0564,-18,0.0534,-17,0.0504,-16,0.0475,
           -15,0.0445,-14,0.0414,-13,0.0384,-12,0.0354,-11,0.0324,
           -10,0.0274, -9,0.0248, -8,0.0221, -7,0.0194, -6,0.0167,
            -5,0.0139, -4,0.0111, -3,0.0084, -2,0.0056, -1,0.0028,
             0,0.0000,
             1,-.0028,  2,-.0056,  3,-.0084,  4,-.0111,  5,-.0139,
             6,-.0167,  7,-.0194,  8,-.0221,  9,-.0248, 10,-.0274,
            11,-.0324, 12,-.0354, 13,-.0384, 14,-.0414, 15,-.0445,
            16,-.0475, 17,-.0504, 18,-.0534, 19,-.0564, 20,-.0593,
            21,-.0622, 22,-.0651, 23,-.0679, 24,-.0707, 25,-.0735,
            26,-.0762, 27,-.0789, 28,-.0815, 29,-.0841, 30,-.0866,
            31,-.0890, 32,-.0914, 33,-.0938, 34,-.0960, 35,-.0982,
            36,-.1003, 37,-.1023, 38,-.1043, 39,-.1080, 40,-.1097,
            41,-.1097, 42,-.1113, 43,-.1128, 44,-.1142, 45,-.1156,
            46,-.1168, 47,-.1180, 48,-.1190, 49,-.1200, 50,-.1208,
            51,-.1216, 52,-.1222, 53,-.1228, 54,-.1232, 55,-.1236,
            56,-.1238, 57,-.1239, 58,-.1239, 59,-.1238, 60,-.1237,
            61,-.1234, 62,-.1230, 63,-.1225, 64,-.1219, 65,-.1211,
            66,-.1203, 67,-.1194, 68,-.1184, 69,-.1173, 70,-.1161,
            71,-.1148, 72,-.1134, 73,-.1119, 74,-.1103, 75,-.1087,
            76,-.1069, 77,-.1051, 78,-.1031, 79,-.1011, 80,-.0991,
 $
C                        Yaw moment coefficient
P$TAB
 TABLE     = 4HCWBT, 1, 4HBETA,161,1,1,1,
           -80,-.0991,-79,-.1011,-78,-.1031,-77,-.1051,-76,-.1069,
           -75,-.1087,-74,-.1103,-73,-.1119,-72,-.1134,-71,-.1148,
           -70,-.1161,-69,-.1173,-68,-.1184,-67,-.1194,-66,-.1203,
           -65,-.1211,-64,-.1219,-63,-.1225,-62,-.1230,-61,-.1234,
           -60,-.1234,-59,-.1238,-58,-.1239,-57,-.1239,-56,-.1238,
           -55,-.1236,-54,-.1232,-53,-.1228,-52,-.1222,-51,-.1216,
           -50,-.1208,-49,-.1200,-48,-.1190,-47,-.1180,-46,-.1168,
           -45,-.1156,-44,-.1142,-43,-.1128,-42,-.1113,-41,-.1097,
```

```
              -40,-.1080,-39,-.1062,-38,-.1043,-37,-.1023,-36,-.1003,
              -35,-.0982,-34,-.0960,-33,-.0938,-32,-.0914,-31,-.0890,
              -30,-.0866,-29,-.0841,-28,-.0815,-27,-.0789,-26,-.0762,
              -25,-.0735,-24,-.0707,-23,-.0679,-22,-.0651,-21,-.0622,
              -20,-.0593,-19,-.0564,-18,-.0534,-17,-.0504,-16,-.0475,
              -15,-.0445,-14,-.0414,-13,-.0384,-12,-.0354,-11,-.0324,
              -10,-.0274, -9,-.0248, -8,-.0221, -7,-.0194, -6,-.0167,
               -5,-.0139, -4,-.0111, -3,-.0084, -2,-.0056, -1,-.0028,
                0,0.0000,
                1,0.0028,  2,0.0056,  3,0.0084,  4,0.0111,  5,0.0139,
                6,0.0167,  7,0.0194,  8,0.0221,  9,0.0248, 10,0.0274,
               11,0.0324, 12,0.0354, 13,0.0384, 14,0.0414, 15,0.0445,
               16,0.0475, 17,0.0504, 18,0.0534, 19,0.0564, 20,0.0593,
               21,0.0622, 22,0.0651, 23,0.0679, 24,0.0707, 25,0.0735,
               26,0.0762, 27,0.0789, 28,0.0815, 29,0.0841, 30,0.0866,
               31,0.0890, 32,0.0914, 33,0.0938, 34,0.0960, 35,0.0982,
               36,0.1003, 37,0.1023, 38,0.1043, 39,0.1080, 40,0.1097,
               41,0.1097, 42,0.1113, 43,0.1128, 44,0.1142, 45,0.1156,
               46,0.1168, 47,0.1180, 48,0.1190, 49,0.1200, 50,0.1208,
               51,0.1216, 52,0.1222, 53,0.1228, 54,0.1232, 55,0.1236,
               56,0.1238, 57,0.1239, 58,0.1239, 59,0.1238, 60,0.1237,
               61,0.1234, 62,0.1230, 63,0.1225, 64,0.1219, 65,0.1211,
               66,0.1203, 67,0.1194, 68,0.1184, 69,0.1173, 70,0.1161,
               71,0.1148, 72,0.1134, 73,0.1119, 74,0.1103, 75,0.1087,
               76,0.1069, 77,0.1051, 78,0.1031, 79,0.1011, 80,0.0991,
 $
C**********************************************************************
C         THE FOLLOWING ARE THE DYNAMIC DAMPING COEFFICIENTS
P$TAB
C   CMQ = THE PITCHING MOMENT DAMPING DERIVATIVE COEFFICIENT DUE TO THE
C         NONDIMENSIONAL PITCH RATE.
  TABLE= 4HCMQT,1,5HALPHA,161,1,1,1,
         -80,0.0404,-79,0.0393,-78,0.0381,-77,0.0368,-76,0.0354,
         -75,0.0339,-74,0.0323,-73,0.0307,-72,0.0290,-71,0.0272,
         -70,0.0253,-69,0.0234,-68,0.0214,-67,0.0193,-66,0.0172,
         -65,0.0150,-64,0.0127,-63,0.0103,-62,0.0079,-61,0.0054,
         -60,0.0028,-59,0.0002,-58,-.0025,-57,-.0053,-56,-.0081,
         -55,-.0110,-54,-.0140,-53,-.0170,-52,-.0201,-51,-.0233,
         -50,-.0266,-49,-.0299,-48,-.0333,-47,-.0368,-46,-.0403,
         -45,-.0440,-44,-.0477,-43,-.0515,-42,-.0554,-41,-.0594,
         -40,-.0634,-39,-.0676,-38,-.0719,-37,-.0762,-36,-.0807,
         -35,-.0853,-34,-.0900,-33,-.0948,-32,-.0997,-31,-.1047,
         -30,-.1099,-29,-.1152,-28,-.1206,-27,-.1262,-26,-.1318,
         -25,-.1376,-24,-.1436,-23,-.1496,-22,-.1557,-21,-.1618,
         -20,-.1680,-19,-.1742,-18,-.1803,-17,-.1862,-16,-.1918,
         -15,-.1970,-14,-.2015,-13,-.2052,-12,-.2077,-11,-.2086,
         -10,-.2288, -9,-.2299, -8,-.2309, -7,-.2318, -6,-.2325,
          -5,-.2331, -4,-.2335, -3,-.2338, -2,-.2339, -1,-.2339,
           0,-.2992,
           1,-.2339,  2,-.2339,  3,-.2338,  4,-.2335,  5,-.2331,
           6,-.2325,  7,-.2318,  8,-.2309,  9,-.2299, 10,-.2288,
```

```
            11,-.2086, 12,-.2077, 13,-.2052, 14,-.2015, 15,-.1970,
            16,-.1918, 17,-.1862, 18,-.1803, 19,-.1742, 20,-.1680,
            21,-.1618, 22,-.1557, 23,-.1496, 24,-.1436, 25,-.1376,
            26,-.1318, 27,-.1262, 28,-.1206, 29,-.1152, 30,-.1099,
            31,-.1047, 32,-.0997, 33,-.0948, 34,-.0900, 35,-.0853,
            36,-.0807, 37,-.0762, 38,-.0719, 39,-.0676, 40,-.0634,
            41,-.0594, 42,-.0554, 43,-.0515, 44,-.0477, 45,-.0440,
            46,-.0403, 47,-.0368, 48,-.0333, 49,-.0299, 50,-.0266,
            51,-.0233, 52,-.0201, 53,-.0170, 54,-.0140, 55,-.0110,
            56,-.0081, 57,-.0053, 58,-.0025, 59,0.0002, 60,0.0028,
            61,0.0054, 62,0.0079, 63,0.0103, 64,0.0127, 65,0.0150,
            66,0.0172, 67,0.0193, 68,0.0214, 69,0.0234, 70,0.0253,
            71,0.0272, 72,0.0290, 73,0.0307, 74,0.0323, 75,0.0339,
            76,0.0354, 77,0.0368, 78,0.0381, 79,0.0393, 80,0.0404,
 $
P$TAB
C   CWR = THE YAWING MOMENT DAMPING DERIVATIVE COEFFICIENT DUE TO THE
C           NONDIMENSIONAL YAW RATE.  THE NAME IN TEXTS IS C_n_r.
  TABLE= 4HCWRT,1,4HBETA,161,1,1,1,
           -80,0.0404,-79,0.0393,-78,0.0381,-77,0.0368,-76,0.0354,
           -75,0.0339,-74,0.0323,-73,0.0307,-72,0.0290,-71,0.0272,
           -70,0.0253,-69,0.0234,-68,0.0214,-67,0.0193,-66,0.0172,
           -65,0.0150,-64,0.0127,-63,0.0103,-62,0.0079,-61,0.0054,
           -60,0.0028,-59,0.0002,-58,-.0025,-57,-.0053,-56,-.0081,
           -55,-.0110,-54,-.0140,-53,-.0170,-52,-.0201,-51,-.0233,
           -50,-.0266,-49,-.0299,-48,-.0333,-47,-.0368,-46,-.0403,
           -45,-.0440,-44,-.0477,-43,-.0515,-42,-.0554,-41,-.0594,
           -40,-.0634,-39,-.0676,-38,-.0719,-37,-.0762,-36,-.0807,
           -35,-.0853,-34,-.0900,-33,-.0948,-32,-.0997,-31,-.1047,
           -30,-.1099,-29,-.1152,-28,-.1206,-27,-.1262,-26,-.1318,
           -25,-.1376,-24,-.1436,-23,-.1496,-22,-.1557,-21,-.1618,
           -20,-.1680,-19,-.1742,-18,-.1803,-17,-.1862,-16,-.1918,
           -15,-.1970,-14,-.2015,-13,-.2052,-12,-.2077,-11,-.2086,
           -10,-.2288, -9,-.2299, -8,-.2309, -7,-.2318, -6,-.2325,
            -5,-.2331, -4,-.2335, -3,-.2338, -2,-.2339, -1,-.2339,
             0,-.2992,
             1,-.2339,  2,-.2339,  3,-.2338,  4,-.2335,  5,-.2331,
             6,-.2325,  7,-.2318,  8,-.2309,  9,-.2299, 10,-.2288,
            11,-.2086, 12,-.2077, 13,-.2052, 14,-.2015, 15,-.1970,
            16,-.1918, 17,-.1862, 18,-.1803, 19,-.1742, 20,-.1680,
            21,-.1618, 22,-.1557, 23,-.1496, 24,-.1436, 25,-.1376,
            26,-.1318, 27,-.1262, 28,-.1206, 29,-.1152, 30,-.1099,
            31,-.1047, 32,-.0997, 33,-.0948, 34,-.0900, 35,-.0853,
            36,-.0807, 37,-.0762, 38,-.0719, 39,-.0676, 40,-.0634,
            41,-.0594, 42,-.0554, 43,-.0515, 44,-.0477, 45,-.0440,
            46,-.0403, 47,-.0368, 48,-.0333, 49,-.0299, 50,-.0266,
            51,-.0233, 52,-.0201, 53,-.0170, 54,-.0140, 55,-.0110,
            56,-.0081, 57,-.0053, 58,-.0025, 59,0.0002, 60,0.0028,
            61,0.0054, 62,0.0079, 63,0.0103, 64,0.0127, 65,0.0150,
            66,0.0172, 67,0.0193, 68,0.0214, 69,0.0234, 70,0.0253,
            71,0.0272, 72,0.0290, 73,0.0307, 74,0.0323, 75,0.0339,
```

```
        76,0.0354, 77,0.0368, 78,0.0381, 79,0.0393, 80,0.0404,
 $
P$TAB
C   CWP = THE YAWING MOMENT DAMPING DERIVATIVE COEFFICIENT DUE TO THE
C         NONDIMENSIONAL ROLL RATE.  THE NAME IN TEXTS IS C_n_p
  TABLE= 4HCWPT,0,0.0,
 $
P$TAB
C   CLLP = THE ROLLING MOMENT DAMPING DERIVATIVE COEFFICIENT DUE TO THE
C          NONDIMENSIONAL ROLL RATE.  THE NAME IN TEXTS IS C_l_p
  TABLE= 5HCLLPT,0,0.0,
 $
P$TAB
C   CLLR = THE ROLLING MOMENT DAMPING DERIVATIVE COEFFICIENT DUE TO THE
C           NONDIMENSIONAL YAW RATE.  THE NAME IN TEXTS IS C_l_R
  TABLE= 5HCLLRT,0,0.0,
 $
C**********************************************************************
C                          MASS PROPERTIES
C                     MOMENTS OF INERTIA TABLES
P$TAB
 TABLE     = 4HIXXT, 0, 61.88,          / ABOUT ROLL
 $
P$TAB
 TABLE     = 4HIYYT, 0, 48.14,          / ABOUT PITCH
 $
P$TAB
 TABLE     = 4HIZZT, 0, 48.14,          / ABOUT YAW
C                     PRODUCTS OF INERTIA TABLES
 $
P$TAB
 TABLE     = 4HIXYT, 0, 0.0,
 $
P$TAB
 TABLE     = 4HIXZT, 0, 0.0,
 $
P$TAB
 TABLE     = 4HIYZT, 0, 0.0,
 $
C                     CENTER OF GRAVITY LOCATIONS
P$TAB
 TABLE     = 4HXCGT, 0, 0.0,            /xcg=0.801666667
 $
P$TAB
 TABLE     = 4HYCGT, 0, 0.0,
 $
P$TAB
 TABLE     = 4HZCGT, 0, 0.0,
 ENDPHS    = 1,
 $
C**********************************************************************
```

```
P$GENDAT
 EVENT     = 10.,
 CRITR     = 4HMACH,
 VALUE     = .8,
 MDL       = 9,
 ENDPHS    = 1,
 ENDPRB    = 1,
 ENDJOB    = 1,
 $
```

APPENDIX D: AERODYNAMIC COEFFICIENTS' DATA*

α	C_A	C_N	C_Y	C_m	C_{mq}	C_n	C_{nr}	C_L	C_D
-80.0	0.03250	-0.89670	0.89670	0.09910	0.04040	-0.09910	-0.04040	-0.12370	0.88872
-79.0	0.04370	-0.89020	0.89020	0.10110	0.03930	-0.10110	-0.03930	-0.12696	0.88218
-78.0	0.05570	-0.88310	0.88310	0.10310	0.03810	-0.10310	-0.03810	-0.12912	0.87538
-77.0	0.06870	-0.87560	0.87560	0.10510	0.03680	-0.10510	-0.03680	-0.13003	0.86861
-76.0	0.08250	-0.86770	0.86770	0.10690	0.03540	-0.10690	-0.03540	-0.12987	0.86188
-75.0	0.09710	-0.85920	0.85920	0.10870	0.03390	-0.10870	-0.03390	-0.12859	0.85505
-74.0	0.11260	-0.85030	0.85030	0.11030	0.03230	-0.11030	-0.03230	-0.12614	0.84840
-73.0	0.12880	-0.84100	0.84100	0.11190	0.03070	-0.11190	-0.03070	-0.12271	0.84191
-72.0	0.14580	-0.83120	0.83120	0.11340	0.02900	-0.11340	-0.02900	-0.11819	0.83557
-71.0	0.16360	-0.82100	0.82100	0.11480	0.02720	-0.11480	-0.02720	-0.11260	0.82953
-70.0	0.18220	-0.81040	0.81040	0.11610	0.02530	-0.11610	-0.02530	-0.10596	0.82384
-69.0	0.20140	-0.79930	0.79930	0.11730	0.02340	-0.11730	-0.02340	-0.09842	0.81839
-68.0	0.22140	-0.78800	0.78800	0.11840	0.02140	-0.11840	-0.02140	-0.08991	0.81356
-67.0	0.24200	-0.77620	0.77620	0.11940	0.01930	-0.11940	-0.01930	-0.08052	0.80905
-66.0	0.26320	-0.76410	0.76410	0.12030	0.01720	-0.12030	-0.01720	-0.07034	0.80509
-65.0	0.28510	-0.75160	0.75160	0.12110	0.01500	-0.12110	-0.01500	-0.05925	0.80167
-64.0	0.30760	-0.73880	0.73880	0.12190	0.01270	-0.12190	-0.01270	-0.04740	0.79887
-63.0	0.33060	-0.72570	0.72570	0.12250	0.01030	-0.12250	-0.01030	-0.03489	0.79669
-62.0	0.35420	-0.71240	0.71240	0.12300	0.00790	-0.12300	-0.00790	-0.02171	0.79530
-61.0	0.37820	-0.69870	0.69870	0.12340	0.00540	-0.12340	-0.00540	-0.00796	0.79445
-60.0	0.40280	-0.68480	0.68480	0.12340	0.00280	-0.12340	-0.00280	0.00644	0.79445
-59.0	0.42780	-0.67060	0.67060	0.12380	0.00020	-0.12380	-0.00020	0.02131	0.79515
-58.0	0.45320	-0.65620	0.65620	0.12390	-0.00250	-0.12390	0.00250	0.03660	0.79665
-57.0	0.47900	-0.64160	0.64160	0.12390	-0.00530	-0.12390	0.00530	0.05228	0.79897
-56.0	0.50510	-0.62680	0.62680	0.12380	-0.00810	-0.12380	0.00810	0.06824	0.80209
-55.0	0.53160	-0.61190	0.61190	0.12360	-0.01100	-0.12360	0.01100	0.08449	0.80615
-54.0	0.55840	-0.59680	0.59680	0.12320	-0.01400	-0.12320	0.01400	0.10096	0.81104
-53.0	0.58540	-0.58150	0.58150	0.12280	-0.01700	-0.12280	0.01700	0.11757	0.81671
-52.0	0.61270	-0.56610	0.56610	0.12220	-0.02010	-0.12220	0.02010	0.13429	0.82331
-51.0	0.64010	-0.55070	0.55070	0.12160	-0.02330	-0.12160	0.02330	0.15088	0.83080
-50.0	0.66770	-0.53510	0.53510	0.12080	-0.02660	-0.12080	0.02660	0.16753	0.83910
-49.0	0.69540	-0.51950	0.51950	0.12000	-0.02990	-0.12000	0.02990	0.18400	0.84830
-48.0	0.72320	-0.50390	0.50390	0.11900	-0.03330	-0.11900	0.03330	0.20027	0.85839
-47.0	0.75110	-0.48820	0.48820	0.11800	-0.03680	-0.11800	0.03680	0.21637	0.86930
-46.0	0.77900	-0.47250	0.47250	0.11680	-0.04030	-0.11680	0.04030	0.23214	0.88103
-45.0	0.80690	-0.45680	0.45680	0.11560	-0.04400	-0.11560	0.04400	0.24756	0.89357
-44.0	0.83470	-0.44120	0.44120	0.11420	-0.04770	-0.11420	0.04770	0.26246	0.90692
-43.0	0.86250	-0.42560	0.42560	0.11280	-0.05150	-0.11280	0.05150	0.27696	0.92105
-42.0	0.89010	-0.41010	0.41010	0.11130	-0.05540	-0.11130	0.05540	0.29083	0.93588
-41.0	0.91760	-0.39470	0.39470	0.10970	-0.05940	-0.10970	0.05940	0.30412	0.95147
-40.0	0.94500	-0.37940	0.37940	0.10800	-0.06340	-0.10800	0.06340	0.31680	0.96779
-39.0	0.97210	-0.36430	0.36430	0.10620	-0.06760	-0.10620	0.06760	0.32865	0.98472
-38.0	0.99890	-0.34920	0.34920	0.10430	-0.07190	-0.10430	0.07190	0.33981	1.00213

*Note that $C_A=C_A(\alpha_{total})$, $C_Y=C_Y(\beta)$, $C_n=C_n(\beta)$ and $C_{nr}=C_{nr}(\beta)$.

α	C_A	C_N	C_Y	C_m	C_{mq}	C_n	C_{nr}	C_L	C_D
-37.0	1.02550	-0.33440	0.33440	0.10230	-0.07620	-0.10230	0.07620	0.35010	1.02025
-36.0	1.05180	-0.31970	0.31970	0.10030	-0.08070	-0.10030	0.08070	0.35959	1.03884
-35.0	1.07770	-0.30520	0.30520	0.09820	-0.08530	-0.09820	0.08530	0.36814	1.05786
-34.0	1.10330	-0.29100	0.29100	0.09600	-0.09000	-0.09600	0.09000	0.37571	1.07740
-33.0	1.12840	-0.27700	0.27700	0.09380	-0.09480	-0.09380	0.09480	0.38226	1.09722
-32.0	1.15310	-0.26320	0.26320	0.09140	-0.09970	-0.09140	0.09970	0.38784	1.11736
-31.0	1.17740	-0.24970	0.24970	0.08900	-0.10470	-0.08900	0.10470	0.39237	1.13783
-30.0	1.20110	-0.23650	0.23650	0.08660	-0.10990	-0.08660	0.10990	0.39573	1.15843
-29.0	1.22430	-0.22360	0.22360	0.08410	-0.11520	-0.08410	0.11520	0.39799	1.17920
-28.0	1.24700	-0.21100	0.21100	0.08150	-0.12060	-0.08150	0.12060	0.39913	1.20009
-27.0	1.26910	-0.19870	0.19870	0.07890	-0.12620	-0.07890	0.12620	0.39912	1.22098
-26.0	1.29060	-0.18680	0.18680	0.07620	-0.13180	-0.07620	0.13180	0.39787	1.24187
-25.0	1.31140	-0.17530	0.17530	0.07350	-0.13760	-0.07350	0.13760	0.39535	1.26262
-24.0	1.33160	-0.16410	0.16410	0.07070	-0.14360	-0.07070	0.14360	0.39170	1.28322
-23.0	1.35110	-0.15340	0.15340	0.06790	-0.14960	-0.06790	0.14960	0.38671	1.30363
-22.0	1.36990	-0.14300	0.14300	0.06510	-0.15570	-0.06510	0.15570	0.38059	1.32372
-21.0	1.38800	-0.13300	0.13300	0.06220	-0.16180	-0.06220	0.16180	0.37325	1.34347
-20.0	1.40530	-0.12350	0.12350	0.05930	-0.16800	-0.05930	0.16800	0.36459	1.36279
-19.0	1.42180	-0.11440	0.11440	0.05640	-0.17420	-0.05640	0.17420	0.35473	1.38158
-18.0	1.43760	-0.10580	0.10580	0.05340	-0.18030	-0.05340	0.18030	0.34362	1.39993
-17.0	1.45250	-0.09770	0.09770	0.05040	-0.18620	-0.05040	0.18620	0.33124	1.41760
-16.0	1.46660	-0.09000	0.09000	0.04750	-0.19180	-0.04750	0.19180	0.31774	1.43459
-15.0	1.47990	-0.08270	0.08270	0.04450	-0.19700	-0.04450	0.19700	0.30314	1.45088
-14.0	1.49220	-0.07600	0.07600	0.04140	-0.20150	-0.04140	0.20150	0.28725	1.46626
-13.0	1.50370	-0.06980	0.06980	0.03840	-0.20520	-0.03840	0.20520	0.27025	1.48086
-12.0	1.51440	-0.06410	0.06410	0.03540	-0.20770	-0.03540	0.20770	0.25216	1.49463
-11.0	1.52410	-0.05890	0.05890	0.03240	-0.20860	-0.03240	0.20860	0.23299	1.50734
-10.0	1.53510	-0.04640	0.04640	0.02740	-0.22880	-0.02740	0.22880	0.22087	1.51984
-9.0	1.54330	-0.04190	0.04190	0.02480	-0.22990	-0.02480	0.22990	0.20004	1.53085
-8.0	1.55070	-0.03740	0.03740	0.02210	-0.23090	-0.02210	0.23090	0.17878	1.54081
-7.0	1.55720	-0.03280	0.03280	0.01940	-0.23180	-0.01940	0.23180	0.15722	1.54959
-6.0	1.56280	-0.02820	0.02820	0.01670	-0.23250	-0.01670	0.23250	0.13531	1.55719
-5.0	1.56760	-0.02360	0.02360	0.01390	-0.23310	-0.01390	0.23310	0.11312	1.56369
-4.0	1.57160	-0.01890	0.01890	0.01110	-0.23350	-0.01110	0.23350	0.09078	1.56909
-3.0	1.57470	-0.01420	0.01420	0.00840	-0.23380	-0.00840	0.23380	0.06823	1.57328
-2.0	1.57680	-0.00950	0.00950	0.00560	-0.23390	-0.00560	0.23390	0.04554	1.57617
-1.0	1.57820	-0.00470	0.00470	0.00280	-0.23390	-0.00280	0.23390	0.02284	1.57804
0.0	1.57860	0.00000	0.00000	0.00000	-0.29920	0.00000	0.29920	0.00000	1.57860
1.0	1.57820	0.00470	-0.00470	-0.00280	-0.23390	0.00280	0.23390	-0.02284	1.57804
2.0	1.57680	0.00950	-0.00950	-0.00560	-0.23390	0.00560	0.23390	-0.04554	1.57617
3.0	1.57470	0.01420	-0.01420	-0.00840	-0.23380	0.00840	0.23380	-0.06823	1.57328
4.0	1.57160	0.01890	-0.01890	-0.01110	-0.23350	0.01110	0.23350	-0.09078	1.56909
5.0	1.56760	0.02360	-0.02360	-0.01390	-0.23310	0.01390	0.23310	-0.11312	1.56369
6.0	1.56280	0.02820	-0.02820	-0.01670	-0.23250	0.01670	0.23250	-0.13531	1.55719
7.0	1.55720	0.03280	-0.03280	-0.01940	-0.23180	0.01940	0.23180	-0.15722	1.54959
8.0	1.55070	0.03740	-0.03740	-0.02210	-0.23090	0.02210	0.23090	-0.17878	1.54081
9.0	1.54330	0.04190	-0.04190	-0.02480	-0.22990	0.02480	0.22990	-0.20004	1.53085
10.0	1.53510	0.04640	-0.04640	-0.02740	-0.22880	0.02740	0.22880	-0.22087	1.51984

α	C_A	C_N	C_Y	C_m	C_{mq}	C_n	C_{nr}	C_L	C_D
11.0	1.52410	0.05890	-0.05890	-0.03240	-0.20860	0.03240	0.20860	-0.23299	1.50734
12.0	1.51440	0.06410	-0.06410	-0.03540	-0.20770	0.03540	0.20770	-0.25216	1.49463
13.0	1.50370	0.06980	-0.06980	-0.03840	-0.20520	0.03840	0.20520	-0.27025	1.48086
14.0	1.49220	0.07600	-0.07600	-0.04140	-0.20150	0.04140	0.20150	-0.28725	1.46626
15.0	1.47990	0.08270	-0.08270	-0.04450	-0.19700	0.04450	0.19700	-0.30314	1.45088
16.0	1.46660	0.09000	-0.09000	-0.04750	-0.19180	0.04750	0.19180	-0.31774	1.43459
17.0	1.45250	0.09770	-0.09770	-0.05040	-0.18620	0.05040	0.18620	-0.33124	1.41760
18.0	1.43760	0.10580	-0.10580	-0.05340	-0.18030	0.05340	0.18030	-0.34362	1.39993
19.0	1.42180	0.11440	-0.11440	-0.05640	-0.17420	0.05640	0.17420	-0.35473	1.38158
20.0	1.40530	0.12350	-0.12350	-0.05930	-0.16800	0.05930	0.16800	-0.36459	1.36279
21.0	1.38800	0.13300	-0.13300	-0.06220	-0.16180	0.06220	0.16180	-0.37325	1.34347
22.0	1.36990	0.14300	-0.14300	-0.06510	-0.15570	0.06510	0.15570	-0.38059	1.32372
23.0	1.35110	0.15340	-0.15340	-0.06790	-0.14960	0.06790	0.14960	-0.38671	1.30363
24.0	1.33160	0.16410	-0.16410	-0.07070	-0.14360	0.07070	0.14360	-0.39170	1.28322
25.0	1.31140	0.17530	-0.17530	-0.07350	-0.13760	0.07350	0.13760	-0.39535	1.26262
26.0	1.29060	0.18680	-0.18680	-0.07620	-0.13180	0.07620	0.13180	-0.39787	1.24187
27.0	1.26910	0.19870	-0.19870	-0.07890	-0.12620	0.07890	0.12620	-0.39912	1.22098
28.0	1.24700	0.21100	-0.21100	-0.08150	-0.12060	0.08150	0.12060	-0.39913	1.20009
29.0	1.22430	0.22360	-0.22360	-0.08410	-0.11520	0.08410	0.11520	-0.39799	1.17920
30.0	1.20110	0.23650	-0.23650	-0.08660	-0.10990	0.08660	0.10990	-0.39573	1.15843
31.0	1.17740	0.24970	-0.24970	-0.08900	-0.10470	0.08900	0.10470	-0.39237	1.13783
32.0	1.15310	0.26320	-0.26320	-0.09140	-0.09970	0.09140	0.09970	-0.38784	1.11736
33.0	1.12840	0.27700	-0.27700	-0.09380	-0.09480	0.09380	0.09480	-0.38226	1.09722
34.0	1.10330	0.29100	-0.29100	-0.09600	-0.09000	0.09600	0.09000	-0.37571	1.07740
35.0	1.07770	0.30520	-0.30520	-0.09820	-0.08530	0.09820	0.08530	-0.36814	1.05786
36.0	1.05180	0.31970	-0.31970	-0.10030	-0.08070	0.10030	0.08070	-0.35959	1.03884
37.0	1.02550	0.33440	-0.33440	-0.10230	-0.07620	0.10230	0.07620	-0.35010	1.02025
38.0	0.99890	0.34920	-0.34920	-0.10430	-0.07190	0.10430	0.07190	-0.33981	1.00213
39.0	0.97210	0.36430	-0.36430	-0.10800	-0.06760	0.10800	0.06760	-0.32865	0.98472
40.0	0.94500	0.37940	-0.37940	-0.10970	-0.06340	0.10970	0.06340	-0.31680	0.96779
41.0	0.91760	0.39470	-0.39470	-0.10970	-0.05940	0.10970	0.05940	-0.30412	0.95147
42.0	0.89010	0.41010	-0.41010	-0.11130	-0.05540	0.11130	0.05540	-0.29083	0.93588
43.0	0.86250	0.42560	-0.42560	-0.11280	-0.05150	0.11280	0.05150	-0.27696	0.92105
44.0	0.83470	0.44120	-0.44120	-0.11420	-0.04770	0.11420	0.04770	-0.26246	0.90692
45.0	0.80690	0.45680	-0.45680	-0.11560	-0.04400	0.11560	0.04400	-0.24756	0.89357
46.0	0.77900	0.47250	-0.47250	-0.11680	-0.04030	0.11680	0.04030	-0.23214	0.88103
47.0	0.75110	0.48820	-0.48820	-0.11800	-0.03680	0.11800	0.03680	-0.21637	0.86930
48.0	0.72320	0.50390	-0.50390	-0.11900	-0.03330	0.11900	0.03330	-0.20027	0.85839
49.0	0.69540	0.51950	-0.51950	-0.12000	-0.02990	0.12000	0.02990	-0.18400	0.84830
50.0	0.66770	0.53510	-0.53510	-0.12080	-0.02660	0.12080	0.02660	-0.16753	0.83910
51.0	0.64010	0.55070	-0.55070	-0.12160	-0.02330	0.12160	0.02330	-0.15088	0.83080
52.0	0.61270	0.56610	-0.56610	-0.12220	-0.02010	0.12220	0.02010	-0.13429	0.82331
53.0	0.58540	0.58150	-0.58150	-0.12280	-0.01700	0.12280	0.01700	-0.11757	0.81671
54.0	0.55840	0.59680	-0.59680	-0.12320	-0.01400	0.12320	0.01400	-0.10096	0.81104
55.0	0.53160	0.61190	-0.61190	-0.12360	-0.01100	0.12360	0.01100	-0.08449	0.80615
56.0	0.50510	0.62680	-0.62680	-0.12380	-0.00810	0.12380	0.00810	-0.06824	0.80209
57.0	0.47900	0.64160	-0.64160	-0.12390	-0.00530	0.12390	0.00530	-0.05228	0.79897
58.0	0.45320	0.65620	-0.65620	-0.12390	-0.00250	0.12390	0.00250	-0.03660	0.79665

α	C_A	C_N	C_Y	C_m	C_{mq}	C_n	C_{nr}	C_L	C_D
59.0	0.42780	0.67060	-0.67060	-0.12380	0.00020	0.12380	-0.00020	-0.02131	0.79515
60.0	0.40280	0.68480	-0.68480	-0.12370	0.00280	0.12370	-0.00280	-0.00644	0.79445
61.0	0.37820	0.69870	-0.69870	-0.12340	0.00540	0.12340	-0.00540	0.00796	0.79445
62.0	0.35420	0.71240	-0.71240	-0.12300	0.00790	0.12300	-0.00790	0.02171	0.79530
63.0	0.33060	0.72570	-0.72570	-0.12250	0.01030	0.12250	-0.01030	0.03489	0.79669
64.0	0.30760	0.73880	-0.73880	-0.12190	0.01270	0.12190	-0.01270	0.04740	0.79887
65.0	0.28510	0.75160	-0.75160	-0.12110	0.01500	0.12110	-0.01500	0.05925	0.80167
66.0	0.26320	0.76410	-0.76410	-0.12030	0.01720	0.12030	-0.01720	0.07034	0.80509
67.0	0.24200	0.77620	-0.77620	-0.11940	0.01930	0.11940	-0.01930	0.08052	0.80905
68.0	0.22140	0.78800	-0.78800	-0.11840	0.02140	0.11840	-0.02140	0.08991	0.81356
69.0	0.20140	0.79930	-0.79930	-0.11730	0.02340	0.11730	-0.02340	0.09842	0.81839
70.0	0.18220	0.81040	-0.81040	-0.11610	0.02530	0.11610	-0.02530	0.10596	0.82384
71.0	0.16360	0.82100	-0.82100	-0.11480	0.02720	0.11480	-0.02720	0.11260	0.82953
72.0	0.14580	0.83120	-0.83120	-0.11340	0.02900	0.11340	-0.02900	0.11819	0.83557
73.0	0.12880	0.84100	-0.84100	-0.11190	0.03070	0.11190	-0.03070	0.12271	0.84191
74.0	0.11260	0.85030	-0.85030	-0.11030	0.03230	0.11030	-0.03230	0.12614	0.84840
75.0	0.09710	0.85920	-0.85920	-0.10870	0.03390	0.10870	-0.03390	0.12859	0.85505
76.0	0.08250	0.86770	-0.86770	-0.10690	0.03540	0.10690	-0.03540	0.12987	0.86188
77.0	0.06870	0.87560	-0.87560	-0.10510	0.03680	0.10510	-0.03680	0.13003	0.86861
78.0	0.05570	0.88310	-0.88310	-0.10310	0.03810	0.10310	-0.03810	0.12912	0.87538
79.0	0.04370	0.89020	-0.89020	-0.10110	0.03930	0.10110	-0.03930	0.12696	0.88218
80.0	0.03250	0.89670	-0.89670	-0.09910	0.04040	0.09910	-0.04040	0.12370	0.88872

VITA

Haisam Kassim Ido was born in Kuwait City, Kuwait on March 29, 1962. He lived in Kuwait for about six years. His father is from the Syrian Arab Republic and his mother is from the Federal Republic of Germany. He attended his first year of elementary school in Salamiyah, Syria. His second through sixth years of elementary school were spent at al-Fārūq Elementary School in Aleppo, Syria. On October 9th 1974 he, his four siblings and parents arrived in New York City, where his father had obtained a post as translator at the United Nations. His seventh and eighth years of education were completed at the United Nations International School on Manhattan Island. His ninth year of education was at Public School 217. He completed his high school education at Hillcrest High School, Jamaica, New York. In the fall of 1980 he attended New York Institute of Technology, to major in Aerospace Engineering Technology, in the Manhattan branch. After two years he transferred to Ohio State University to study Aeronautical-Astronautical Engineering. In June of 1985 he received a Bachelor of Science. Again in June of 1988 he received a Bachelor of Science in Applied Mathematics. After being employed as a civil servant at the Ohio State University Libraries for two and a half years, as an assistant to an Arabic Language Cataloger, he and his wife moved to Tullahoma, Tennessee, where he pursued a Master of Science in Aerospace Engineering at the University of Tennessee Space Institude. He was employed as a Graduate Research Assistant at the Computer Center, from October 1990 to July 1991. From August 1991 to May of 1992, he was employed as a Graduate Research Assistant at the UT-Calspan Center for Space Transportation and Applied Research. Haisam received his Master of Science degree in August of 1992.

INDEX